PERFORMANCE OF AUTOCLAVED AERATED CONCRETE INFILL WALLS UNDER IN-PLANE AND OUT-OF-PLANE SEISMIC DEMANDS

A THESIS SUBMITTED TO
THE GRADUATE SCHOOL OF NATURAL AND APPLIED SCIENCES
OF
MIDDLE EAST TECHNICAL UNIVERSITY

BY

SEMA MELEK YILMAZTÜRK

IN PARTIAL FULFILLMENT OF THE REQUIREMENTS
FOR
THE DEGREE OF DOCTOR OF PHILOSOPHY
IN
CIVIL ENGINEERING

SEPTEMBER 2023

Approval of the thesis:

PERFORMANCE OF AUTOCLAVED AERATED CONCRETE INFILL WALLS UNDER IN-PLANE AND OUT-OF-PLANE SEISMIC DEMANDS

submitted by **SEMA MELEK YILMAZTÜRK** in partial fulfillment of the requirements for the degree of **Doctor of Philosophy** i**n Civil Engineering, Middle East Technical University** by,

Prof. Dr. Halil KALIPÇILAR
Dean, Graduate School of **Natural and Applied Sciences** _____

Prof. Dr. Erdem CANBAY
Head of the Department, **Civil Engineering** _____

Prof. Dr. Barış BİNİCİ
Supervisor, **Civil Engineering, METU** _____

Examining Committee Members:

Prof. Dr. Güney ÖZCEBE
Civil Engineering, TEDU _____

Prof. Dr. Barış BİNİCİ
Civil Engineering, METU _____

Prof. Dr. Erdem CANBAY
Civil Engineering, METU _____

Prof. Dr. Ahmet YAKUT
Civil Engineering, METU _____

Assoc. Prof. Dr. Alper ALDEMİR
Civil Engineering, Hacettepe University _____

Date: 11.09.2023

I hereby declare that all information in this document has been obtained and presented in accordance with academic rules and ethical conduct. I also declare that, as required by these rules and conduct, I have fully cited and referenced all material and results that are not original to this work.

Name Last name : Sema Melek Yılmaztürk

Signature :

ABSTRACT

PERFORMANCE OF AUTOCLAVED AERATED CONCRETE INFILL WALLS UNDER IN-PLANE AND OUT-OF-PLANE SEISMIC DEMANDS

Yılmaztürk, Sema Melek
Doctor of Philosophy, Civil Engineering
Supervisor: Prof. Dr. Barış Binici

September 2023, 117 pages

According to past studies, it is observed that infill walls increase the lateral stiffness and strength of the frame under earthquakes with low intensities causing in-plane (IP) loading. However, the combined effect of IP and out-of-plane (OOP) excitations can lead to the premature failure of infill walls. Autoclaved aerated concrete (AAC) is a lightweight, precast building material made from natural raw materials such as sand, cement, lime, and water. It is known for its excellent thermal insulation properties, high load-bearing capacity, and fire resistance. AAC is a relatively newer material compared to traditional masonry; therefore, there are fewer studies on the seismic performance of AAC-infilled reinforced concrete (RC) frames until recent years. This study investigates the performance of an insulated wall system made of AAC blocks and thermal insulation plates. This system aims to create monolithic, mineral-based, non-combustible facades that can easily meet the regulations and standards. Two types of walls are prepared, and experiments are conducted in the laboratory under different loadings. The objective of the study is to understand the behavior of these insulated walls (single cross-section wall system) under the combined effect of in-plane and out-of-plane loads during earthquakes. Additionally, it was aimed to assess the in-plane drift capacity of AAC infill walls under the influence of out-of-plane loads and develop a model to estimate the drift ratio of

AAC infill walls under combined in-plane and out-of-plane demands. Total of eight tests are conducted for the insulated wall system. The behavior of the insulated wall system is found to be similar to other infill wall types. The main contribution to literature is to show the performance of an insulated wall system with AAC infill walls under seismic forces. It was observed that the combined in-plane and out-of-plane loading causes a reduction in the displacement capacities and drift ratios.

Keywords: AAC infill wall, in-plane behavior, out-of-plane behavior, combined IP and OOP effect, experimental test

ÖZ

GAZ BETON DOLGU DUVARLARININ DÜZLEM İÇİ VE DÜZLEM DIŞI SİSMİK YÜKLER ETKİSİNDEKİ PERFORMANSININ İNCELENMESİ

Yılmaztürk, Sema Melek
Doktora, İnşaat Mühendisliği
Tez Yöneticisi: Prof. Dr. Barış Binici

Eylül 2023, 117 sayfa

Dolgu duvarlarının düşük derecedeki depremlerde çerçevenin yanal rijitlik ve dayanımının artırdığı bilinmektedir. Ancak birleşik düzlem içi ve düzlem dışı hareketler, dolgu duvarlarının sadece düzlem içi harekete göre daha erken yıkılmasına sebep olabilmektedir. Gaz beton dolgu duvar geleneksel tuğla duvar uygulamalarına kıyasla nispeten daha yeni bir malzemedir. Bu yüzden literatürde bulunan dolgu duvar çalışma sayılarının daha az olması anlaşılabilir bir durumdur. Dolgu duvar çalışmalarında gaz beton duvar çalışmalarının sayıları özellikle ilave izolasyonlu durumlar için yetersizdir. Gaz beton; kum, çimento, kireç ve su gibi doğal hammaddelerden yapılmış, hafif prekast bir yapı malzemesidir. Mükemmel ısı yalıtım özellikleri, yüksek yük taşıma kapasitesi ve yangına dayanıklılığı ile bilinir. Bu çalışmada tek kesit cephe sistemlerinin deprem performanslarının incelenmektedir. Tek kesitli duvar; gaz beton duvar ile izolasyon plakaların birlikte kullanılmasından oluşmaktadır. İki farklı tipte duvar hazırlanarak laboratuvarda farklı yükleme durumları altında deneyler yapılmıştır. Bu araştırmanın amacı; deprem sırasında bileşik düzlem dışı ve düzlem içi yüklerinin etkisi ile tek kesitli (Gaz beton + Minepor) duvarların davranışlarını anlamak; Gaz beton dolgu duvarının düzlem içi yatay ötelenme kapasitesini düzlem dışı etki altında incelemek,

tasarıma yönelik öneriler geliştirebilmek ve gaz beton dolgu duvarlarının birleşik düzlem içi ve dışı yükler altında davranışlarının ve yatay ötelenme oranını tahmin edebilen bir model oluşturmaktır. Yalıtımlı duvar sistemi için toplam sekiz test yapılmıştır. Yalıtımlı duvar sisteminin test sonuçları diğer dolgu duvar tiplerinin davranışına benzer bir davranış göstermiştir. Bu çalışmanın literatüre katkısı gaz beton dolgu duvarlı yalıtımlı duvar sisteminin deprem kuvvetleri altındaki performansının belirlenmesi ve gösterilmesidir. Birleşik düzlem içi ve düzlem dışı yükün, sistemde yer değiştirme kapasitelerinin ve yatay ötelenme oranlarının azalmasına neden olduğu gözlenmiştir.

Anahtar Kelimeler: Gaz beton dolgu duvar, düzlem içi davranış, düzlem-dışı davranış, birleşik etki (düzlem içi ve düzlem dışı), deneysel test çalışmaları.

To my beloved mother and in the memory of my beloved father

ACKNOWLEDGMENTS

First of all, I wish to express my deepest gratitude to my supervisor, Prof. Dr. Barış Binici, for his guidance, advice, criticism, encouragement, and insight throughout the research since 2010, the beginning of my master's degree studies.

I am also thankful to Prof. Dr. Güney Özcebe and Prof. Dr. Erdem Canbay for their support, guidance, and contribution to my PhD research.

I cannot forget the help of my friend and assistant, İsmail Ozan Demirel, during my experiments and for preparing the test setup in the laboratory. Whenever I had a question about the experiment, he always answered sincerely. Moreover, I am thankful to Labor Murat for constructing the infill wall and applying plasters.

I am fortunate to have become friends with Meltem Tangüler Bayramtan and Burhan Alam after meeting them in the Materials Laboratory. Moreover, I would like to thank Melis Yıldız Yılmaz for her support.

I want to thank my colleagues in Mega Engineering, Kamil Ergüner, Fulya Deneyen, Öykü Beyaziler, and Mehmet Can Beyaziler, for their support.

I am also thankful to my dear friends Başak Bingöl Taştankaya, Fatoş İlbi, Seçil Üstünkol, and Cansu Direk Ateş for being my best friends for 20 years.

Special thanks go to my dear family members: my mother, Gülhun Yılmaztürk, my brother Mehmet Yılmaztürk and Seher Yılmaztürk. Without their support, I cannot achieve this. They always support me with their love. I wish my father could see this moment, but I feel his presence all around me all the time. The most important person in my life, my dear son Kuzey Kasapgil, deserves the last and most special thanks for always being with me during experiments in the period of pregnancy.

My primary motivation to start my Ph.D. research was to develop myself in engineering and become a fully equipped, successful, and experienced structural

design engineer. I have studied many subjects and topics related to structural engineering and gained huge amount of knowledge throughout these years. Nevertheless, I postponed finalizing the Ph.D. degree because I could not feel competent enough. I wondered if I would be perfect and know everything when I get the Ph.D. Now it is time to finalize my research as I am. I always tried my best and never gave up studying, although I had many tears over the years. I feel that learning is a never-ending process and I should continuously improve myself. It was a long journey that has improved me and my ideas about life. Thanks for all your support. The key to success is not to give up.

A new chapter of my life with my dear son Kuzey is beginning since he has started his preschool education, and now, I am the caregiver. Today is the last day of my life as a student and the first day of Kuzey's preschool education. I am ready for new adventures.

TABLE OF CONTENTS

ABSTRACT v

ÖZ vii

ACKNOWLEDGMENTS x

TABLE OF CONTENTS xii

LIST OF TABLES xiii

LIST OF FIGURES xiv

LIST OF ABBREVIATIONS xvii

LIST OF SYMBOLS xviii

CHAPTERS

1 INTRODUCTION 1

2 LITERATURE REVIEW 9

3 EXPERIMENTAL PROGRAM- TEST SET-UP 27

4 EXPERIMENTAL RESULTS AND DISCUSSIONS 44

5 NUMERICAL SIMULATIONS 66

6 CONCLUSIONS 92

REFERENCES 96

CURRICULUM VITAE 117

LIST OF TABLES

TABLES

Table 1.1. Material properties of AAC 2
Table 1.2. Properties of Minepor Thermal Insulation Plate..... 5
Table 3.1. Specimen Properties 38
Table 3.2. Material Strengths..... 39
Table 4.1. Summary of test results..... 58
Table 4.2. Bare Frame (BF) and AAC infill wall results of studies of Binici et al. (2019)..... 60
Table 5.1. Strut properties for Models 72
Table 5.2. Parameter for the calculation of effective strut material properties..... 78
Table 5.3. Summary of strut parameters with presence of plaster- Type 1 78
Table 5.4. Summary of calculation the effective strut width..... 78
Table 5.5. Parameter for the calculation of effective strut material properties..... 86
Table 5.6. Summary of strut parameters with presence of plaster- Type 2 87
Table 5.7. Summary of calculation the effective strut width..... 87

LIST OF FIGURES

FIGURES

Figure 1.1. AAC manufacturing in large scale (Y som i Yxhult by Linda Gustafsson, 1929) 2
Figure 1.2. Different applications of AAC construction material 3
Figure 1.3. Single Cross Section Facade system 4
Figure 2.1. Relative effectiveness of vertical and horizontal shear stress (Priestly & Bridgeman, 1974) 15
Figure 2.2. Out-of-plane mechanism a) Arching effect b) Crack pattern under OOP 21
Figure 2.3. λ_2–(h/t) points and possible best fitting curve (FEMA-356) 22
Figure 2.4. Strut and Tie macro model scheme by Hashemi and Mosalam (2006) 23
Figure 2.5. Model scheme of Kadysiewski and Mosalam (2009) 23
Figure 3.1. Portal frame system dimensions and reinforcement detail 29
Figure 3.2. Dimensions of AAC block (300x125x125 mm) 30
Figure 3.3. Procedures of preparing the Type 1 wall 31
Figure 3.4. Application of CLIP on the surface of the frame 31
Figure 3.5. AAC block mortar, CLIP adhesive and Plaster 32
Figure 3.6. Test samples for determination of flexural strength (40x40x160 mm) and uniaxial compressive strength (50x50x50mm) 32
Figure 3.7. Instrumentation (Todorovic, 2019) 34
Figure 3.8. In-plane loading instrumentation 34
Figure 3.9. Out-of-plane loading instrumentation 35
Figure 3.10. In-plane loading protocol 36
Figure 3.11. Locations of LVDTs of OOP test 36
Figure 3.12. System dimensioning and 3D view for Type 1 a) to d) and for Type 2 e) to h): 38
Figure 3.13. Compressive strengths of mortar types (MPa) 40
Figure 3.14. Stiffness calculation in cyclic load (Akin, 2011) 41

Figure 3.15. Idealized bi-linear curve for equal area concept..... 42
Figure 3.16. Dissipated energy of the frame..... 43
Figure 4.1. S1 test results..... 46
Figure 4.2. S2 test results..... 47
Figure 4.3. S3 test results..... 48
Figure 4.4. S4 test results..... 50
Figure 4.5. S5 test results..... 51
Figure 4.6. S6 test results..... 52
Figure 4.7 S7 test results..... 55
Figure 4.8 S8 test results..... 56
Figure 4.9. Effect of plaster on a) Behavior of Type 1 wall under in plane loading, b) cumulative energy dissipation versus drift ratio..... 59
Figure 4.10. Effect of OOP Load Level for Type 1 Specimens..... 61
Figure 4.11. OOP displacement-OOP Load Level 61
Figure 4.12. Comparison of various system behavior under IP loading..... 62
Figure 4.13. Comparison of various system behavior under OOP loading 63
Figure 4.14. Comparison of various system behavior under IP+OOP loading 64
Figure 4.15. OOP force ratio- in-plane DR capacity 65
Figure 5.1. Modeling properties of Type 1 wall, a) Frame set-up b) plan view c) detail..... 66
Figure 5.2. Modeling properties of Type 2 wall, a) Frame set-up b) plan view..... 67
Figure 5.3. Hognestad concrete model for unconfined concrete 67
Figure 5.4. Mander's concrete model for confined concrete..... 68
Figure 5.5. Cross sections of column and flanged beam 69
Figure 5.6. Modified Giuffré–Menegotto–Pinto uniaxial material constitutive model for structural steel 69
Figure 5.7. Different Material properties of infill strut a) Concrete01 model b) Concrete06 model ..... c) Hysteretic Material model 70

Figure 5.8. Fiber-based modeling of strain penetration effect (Zhao and Sritharan, 2007) 70
Figure 5.9. Modeling system a) Node Labeling b) Element Labeling 71
Figure 5.10. Diagonal, horizontal and horizontal strut widths (Trapani, 2018) 73
Figure 5.11. Material property of strut (Shing and Stavridis, 2014) 73
Figure 5.12. Verification of Model 1 Analysis with test (IP loading without plaster) 75
Figure 5.13. Infill strut stress-strain model 77
Figure 5.14. Infill extrusion detail for Type 1 79
Figure 5.15. Verification of Model 2 Analysis with test 81
Figure 5.16. Verification of Model 3 Analysis with test (OOP loading with plaster) 82
Figure 5.17. Verification of Model 4 Analysis with test 84
Figure 5.18. Verification of Model 5 Analysis with test 85
Figure 5.19. Verification of Model 6 Analysis with test (OOP)-Type2 88
Figure 5.20. Verification of Model 7 Analysis with test 90

LIST OF ABBREVIATIONS

ABBREVIATIONS

AAC: Autoclaved aerated concrete

BF: Bare Frame

CLIP: Mineral-based cementitious lightweight insulation panels

DR: Drift ratio

IP: In-plane loading

IP+OOP: Combined effect of in-plane and out-of-plane loading

OOP: Out of plane loading

RC: Reinforced concrete

SBC: Styrol Butadiene Copolymer

ULS: Ultimate limit State

LIST OF SYMBOLS

SYMBOLS

β_1 Coefficient depending on aspect ratio of panels (2.9)

f_t Tensile strength (2.9)

h Height of infill wall

q_u Maximum lateral pressure (2.9)

t thickness of infill wall

CHAPTER 1

INTRODUCTION

1.1 General

The use of reinforced concrete frame structures with infill walls, particularly with autoclaved aerated concrete (AAC) blocks and panels, has become popular in residential buildings and schools worldwide. AAC offers several advantages as a construction material. It was first invented by Hoffman in Germany in 1889 when he discovered concrete aeration with carbon dioxide. Since then, AAC has been widely manufactured on large scales in the industry. AAC is made by mixing cement, gypsum, lime, fine sand, and aluminum powder. This mixture undergoes expansion, tripling its volume creating a lightweight and porous material. The resulting AAC blocks and panels have numerous benefits, including high thermal insulation, fire resistance, and excellent acoustic performance. They also provide good load-bearing capacity and are easy to handle, making construction processes more efficient. An example of AAC manufacturing at a large scale is shown in Figure 1.1. The use of AAC in infill walls has gradually replaced traditional masonry construction due to its versatility and improved performance by up to 30%. This material has proven reliable and has been widely adopted in many countries, including Turkey. Its sustainable nature and energy-saving properties make AAC desirable for modern construction projects. It is a lightweight, fire-resistant, good insulation material that is easy to construct with thin bed mortar glue. AAC can be used for exterior walls in warm climate regions due to its low thermal conductivity coefficient (0.1-0.2 W/mK). It has a low density because its porous structure results in low weight. However, the mechanical properties satisfy the durability limitations of concrete with lightweight. The only disadvantage of the AAC is its water absorption and

brittle character. When exposed to water, cracks can appear due to water absorption from the porous behavior.

Figure 1.1. AAC manufacturing in large scale (Y som i Yxhult by Linda Gustafsson, 1929*)*

The use of AAC members in Turkey started after the 1950s with the imports from Germany. The most used products are blocks and lintels as filler walls. In factories, it is also possible to obtain rounded or U-shaped blocks. Moreover, by positioning steel mesh inside the blocks, load-bearing reinforced walls with reinforced elements have become valid and popular in recent years. The different application areas of AAC technology as a construction material are shown in Figure 1.2.

Table 1.1. Material properties of AAC

Property	**AAC**	**Normal Concrete**
Density (kg/m^3)	300-1000	1280-2400
Compressive strength (MPa)	1.5-10	6.9-69
Thermal Conductivity (W/m°K)	0.07-0.26	1.4-3.6
Fire rate (hours)	<8	<6

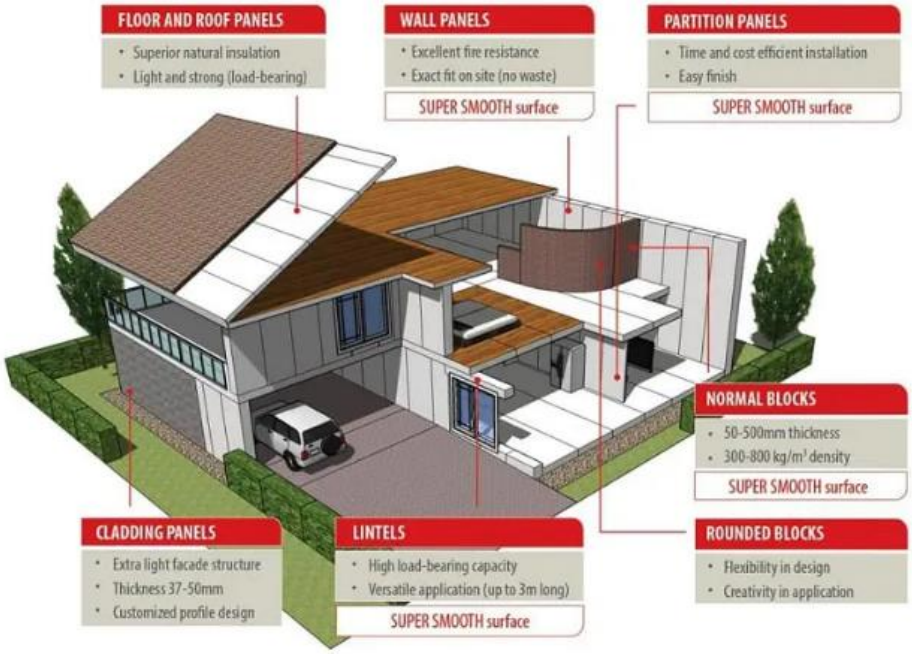

Figure 1.2. Different applications of AAC construction material

1.2 Cementitious Lightweight Insulation Panels (CLIP)

Minepor insulation plate is a mineral-based autoclaved aerated concrete heat insulation covering material used inside and outside buildings, slabs, and roofs as the insulator. The mechanical properties and performance values of the AAC material are listed in Table 1.2. The short-term water absorption capacity is calculated as 6.46 kg/m^2 as an average value according to TS EN 1609 Method B. The long-term water absorption capacity is calculated according to the TS EN 12087 Method-1B and found to be 7.13 kg/m^2. The resistance coefficient of water vapor permeability is 1.3 (TS EN 12086).

Figure 1.3. Single Cross Section Facade system

The single cross-section facade system offers a breathing and fireproof solution not affected by heat or cold weather. The infill walls of AAC blocks are positioned on the reinforced concrete frame; then, the minepor thermal insulation plates are covered only on the reinforced concrete frame, as shown in red dots in Figure 1.3. Therefore, without the need for extra insulation on the infill walls, compliant with regulations and standards, non-combustible, breathing, heat-insulated facades and thermally comfortable living spaces are obtained.

Table 1.2. Properties of Minepor Thermal Insulation Plate

General Requirements	**Property**	**Performance Value**
Fire resistance	Reaction to fire	A1
Health, environment and hygiene	Short period water absorption	Max. 10 kg/m^2
	Long period water absorption	Max. 12kg/m^2
	water vapor permeability	Max. 10
Energy saving and heat preservation	Heat insulation	Measured value
	Dimensions	Max. deviation 2 mm
	Density	Max. 160 kg/m^3
	Under point load behavior	Min. 2000 N
	Compressive strength	>400 kPa
	Tensile strength perpendicular to surfaces	Min. 100 kPa
	Flexural strength	Min. 150 kPa

1.3 Objective and Scope

Recently, many studies have been related to infill wall performance with different material types. It was observed that more research on infill walls with insulation materials is needed. The main difference in this research is the type of wall construction with the eccentric location of AAC blocks on the reinforced concrete frame and covering the cementitious-based lightweight insulation plates as the insulated exterior wall system.

The objective of this research is :

- to understand the behavior of single cross-section (AAC+Minepor) walls with the effect of combined OOP and IP loads during earthquake
- to investigate the in-plane drift capacity of AAC infill wall under the effect of out-of-plane
- to investigate the performance of two different types of infill wall systems with insulation plates (Type-1 and Type-2)
- to provide an analytical model for the evaluation and verification of the experimental test results
- to provide a model for estimating the drift ratio of AAC infill walls under combined IP and out-of-plane demands.

1.4 Organization of The Thesis

The thesis includes seven chapters. The content of the study, as submitted in the following chapters, is outlined:

In Chapter 2, the literature review of the studies of AAC infill walls with reinforced concrete frame behavior under the different direction of loadings is covered. It is divided into two parts: research including laboratory experimental tests and analytical models using computer technology.

In Chapter 3, the test setup is introduced with geometrical and material properties, procedure of construction of test sample, instrumentation, and application of different loading directions.

In Chapter 4, the experimental test results are presented and discussed. The monitored response parameters are shown through hysteretic curves, and pictures taken during the experiments are figured. The subdivisions of wall types are used for Type 1 and Type 2 systems and different loading conditions.

In Chapter 5, the computer validation of analytical models is done and compared with test results. Numerical simulation includes the modeling parameters, material, section, and element properties.

In Chapter 6, the overall study is summarized, and the conclusions and further recommendations are given.

CHAPTER 2

LITERATURE REVIEW

2.1 General

The studies on the performance of AAC infill walls in the literature survey are divided into categories studies, including experimental tests conducted in laboratories in Chapter 2.2 and the analytical studies on infilled frame systems in Chapter 2.3.

2.2 Studies of Experimental Tests

Tomazevic and Gams (2011) tested different geometrical properties, ¼ scaled AAC confined masonry buildings under one directional shaking table effect. Plan views of the buildings were the same; however, the number of stories differed to three or four. Furthermore, prefabricated slabs and in-situ reinforced concrete slabs were considered for the slab types. The first model, M1, had three stories of building with prefabricated slabs and exhibited seismic excitation from the shaking table along the symmetry axis of the building. In the M2 model, the seismic force is applied in the orthogonal direction of the three-story building with cast-in-place reinforced concrete slab. Finally, Model 3 was like the M2 model except for having four-story heights. In all cases, the typical diagonal shear failure mode of walls in the base level floor of the buildings was observed. It was essential to have the orthogonal walls contribute a box-type behavior of the models despite the failure mechanism being the shear failure of the walls in the excitation direction. Tie columns improved the walls' flexural capacity and provided the structure's integration at its ultimate state.

In addition, a nonlinear numerical model had been studied with concentrated story mass. Push-over method and hysteretic rules were used to calculate story resistances and behaviors. The numerical models were validated with the experimental results. The idealization of the story resistance curve calculations was done with a tri-linear envelope, which was determined by the resistance and displacements at the crack limit state, maximum force, and ultimate limit state. In conclusion, the structural behavior factor q was recommended as 2.5 for the AAC masonry buildings according to Eurocode 8.

Kurt et al. (2011) conducted pseudo-dynamic tests on a two-story, three-bay reinforced concrete frame with three different scales of ground motions on a frame with deficient reinforcement details with respect to seismic codes. The required confining steel reinforcement was calculated as 0.25% and 135-degree hooks according to the Turkish Earthquake Code (2007); the tested frame has transverse reinforcement with 90-degree hooks and a volumetric ratio of 0.16% at plastic hinge locations. Moreover, there was less reinforcement at the critical beam-column joint locations. The frame was tested under nonlinear time history analyses by scaling the acceleration time series of half capacity, total capacity, and 1.4 greater values of Duzce ground motion 1999. The results showed that the fundamental period of the frame changed with the level of ground motions, and the damping ratio of the frame showed oscillation between values of 2 and 15 %. In addition, the fundamental period change fits the method of secant stiffness calculations. Then, nonlinear time history analyses were performed in Opensees to show the dynamic response of the test frame. The properties of infill units were calculated according to Binici and Ozcebe's 2006 studies. Infill wall contribution was about 65% of the lateral strength capacity. A soft-story was formed upon failure at a drift ratio of 1.2%, with an inter-story drift level of 1.5%.

Sucuoglu et al. (2014) conducted pseudo-dynamic tests on two reinforced concrete bare frames with deficiencies of non-seismic construction on a scale of ½, 3x3 frame. The main difference between the two specimens was the insufficient lap splice at the bottom of the columns, whereas the other reinforcement details were continuous and

sufficient. Analytical models were prepared which predicted the response of global deformation using nonlinear frame models with dynamic analyses.

Okuyucu D. (2011) conducted 15 experimental tests on three aspect ratios of reinforced concrete infill frames with 1:3 scaled one-bay, two-story frames with a precast panel strengthening technique. The idea was to increase the seismic performance of the load-carrying capacity of the non-structural infill walls by applying easy precast panels. The equivalent diagonal strut concept influenced the simulation of the infills in the analysis models. Nonlinear push-over analysis was performed in Opensees and compared with experimental responses. The performance of the PC panel method by 3D shaking table tests was verified on the improvements in the load-carrying capacity of the infill walls.

Schwarz et al. (2015) tested the seismic resistance of reinforced concrete frames with AAC blocks for infill walls. Four parameters were investigated using nine half-scaled specimens under in-plane cyclic loading with low cycles. These parameters were panel aspect ratio, method of construction of the wall, presence of openings, and the applied vertical force. It was observed that the presence of the infill wall resulted in a twofold increase in the load-carrying capacity and a 60% reduction in ductility. Higher ductility was obtained in narrow panels. Integral walls have a higher capacity and less ductility when compared with the infill walls that were built after reinforced concrete frame casting. The openings caused a decrease in the load-carrying capacity of the wall of the whole infill wall. However, the maximum loads were more significant than the bare frame behavior. Moreover, the ductility of the wall with openings was between the level of the whole infill wall and the bare frame. Finally, the vertical load on the infill wall has a positive effect, with a 50% increase in the maximum load and approximately 120% in the dissipated energy level.

The strong frame-weak infill principle was suggested by Huang et al. (2016) to form a two-line system for seismic resistance. Reinforced concrete frames with two lightweight infill walls were tested under reversed cyclic loading on a single-story, single-bay, large-scale (1/2) test specimen. The lateral strength and stiffness for these

frames were studied using macro models. The aerated concrete blocks had 600 x 240 x 120 mm dimensions commonly used in Chinese commercial markets. The aspect ratio of 1.5 was considered with a 1.375 m story height and a corresponding span length of 2.250 m. There were no shear connectors between the infill panel and the surrounding frame. The compressive strength of aerated concrete blocks was 7.2 MPa, and the concrete had a 34.5 MPa of 28 days compressive strength.

Moreover, the special mortar for the AAC was 6.2 MPa. Weak-infilled frames were observed to meet the multi-line defense concept under seismic actions. The first defense was the infill wall, providing strength and stiffness under small deformations. When diagonal cracks were observed, the strength decreased rapidly. This type of frame was an example of the concept of strong frame-weak infill, where the infill did not influence the change in the failure mode of the frame. However, it affected the internal force distribution of the columns. The location of the contra flexure point moved upward when compared with the bare frame column, increasing the shear demands.

The energy contribution of the infill panel with AAC was 10% greater than the bare frame. "The equivalent damping ratio of the bare frame is greater than that of infilled frames at each cycle, showing the remarkable pinching effect of hysteretic loops of infilled frame specimens due to the large slip-along bed joints of infills."

Zockvic, Sigmund, and Guljas (2013) conducted experimental studies on reinforced concrete one-bay one-story frame specimens with a scale of 1:2.5 under constant vertical and in-plane cyclic lateral loads with different infill materials. Ten frames were tested with three different wall strength values: strength hollow clay brick blocks, medium-strength hollow clay brick blocks, and low-strength lightweight autoclaved aerated concrete blocks. The presence of the infill wall increased stiffness, damping, and initial strength when compared with the bare frame. The ductility of the system depended on the frame's span-to-height ratio, detailing of the frame in terms of confinement, stiffness, and strength ratios of infill versus

reinforced concrete frame. These were also effective in the failure mechanism of the system. The strong frame-weak infill was suggested as the best alternative.

AAC block infilled frame had different crack patterns than the masonry walls since the mortar glue was strong and AAC itself was the weak component. Cracks occurred in X-shaped after the interface of infill and reinforced concrete frame. When the hysteretic behavior of lateral displacement and load relationship was considered, AAC-type infill resulted in higher energy dissipation with smaller strength values. The stiffness degradation in AAC infilled frame was observed to be the smallest compared with other masonry types in terms of lateral stiffness. It appeared that stronger infill had more energy dissipation capacity. When the shear friction was reached at the interface between the masonry and concrete frame, the composite behavior was separated at that moment level. It was observed that at up to drift levels of 0.3%, infill contribution was reduced, and maximum load-carrying capacity was attained. Subsequently, the damage on the infill walls increased at 0.75% drift ratio, and no more infill contribution could be considered. The concrete frame remained intact until the 1% drift ratio without severe damage.

Siddiqui et al. (2013) conducted experimental research on pseudo-dynamic testing of reinforced concrete frames with AAC block infill walls. The study was related to the seismic performance of 3-bay three-story reinforced concrete frames with low-strength AAC block masonry and comparison with the bare frame to understand the presence of infill wall—the weak infill wall reduced deformation in the second and third stories. However, at the first story level, the influence of weak infill had a negative effect. The effect of AAC infills on inter-story drifts reduced as drift demands increased. It was observed that the residual drifts at all stories are reduced with the presence of an infill wall.

Under moderate ground motions, infills with low strength do not influence the seismic response of the frame. However, the significance of infills is observed by reducing the deformations in the upper stories when the earthquake's intensity increases. At the first story level, the damage is localized by increasing stresses. The

positive contribution of low-strength infills is obvious in reducing residual drifts of the frames.

Penna et al. (2015) conducted experiments on AAC masonry panels with flat-truss bed joint reinforcements located horizontally under in-plane cyclic loading tests. Two alternatives were possible for horizontal reinforcement inside the AAC masonry. The first was to locate the traditional bars inside the bed joints of special grooved blocks, whereas the other option was the flat reinforcement lodged within the thickness of the joint. This study applied and tested a truss-like reinforcement obtained by diagonal wires welded between two parallel galvanized steel plates as horizontal reinforcement. The main objective of these tests was to provide lateral confinement through the wall thickness by the diagonals, increase ductility capacity and in-plane deformations, and provide resistance to out-of-plane bending with the presence of horizontal reinforcement. In a past study, Priestly and Bridgeman (1974) showed that horizontal steels carry shear by tension. In contrast, vertical steel carries shear by dowel effect in diagonal cracks with an amount of three times less than the horizontal shear stress. Horizontal shear capacity was from

$$V_H = 0.785 * n * d^2 * f_y \tag{2.1}$$

$$V_V = 0.24 * n * d^2 * f_y \tag{2.2}$$

Where n is the number of bars, d diameter crossing the shear crack, and f_y is the yield stress.

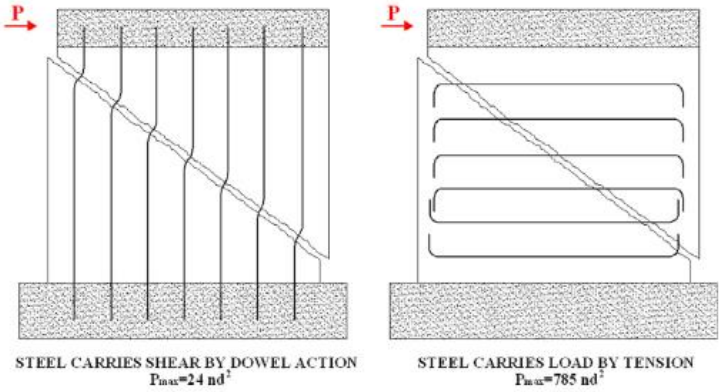

Figure 2.1. Relative effectiveness of vertical and horizontal shear stress (Priestly & Bridgeman, 1974)

The reinforcement effectively prevented the failure of outer portions of the hourglass cracking pattern, changing the damage pattern. The initial stiffness of models with and without horizontal reinforcements was similar under in-plane loading. However, an increase in maximum shear strength of approximately 20 % was observed with the addition of flat-truss bed-joint reinforcement. Moreover, maximum displacement versus drift capacity was increased by 75%.

Rosti et al. (2016) studied in-plane cyclic tests of unreinforced masonry with AAC blocks with six full-scale tests. The dimensions of AAC blocks were 500x250x300 mm. The dimensions of the walls were 1000x1250x300 mm constructed in the laboratory, and compressive force was applied using a force-controlled hydraulic device. Vertical compression tests, diagonal compression tests, and cyclic shear-compression tests were conducted. Then, experimental results were compared with derived analytical strengths. It was observed that the level of applied vertical load on the wall affects the displacement of piers under in-plane loading. Residual vertical strengths of walls were also investigated.

The lateral strength of the wall under in-plane loading, which fails in bending, was formulated below:

$$V_{u,f} = \frac{P * l}{2\ h_o} * (1 - 1.15 * \frac{P}{f_m * l * t})$$ (2.3)

Where P is the axial load, l and t are dimensions of wall length and thickness, respectively, and h_o is the distance between the contra flexure point of flexural capacity and the section.

The formulation of Turnsek and Sheppard (1980) was given for the maximum lateral resistance due to the diagonal cracking mechanism as follows:

$$V_u = \frac{f_t * l * t}{b} \sqrt{1 + \frac{P}{f_t * l * t}}$$ (2.4)

In which f_t is the tensile strength of masonry, b is the shear stress distribution factors ranging between 1-1.5. The shear strength of masonry is formulated according to this study is related to the applied vertical compression force:

$$f_{vlt} = 0.45 * f_{bt} * \sqrt{1 + \frac{P}{f_{bt} * l * t}}$$ (2.5)

Where f_{bt} is characterized as 0.475 MPa in the tests.

Kaluza (2017) studied the behavior of AAC block infills under in-plane loading while conducting laboratory tests. The aim was to develop the shear parameters of AAC walls by using different GRFP external strengthening methods. The performance of AAC blocks with thin bed joints and unfilled head joints strengthened with GFRP was compared with bare AAC block walls. The use of thin bed joints and unfilled head joints is required by the technology for erecting walls constructed of AAC blocks, which has an adverse effect on the deformability of such erecting parts.

Liu et al. (2020) conducted six experiments on AAC self-insulation block masonry walls under pseudo-static tests. Three different situations were considered as two of the tests are self-insulation mortar joints, two with thin-layer mortar joints, and the last two have vertical mineral wool plate joints accompanying horizontal thin-layer mortar joints. The tests' failure mode, maximum load-carrying capacities, stiffnesses, drift ratios, and dissipated energy capacities were investigated and compared. The in-plane loading was applied with two cycles for the load levels of two or three times the cracking grade until the damage. A typical crack pattern with diagonal inclined cracks was observed on the AAC self-insulation blocks, whereas on walls with vertical joints filled with mineral wool plates, more vertical cracks took place. The best seismic performance was observed in the walls with thin-layer mortar joints. A reduction in the stiffness and energy dissipation appeared due to the weakness of the integrality of walls by the vertical joints filled with mineral wool plates. In addition, the amount of vertical compressive stress on the wall increased the stiffness of the wall, with a decrease in the total dissipated energy.

Artino et al. (2019) studied the retrofit strategy of reinforced concrete framed buildings by replacing the external layer of old-type infill walls and placement of AAC blocks with high-performing ones—the macro-element modeling approach in which the contribution of masonry infill walls was considered. At the damage limit state, the most significant improvement was obtained by involving the proposed retrofitting. Regarding energy consideration, 4-10 % improvements were obtained for heating and cooling by replacing the outer layer of hollow bricks with AAC blocks. This was also stated to minimize the disruptions during renovation and an economic and temporal solution. It provided stiffness and resistance increases; higher base shear values were obtained due to the lower fundamental periods of the system. An apartment block in Catania was selected as the case study, constructed between the 1950s and 1980s. It was a 4-stories building with two houses per story in a rectangular shape with dimensions of 18.1 m to 11.8 m.

The seismic performance of reinforced concrete frames with infill walls composed of autoclaved aerated concrete blocks was studied by Binici et al. (2019) with a test

setup of a half scaled story bay of a 5-stories prototype structure at the Laboratory of Structural Mechanics department of Middle East Technical University. The study provided eight experiments, including AAC blocks infill and one bare frame exposed to in-plane loading as a reference test. The main idea of that was the effect of out-of-plane loading on the reduction of the lateral deformation capacity of the AAC infill wall. As a result, the aim was to develop an innovative system by supporting the induced forces in the in-plane direction while protecting the out-of-plane direction.

Demirel I.O. (2023) studied the seismic performance of reinforced concrete frames with different infill types and proposed retrofit techniques to develop resistance to seismic forces. He conducted 22 frame tests in the laboratory under different loading conditions: in-plane, out-of-plane loading, and combined effects of two different directions of loadings. Damages of the frame, modes of failures, strength and stiffness properties, and hysteretic response of the frames were investigated throughout the test results. In addition, the performance of the infill wall was assessed and compared with previous studies and seismic code limitations.

2.3 Studies of Analytical Models

Researchers have studied modeling the performance of infilled frames with different approaches. Micro and macro models are available in the literature.

In studies of Fiora et al. (2012), macro models provide the simulation of infill-frames in global and local analyses by setting two non-parallel struts. Finite element analyses were performed by using plate elements to model the frame and infills. Applied loads were considered the combination of in-plane and out-of-plane stiffness so that local effects on the contact region of the frame and infill could be included—a one-dimensional truss element with only compression property provided for the interface contact between infill and concrete frame.

The first reference models were two one-bay, two-story models with a soft story at the bottom. 1:1 and 2:1 aspect ratio of the infills were considered. Moreover, various Coefficient of friction (0-0.4) values were used for the interface of contact forces. These affected mainly the interface's local response, not the infilled frame's global behavior. Six different methods for analyzing the behavior of the infilled frame were studied. The frame was modeled through plate elements in the first three models, whereas infills were modeled with inclined trusses, two struts, and single struts, respectively. Then, the following three models with beam elements were used for the reinforced concrete frames with corresponding infill mechanisms as listed. According to the results, the evaluation of reinforced concrete infilled systems under vertical and horizontal loads, the two-strut mode highlights the local effects. In addition, it was a bare structure model with a reduced period that was able to reproduce the global behavior.

Ferratti (2015) studied experiments of mechanical characterization of AAC masonry blocks and the prepared macroscopic anisotropic constitutive models. The tests have been performed under uniaxial compression tests of AAC panels with force-controlled and displacement-controlled tests, diagonal compression tests, biaxial compression tests, and three-point bending tests on masonry panels. The macro model involves the push-over test of a full-scale AAC masonry wall. The following results are obtained. AAC masonry has a weak anisotropy due to the realization of thin joints adopted by cementitious glue. The proposed model for traditional masonry is also valid for AAC masonry modeling.

Milanesi et al. (2018) studied a one-bay, one-story full-scale specimen of a reinforced concrete frame with AAC masonry infill simulation using finite element methods under in-plane loading with pseudo-static cyclic loads. The analyses were compared with bare frame structure for moment and shear demand changes on the local effects. The reference test samples of experimental results were chosen from Calvi and Bolognini (1999) and Penna and Calvi (2006) studies. The AAC masonry infill experimental tests by Penna and Calvi (2006) were considered only in-plane loading up to a drift of 1.2 %.

Meso-modeling was carried out as the approach of analysis. The study's main aim is to estimate the extra shear and contact length activated by the AAC masonry infill on the reinforced concrete frame and determine the local effects on the system.

At the ultimate limit state (ULS) condition of design codes, the out-of-plane seismic force acting on the infill can be determined by applying force at the mass center of the infill and considering inter-story drift limitations to avoid failure of the non-structural components. In Eurocode 8, the critical length for the contact length is suggested as the ground level's column total height or full contact length with infill on one side for the investigation of local effects.

In meso-modeling, the masonry was considered as a homogeneous material. The reinforced concrete frame was modeled according to Vecchio and Collins's original smeared crack criterion (1986). Both RC frame and AAC block infill were modeled with plane stress elements with eight-node quadrilateral iso-parametric properties. There were 4 Gauss integration points per element. The interface elements between frame and AAC were modeled with six-node interface elements. The fixed boundary condition at the base of the frame was assumed. Analysis results showed that with the increasing levels of drifts, the behavior of infilled frames differs from the bare frame.

Asteris et al. (2017) prepared computational models that predict infilled reinforced concrete frames' combined in-plane and out-of-plane response. The observations of earthquakes show the development of an arching mechanism on the infill when the out-of-plane load is considered.

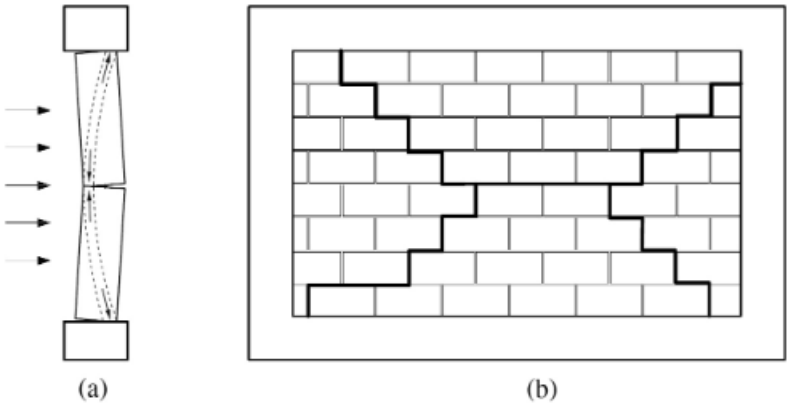

Figure 2.2. Out-of-plane mechanism a) Arching effect b) Crack pattern under OOP

The out-of-plane capacity was generally measured as flexural action-based models in the literature. The first theory of Timoshenko considered linearly elastic, isotropic material; the maximum lateral pressure is calculated as

$$q_u = \frac{f_t}{6\beta_1(^h/_t)^2} \tag{2.6}$$

Where $_{it}$ is tensile strength, β_1 is a coefficient depending on the panel's aspect ratio.

Angel (1994) and Abrams et al. (1996) conducted the most comprehensive experimental studies of combined in-plane and out-of-plane loading effects on infill walls. Then, the wall was repaired with cement plaster, and steel bolts embedded in wire mesh were applied to investigate the reinforcement effect on retested samples. The crack pattern of the wall was observed as the yield line pattern of two-way slabs. The infill restrained by the frame behaves as a plate; therefore, the two-way arching action occurs. The compressive strength of masonry had an essential role in the arching mechanism of the wall. The out-of-plane strength of the wall was reduced with the level of in-plane loading during the cycles. However, the repaired panels with reinforcement increased the capacity of the wall at the ultimate, whereas the final strength did not depend on the accumulation of the damage.

The main parameters affecting the capacity of the wall are the compressive strength of masonry and the aspect ratio of h/t. As the h/t ratio increases, the ultimate load of the out-of-plane direction decreases rapidly. The formula of strength capacity is given in FEMA 273 as

$$q_u = \frac{0.7 f_m \lambda_2}{(h/t)} \tag{2.7}$$

Where λ_2 is a constant depending on h/t ratio as shown in Figure 2.3.

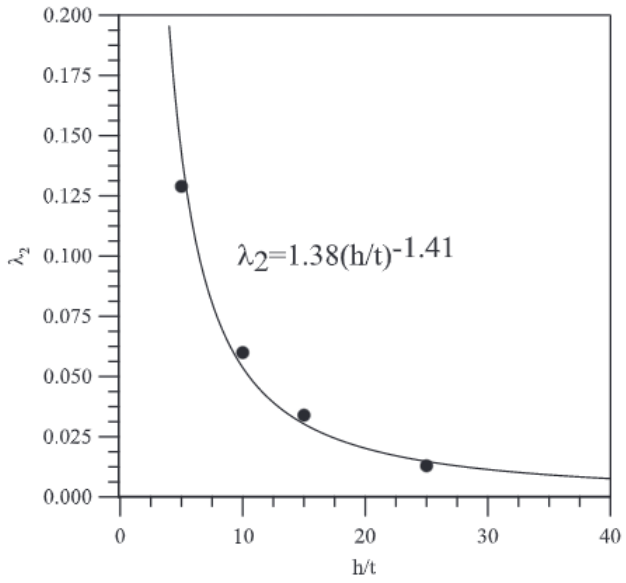

Figure 2.3. λ_2–(h/t) points and possible best fitting curve (FEMA-356)

In recent studies of integrated macro models, Hashemi and Mosalam (2006) proposed a three-dimensional strut and tie model. The midspan joint of each strut is shifted in the out-of-plane direction to provide the arching mechanism, as shown in Figure 2.4.

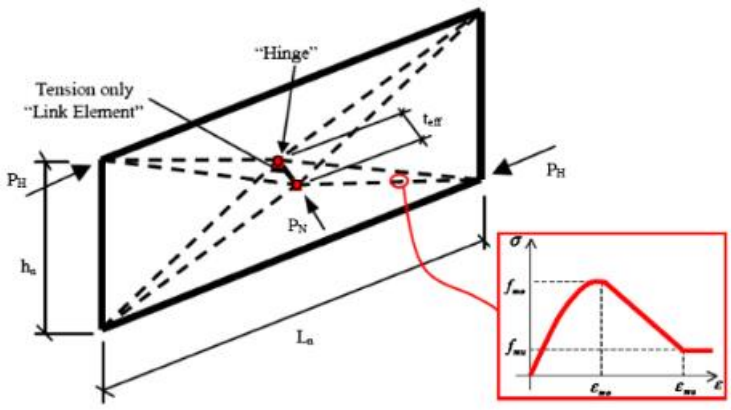

Figure 2.4. Strut and Tie macro model scheme by Hashemi and Mosalam (2006)

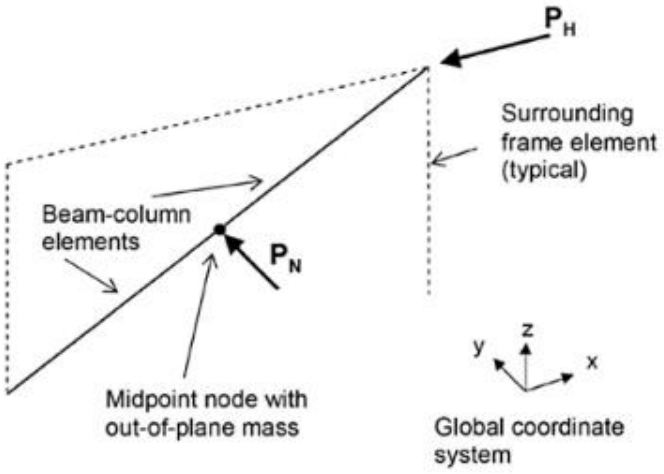

Figure 2.5. Model scheme of Kadysiewski and Mosalam (2009)

$$\left(\frac{P_N}{P_{N0}}\right)^{\frac{3}{2}} + \left(\frac{P_H}{P_{H0}}\right)^{\frac{3}{2}} \leq 1.0 \qquad (2.8)$$

In the single strut model reacting both in compression and tension of Kadyiewski and Mosalam's (2009) study, the strut is identified to reproduce the in-plane behavior of strength and stiffness with the same response frequencies in the out-of-plane

direction. The combined effect of wall behavior under the effect of in-plane and out-of-plane direction is calculated in equation (2.8). In the formula, N stands for in-plane loading, and H for the out-of-plane force. The abbreviation 0 is used in $P_{N0}\ and\ P_{H0}$ to identify the forces' absence in the in-plane or OOP direction, respectively. Reliable results of arching action can be obtained by analyzing complex three-dimensional models with proper calibrations.

Panto et al. (2018) studied the numerical simulation of a hybrid method for the out-of-plane behavior of infill walls with brick masonry-reinforced concrete frames using macro-modeling. Beam-column elements with concentrated plasticity were used for the surrounding frame, whereas a three-dimensional discrete macro-element was chosen to perform the nonlinear masonry behavior. Two types of brick masonry infill walls were modeled and compared with experimental results. The first type of brick wall consists of a 100 mm thickness of single-leaf masonry Wall laid in a vertical direction, creating interlocking joints continuously with vertical steel bars. In the second system, truss elements were in the single-leaf clay masonry wall bed joints as horizontal reinforcement.

One of the aims of the study was to investigate the effective material and geometric parameters on the performance of the brick infill wall under out-of-plane loading and predict the failure mechanism. It was observed that the aspect ratio of length to height of the infill wall is an important parameter affecting the behavior of the infill wall under out-of-plane loading. The two-way bending mechanism changed to a one-way mechanism as the increase in aspect ratio leads to a decrease in resistance to out-of-plane loading. The uniformly distributed load on the top RC beam has a negative impact on the out-of-plane performance of brick infills. In general, since brick infills are regarded as non-structural, no additional vertical stresses are supposed to be placed on them. However, if additional loads are induced in the brick infills because of construction flaws or long-term behavior, these can increase the structure's seismic sensitivity.

Some of the research on the performance of autoclaved aerated concrete walls includes AAC panels infills inside steel frames (Liu et al., 2004). Zhenggang et al. (2017) studied two prefabricated steel frames with a two-story, single-bay frame in a half-scale experiment under in-plane cyclic reversed loads. Then, analytical models were prepared. Similar to results in reinforced concrete frames, the presence of AAC infill results in maximum load-carrying capacity in steel frames when compared with steel bare frames. In addition, initial stiffness is greater, and ultimate drift ratios of the frame and dissipated energy are larger in AAC panel frames. The mechanical properties of the AAC panel, such as the width and thickness of the panel, are affected by the behavior of the wall.

According to the literature research, it was observed that the performance of infilled wall types with AAC block infilled walls and the modeling techniques of diagonal strut modeling as the idealization of the infill wall. Literature has yet to find studies of infilled walls with insulated materials. Therefore, it aimed to provide a study on the performance of infilled wall types, including insulated elements under different loadings with two different arrangements of wall types. Experimental studies conducted in the Structural Laboratory of Middle East Technical University and computer models for the test results are presented in the following chapters.

CHAPTER 3

EXPERIMENTAL PROGRAM- TEST SET-UP

3.1 General

In the experimental part of the current study, a similar portal frame was constructed in the Structural Mechanics Laboratory of Middle East Technical University (Binici, 2019; Todorovic, 2019; Demirel, 2023), and the AAC infill wall with cementitious insulation material was investigated. Two different types of systems for insulation material-AAC blocks were prepared. The main objectives were to study the performance of insulated AAC infill walls under different loading conditions and to observe the change in the in-plane drift capacity when the combined loading was current. The selection of the specimen is described in Section 3.2. Section 3.3 explains the details of reinforced concrete frames regarding concrete, reinforcement material properties, and construction techniques. In Section 3.4, instrumentation is presented. Lastly, the properties of frame tests in terms of material characteristics and key considerations determined for the analysis and comparison of test results are found in Section 3.5.

3.2 Specimen

The concrete specimen was chosen from a first-level frame of a 5-story 5x4 bay building model designed according to the Turkish Earthquake Code (2007). The selected frame had a 5 m span length and 3 m height designed with 400 mm square columns and 300 x 400 mm beam dimensions. It was in the first seismic zone with a corresponding PGA of 0.4 g. It was designed according to high ductility level where the response reduction factor, R, was taken as 8. The compressive strength of reinforced concrete was 25 MPa at the 28-day level, whereas the reinforcements had

a yield strength of 420 MPa, with grade S420. The combination of G+0.3Q was considered with an average axial load of 0.175 ratios to decide on the seismic weight of the structure.

3.3 Frame Details

The half-scale of the inner frame is selected as the specimen and constructed in the laboratory. The portal frame has dimensions of 2700 mm x 1500 mm in horizontal and vertical directions, respectively, having a clearance of 2300 mm x 1300 mm for the infill wall. Columns of the frames were square with 200 mm dimension and had eight longitudinal bars with 8 mm diameter deformed bars with 424 MPa yield strength. The lateral reinforcement was stirrups with 6 mm diameter plain bars having 448 MPA yield strength. The ultimate strengths of 8 mm and 6 mm bars were 567 and 504 MPa, respectively. The spacing of the stirrups was 50 mm at the confined region of 300 mm distance away from the end of the column. The spacing was 100 mm for the rest of the column region. A flanged beam was constructed to simulate the slab's contribution and allow placing steel blocks to simulate gravity loads from the slabs. A distributed load of 10.25 kN/m was applied to the structure. The transverse reinforcement spacing in the confined and middle regions of the beam was 50 mm and 100 mm, respectively. The reinforcement ratio of columns and beams was 1 %, whereas the tensile beam reinforcement was calculated as 0.56 %. The stirrup ends were hooked at 135° according to the reinforcement detailing rules in the Turkish Earthquake Code. The cross-sections of column and beam are shown in Figure 3.1.

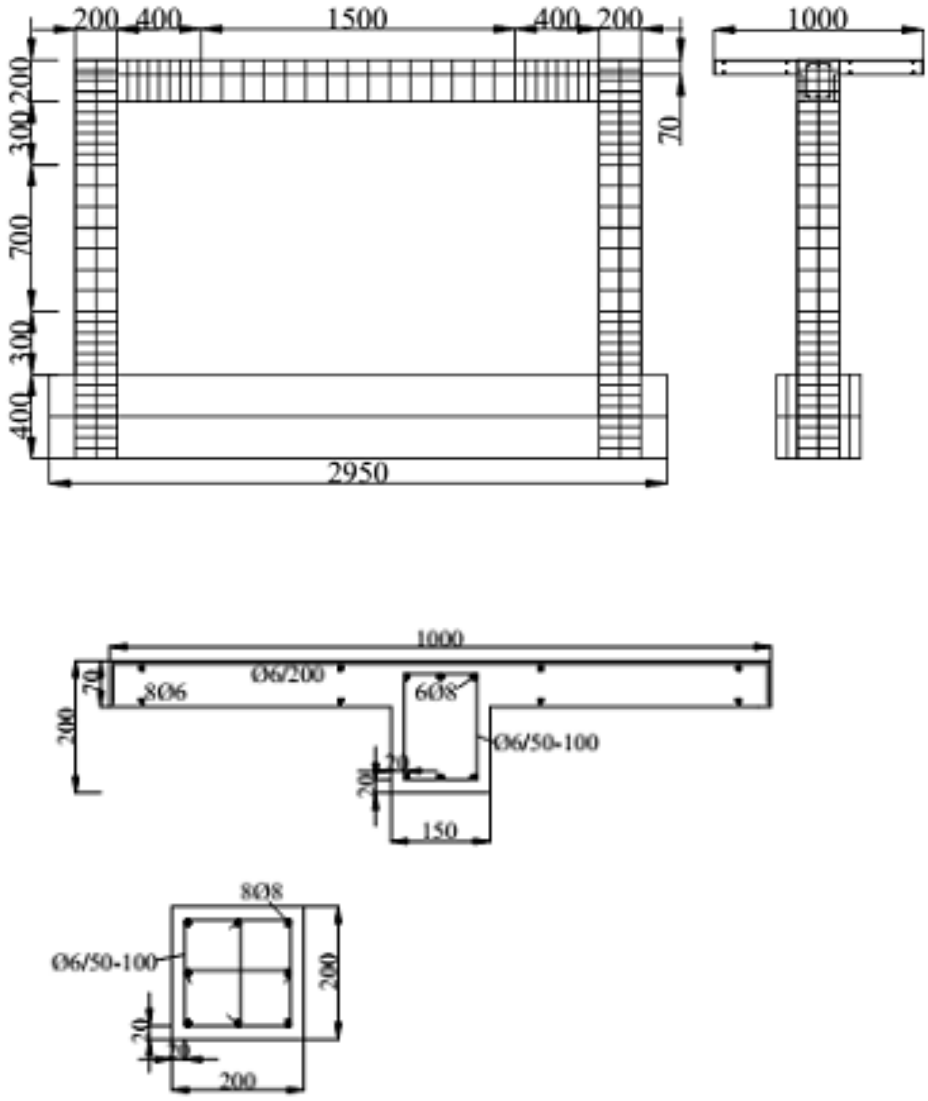

Figure 3.1. Portal frame system dimensions and reinforcement detail

The moment-curvature analysis of column and beam sections was calculated. The axial compressive load of the column was found to be 193 kN under 0.175 ratio. The ultimate moment capacity of the column was calculated as 28.2 kNm.

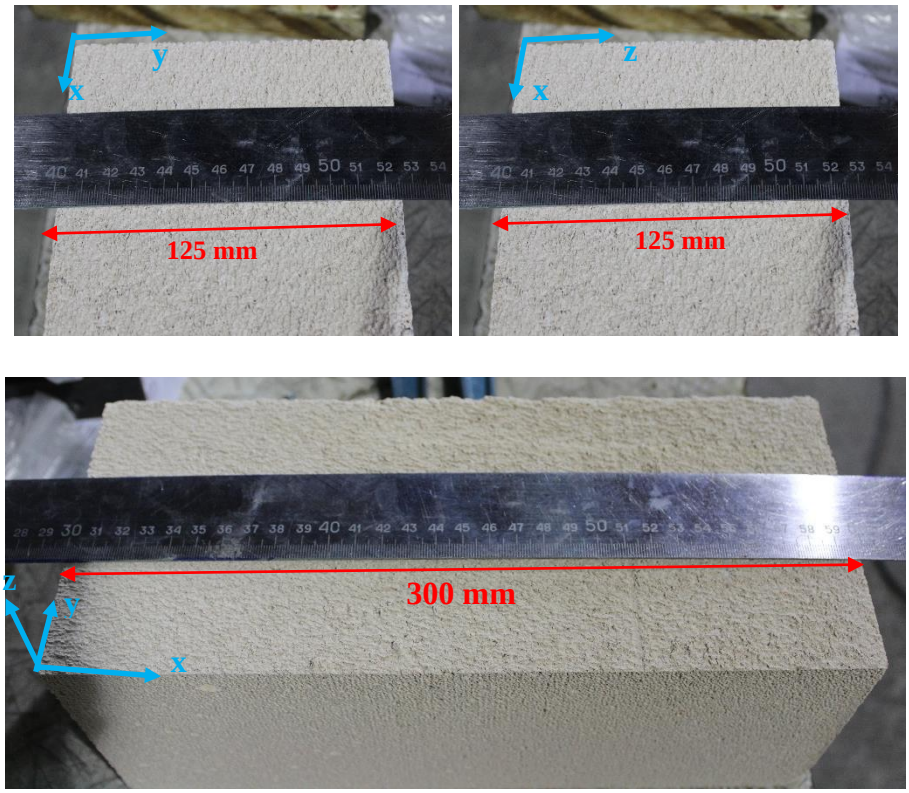

Figure 3.2. Dimensions of AAC block (300x125x125 mm)

The infill wall material is AAC blocks with dimensions of 300x125x125 mm (Figure 3.2) with a compressive strength of 2.45 MPa with a modulus of elasticity of 1520 MPa according to the Masonry Standards Joint Committee (MSJC, 2011) study. The dry density is 350 kg/m3, as specified by AKG-Gazbeton. The material tests of AAC blocks are conducted according to ASTM C1692-11 and ASTM C1693-11.

The construction of the Type-1 infill wall started with applying leveling mortar with a 10 cm width. Then, AAC blocks were placed with 30 mm eccentrically from the column face. In the second layer, the blocks are staggered to obtain a resistant wall like a typical brick wall. The thickness of AAC mortar is 2 mm between the layers of blocks. The procedure of preparation of the wall is shown in Figure 3.3.

The CLIPs were applied on the concrete frame surfaces using CLIP adhesive mortar, as shown in Figure 3.4. The performance of exterior insulation material multipor was performed in recent studies (Carrigan et al., 2018) on a test building.

A special liner was painted on the wall's surface before applying the plaster. Two layers of plaster were placed in between the fiber-reinforced mesh, Styrol Butadiene Copolymer (SBC), which had a weight, grid size, width, and thickness of 160 gr/m2, 5 mm, 1.2 mm, and 0.5 mm, respectively.

Figure 3.3. Procedures of preparing the Type 1 wall

Figure 3.4. Application of CLIP on the surface of the frame

The samples of the bags of AAC block mortar, CLIP adhesive, and plaster are shown in Figure 3.5 to clarify the materials' properties. While preparing the mortars, three cubic samples were taken with dimensions of 50x50x50 mm according to ASTM C109 for the determination of the uniaxial compressive strength of the cubic specimens. Moreover, following ASTM C348-18, three samples of rectangular prisms with dimensions of 40x40x160 mm were prepared for the flexural strength determination (Figure 3.6). At the end of flexural strength testing, the halves of the samples were also tested under uniaxial compressive strength. The material properties of each test are listed in Chapter 3.6.1.

Figure 3.5. AAC block mortar, CLIP adhesive and Plaster

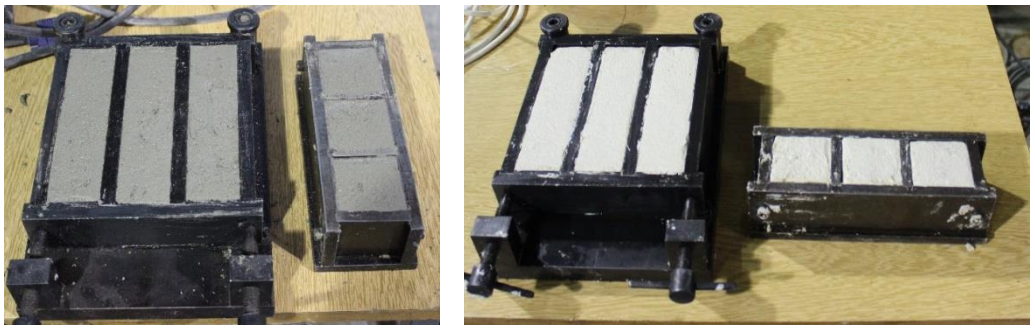

Figure 3.6. Test samples for determination of flexural strength (40x40x160 mm) and uniaxial compressive strength (50x50x50mm)

3.4 Instrumentation

The test setup comprises a strong floor, reinforced concrete frame, hydraulic actuator, steel plates, and hydraulic jacks, as shown in Figure 3.7. A hydraulic actuator is a displacement-controlled tool used to apply the lateral loads on the frame for in-plane loading tests. Two-cylinder hydraulic jacks at the top of the columns are pin-connected to the force-controlled rigid exterior frame. Concentrated axial force is applied with an axial load ratio of 0.175 on the columns to simulate the axial forces coming from the upper stories. Moreover, the vertical loads applied on the slabs using steel blocks provide a 10.25 kN/m distributed load.

Load cells monitor the applied forces in each direction, lateral or axial—the corresponding story displacements are measured with Linear Variable Differential Transformers (LVDTs). The locations of the LVDTs are at the plastic hinge lengths of the columns, 180 mm away from the column and beam ends.

The application of out-of-plane loading on the infill wall is satisfied with an airbag on a stiffened wooden plank (Figure 3.9). A hydraulic cylinder was used to approach the airbag to the wall's surface. An air pump provides the load-controlled application of out-of-plane loading on the wall by pushing the airbag. There is a Teflon sheet with a thickness of 2mm located between the airbag and the infill wall to minimize the friction forces with a coefficient of friction equal to 0.1.

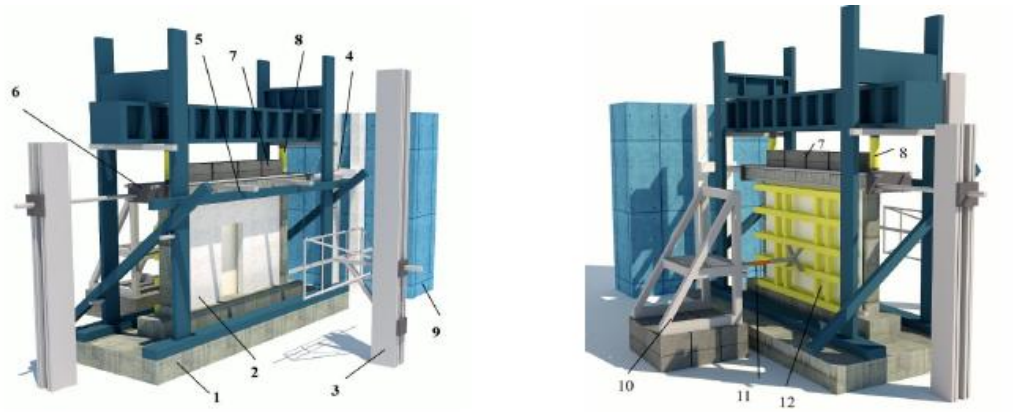

Figure 3.7. Instrumentation (Todorovic, 2019)

Figure 3.8. In-plane loading instrumentation

Figure 3.9. Out-of-plane loading instrumentation

3.5 Test Procedure

The aim of this study is to investigate the two different arrangements of cementitious insulation panels on the AAC infills under different loading conditions. These are in-plane loading, pure out-of-plane loading, and the considerations of simultaneously in-plane loading and out-of-plane loading. The level of out-of-plane loading is also studied.

3.5.1 In-plane loading

The in-plane loading is applied in a displacement-controlled manner. Cyclic displacement history is introduced, and two cycles are repeated for each drift ratio level. Inter-story drift ratios are obtained by dividing the lateral top displacement by the height of the story. First, it started with a 0.35% drift ratio, continued with 0.5%, and then increased by 0.5%, corresponding to 1%, 1.5%, and 2%.

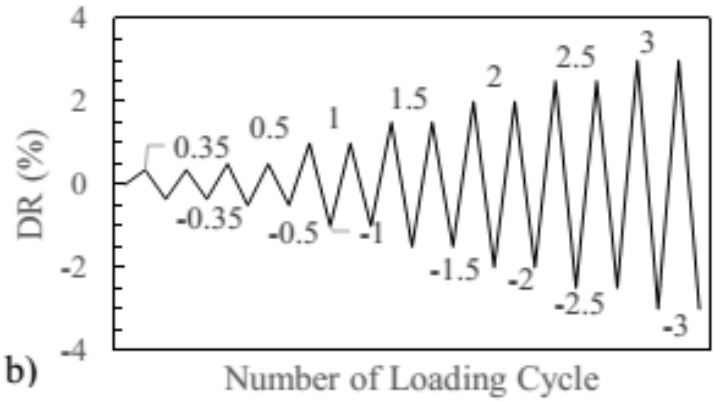

Figure 3.10. In-plane loading protocol

3.5.2 Out of plane loading

In the case of only out-of-plane loading application, the hydraulic cylinder continued to press the airbag to increase the force control till the collapse of the infill wall. The locations of displacement records of the test of pure out-of-plane loading are shown in Figure 3.11. 13 LVDTs are located. The load-carrying capacity of the wall under the effect of only out-of-plane direction is obtained.

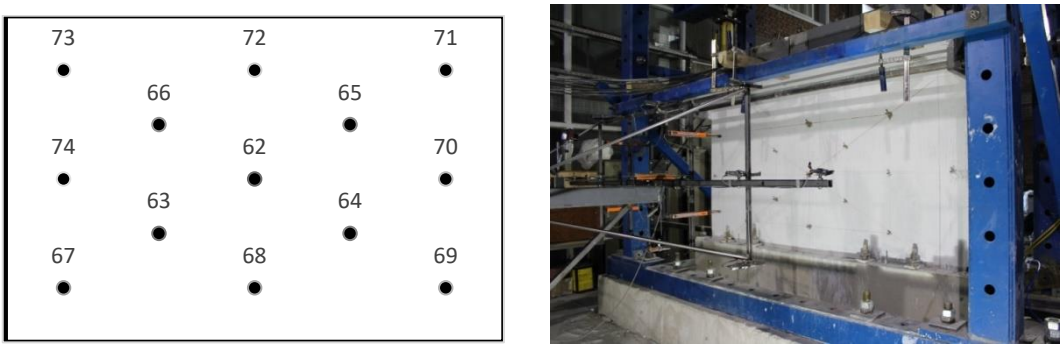

Figure 3.11. Locations of LVDTs of OOP test

3.5.3 Combined out-of-plane loading and in-plane Loading

When both the effects of out-of-plane loading and in-plane loading are considered, firstly, the out-of-plane loading is applied up to a determined capacity level and kept constant. Then, the in-plane loading starts. The levels of 1/3 and 1/6 of out-of-plane capacity are considered in the tests.

3.6 Frame Tests

Eight specimens with two different infill wall details were investigated under in-plane, out-of-plane, or combined in-plane and out-of-plane loadings. The first type of infill wall system (Type 1) had the infill walls eccentrically placed from the frame's front face such that a flush surface could be obtained upon bonding CLIPs on the reinforced concrete beams and columns. In this way, the insulation of the frame with AAC infill wall and CLIPs over the reinforced concrete members was simulated. There is no plaster on the surface of the infill wall in the S1 and S2 test specimens to investigate the effect of the plaster on the in-plane loading by comparing the results with the presence of plaster as in the case of the S3 specimen.

In the second type of infill wall system (Type 2), the AAC infill wall was constructed flush to the beams and columns' faces, and CLIPs were bonded on both the AAC infill wall and reinforced concrete member surfaces to provide additional insulation. This situation simulates the installation of full insulation of the building façade, resulting in a less economical solution than Type 1. In the following table, the labels of the tests with corresponding loading types are listed for both systems, Type 1 and Type 2.

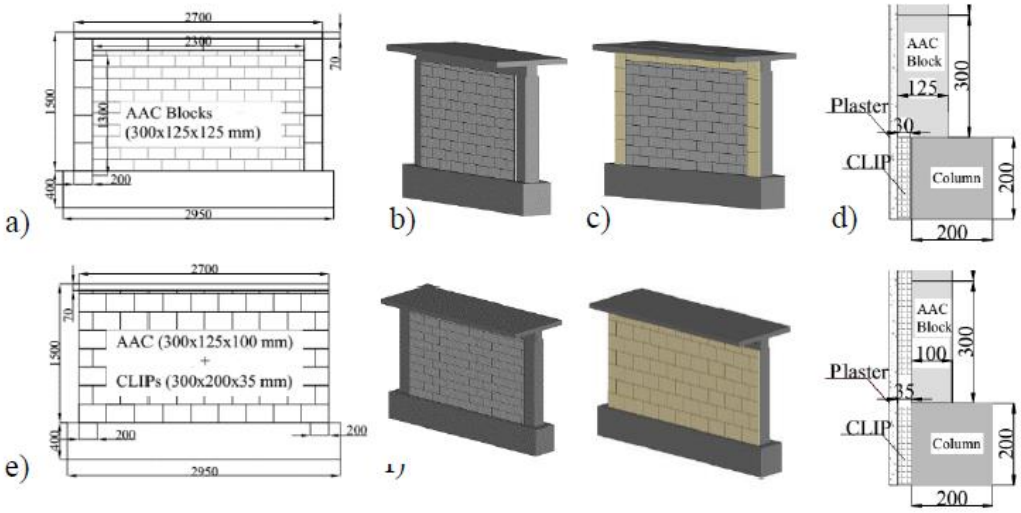

Figure 3.12. System dimensioning and 3D view for Type 1 a) to d) and for Type 2 e) to h):

a) Type 1 dimensioning, b) 35 mm of protrusion of AAC block from the frame, c) insertion of CLIPs, d) top view of Type 1, e) Type 2 dimensioning, f) 100 mm AAC block adjacent to frame, g) Full CLIPs application, h) top view of Type 2

Table 3.1. Specimen Properties

System	Specimen	Plaster	Loading	Age of Wall at Test Day
Type 1	**S1**	No	IP	2 days
	S2	No	IP	15 days
	S3	Yes	IP	15 days
	S4	Yes	OOP	26 days
	S5	Yes	OOP 1/3 +IP	10 days
	S6	Yes	OOP 1/6 +IP	8 days
Type 2	**S7**	Yes	OOP	9 days
	S8	Yes	OOP 1/3 +IP	15 days
Abbreviations	IP: in-plane, OOP: out-of-plane, OOP 1/3+ IP: combined 1/3 capacity of out-of-plane and in-plane loading, OOP 1/6+ IP: combined 1/6 capacity of out-of-plane and in-plane loading			

3.6.1 Material Properties

In the tests, the compressive strength of the reinforced concrete is calculated as 28 MPa for the Type 1 frame and 22.2 MPa for the Type 2 frame. The AAC blocks have a compressive strength of 2.45 MPA, and CLIP plates have 0.42 MPa compressive strength; both were manufactured from AKG-Gazbeton.

The summary table of compressive strengths of each test with mean values of compressive strengths obtained from the test specimen according to ASTM standards is shown in Table 3.2. The detail of each calculation is given in Appendix 1. The wall specimen's age at the day of experiment is listed in Table 3.1. The early age of 2 days of S1 resulted in small compressive strengths of AAC mortar and CLIP adhesive than the others.

Table 3.2. Material Strengths

System	**Specimen**	**Compressive Strength (MPa)**					
		Concrete	AAC block	AAC mortar	CLIP	CLIP Adhesive	Plaster Overlay
Type 1	**S1**	28	2.45	1.13	0.42	4.07	-
	S2	28	2.45	7.4	0.42	9.6	-
	S3	28	2.45	16.53	0.42	9	7.6
	S4	28	2.45	8.33	0.42	13.87	15.23
	S5	28	2.45	10.23	0.42	10.6	19.1
	S6	28	2.45	7.3	0.42	7.03	14.03
Type 2	**S7**	22.2	2.45	6.8	0.42	7.6	18.8
	S8	22.2	2.45	8.3	0.42	9.7	16.5

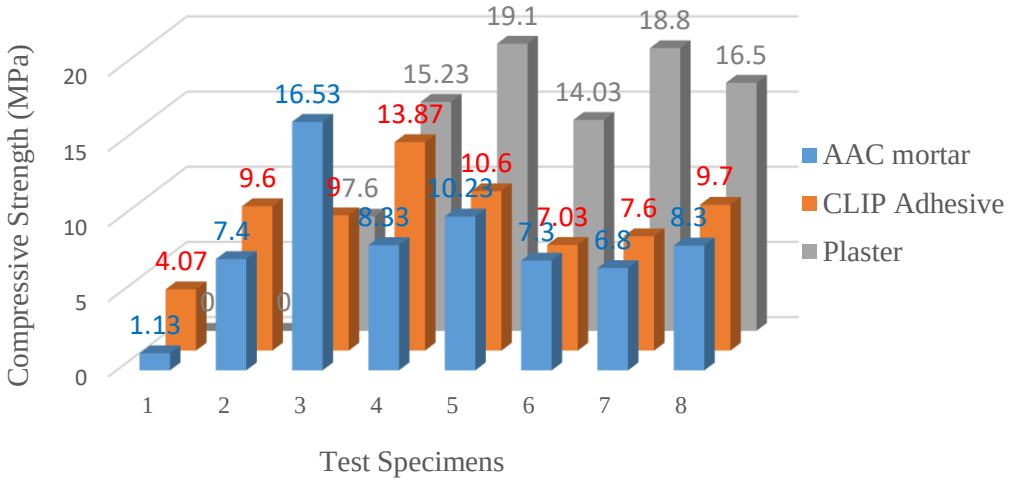

Figure 3.13. Compressive strengths of mortar types (MPa)

3.6.2 Key Considerations

In this part, the evaluation properties of the test results are described in terms of strength, stiffness, ductility, and dissipated energy.

3.6.2.1 Maximum Load Carrying Capacity

In each test, the first parameter considered is the maximum load-carrying capacity. The loading type, age of mortars and plaster, and type of wall system directly affect the maximum load capacity of the wall.

3.6.2.2 Stiffness

The initial stiffness is assumed to be the secant stiffness, calculated by the slope of the line, corresponding to 0.7 times the ultimate load.

When in-plane loading is applied in cyclic loading, the damage occurs in the inelastic range, reducing the system's stiffness.

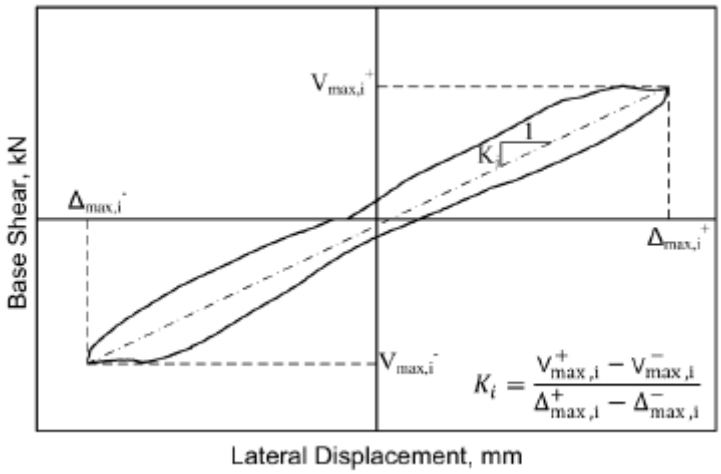

Figure 3.14. Stiffness calculation in cyclic load (Akin, 2011)

Yield displacement is defined as the displacement of a hypothetical yield point of an equivalent linearly elastic-perfectly plastic system whose initial elastic stiffness and yield strength are respectively equal to the secant stiffness at 0.7 times the maximum load and maximum load.

Ultimate displacement is obtained as the displacement corresponding to the load level of 0.85 times the maximum load-carrying capacity.

The drift ratio is calculated by dividing the top displacement of the frame by the height of that story. Therefore, the yield drift ratio is obtained by yield displacement divided by the story height and, similarly, the ultimate drift ratio with ultimate displacement.

3.6.2.3 Ductility

Ductility is determined as the ratio of ultimate displacement to the yield displacement. The definition of ductility is the degree to which a material can sustain plastic deformation under tensile stress before failure. Using idealized bi-linear curves of the forward cycle of the base shear-displacement graph, equal area concepts of study by Dimova and Negro (2005), the ductility is calculated.

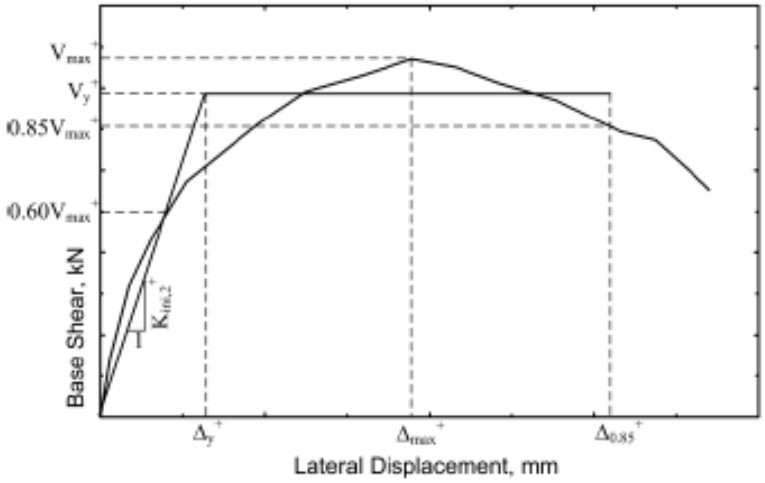

Figure 3.15. Idealized bi-linear curve for equal area concept.

3.6.2.4 Energy Dissipation

The dissipated energy of the frame under the hysteretic loop is calculated by the enclosed area under the base shear versus lateral displacement curve. The amount of dissipated energy of inelastic actions under dynamic excitations is determined. The relationship between the drift ratio and the amount of dissipated energy is presented in the further chapters (Figure 4.9 b).

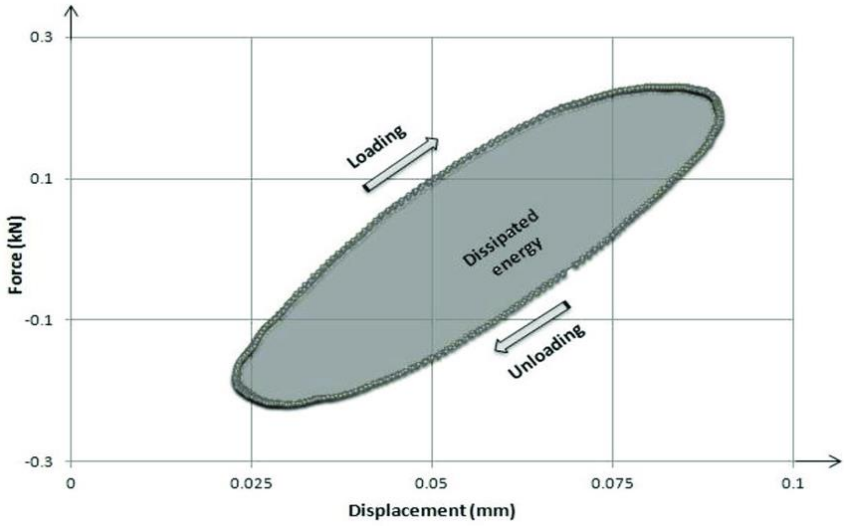

Figure 3.16. Dissipated energy of the frame

CHAPTER 4

EXPERIMENTAL RESULTS AND DISCUSSIONS

4.1 General

This chapter presents the results of infill wall-reinforced concrete frame tests for Type 1 and Type 2. Moreover, the responses of specimens are presented in the form of base-shear versus top displacement for the in-plane loading. The graphs present the relation between the out-of-plane load level and displacement in the out-of-plane loading case. Crack patterns are investigated during load application and shown in photos of the test specimen and sketch drawings for the system's failure.

4.1 Type 1 Wall Experiments

4.1.1 IP Loading (S1, S2, S3 Specimens)

Firstly, the reinforced concrete frame with application of AAC block as infill according to the previously defined Type 1 wall condition without the presence of plaster is tested under only in-plane loading. The base shear versus top displacement graph is shown in Figure 4.1 for specimen S1. Furthermore, the drift ratio is calculated by dividing the lateral displacement by the height of the frame and is shown at the top of the graph's horizontal axis. The load-deformation response curves also show the yield (according to FEMA356) and ultimate (according to 15% capacity drop) drift ratios.

The initial cracking of the wall occurred at about 0.1% drift ratio for the S1 specimen. Cracks appeared at the top corner of the frame, extending along the diagonal

direction. The first yield point of the S1 specimen was observed at a 0.3 % drift ratio at which the right column yield curvature was 12 rad/km. The lateral force increased up to a maximum value of 67.64 kN at a 1% drift ratio, after which a sudden loss of lateral strength was observed due to corner crushing like some of the past test observations (Asteris 2011 and Mehrabi 1996) with low bed joint strength. This result shows the importance of AAC bed joint strength for the observed limited deformability of AAC-infilled frames. The ultimate curvature of the column plastic hinge regions recorded during the test was measured as 47 rad/km, corresponding to a curvature ductility of about 3.33.

Specimen S2, with higher AAC mortar and CLIP adhesive strength than specimen S1, was tested under IP loading. The initial cracking and yield displacements were identical to the S1 specimen. The yield curvature of the column was calculated as 13 rad/km. The maximum load-carrying capacity was 87.83 kN at 1% drift ratio. The ultimate column end curvature was measured as 96 rad/km at a 1.9% ultimate drift ratio. The 25% higher lateral strength and 90% increase in the drift capacity observed in Specimen S2 compared to Specimen S1 can be attributed to the higher bed joint strength. The failure mode of the specimen was a distributed diagonal cracking, resulting in more ductile compared to the brittle corner crushing failure mode observed in specimen S1.

Two layers of plaster were applied on the surface of the wall in the case of the S3 specimen to observe the change in the load-carrying capacity of the system. In the S3 specimen, the first diagonal cracks were observed at the 0.1 % drift ratio level. In addition, horizontal cracks occurred at the contact region of the concrete beam and the top of the wall. The maximum load-carrying capacity was measured as 109.22 kN, corresponding to a 1% drift ratio. The plastic hinge was first observed at the base of the left column at a 0.6% inter-story drift ratio. The yield curvature of the left column was 7 rad/km. The right column base plastic hinging took place at 0.95%. Ultimate column curvature was obtained as 70 rad/km.

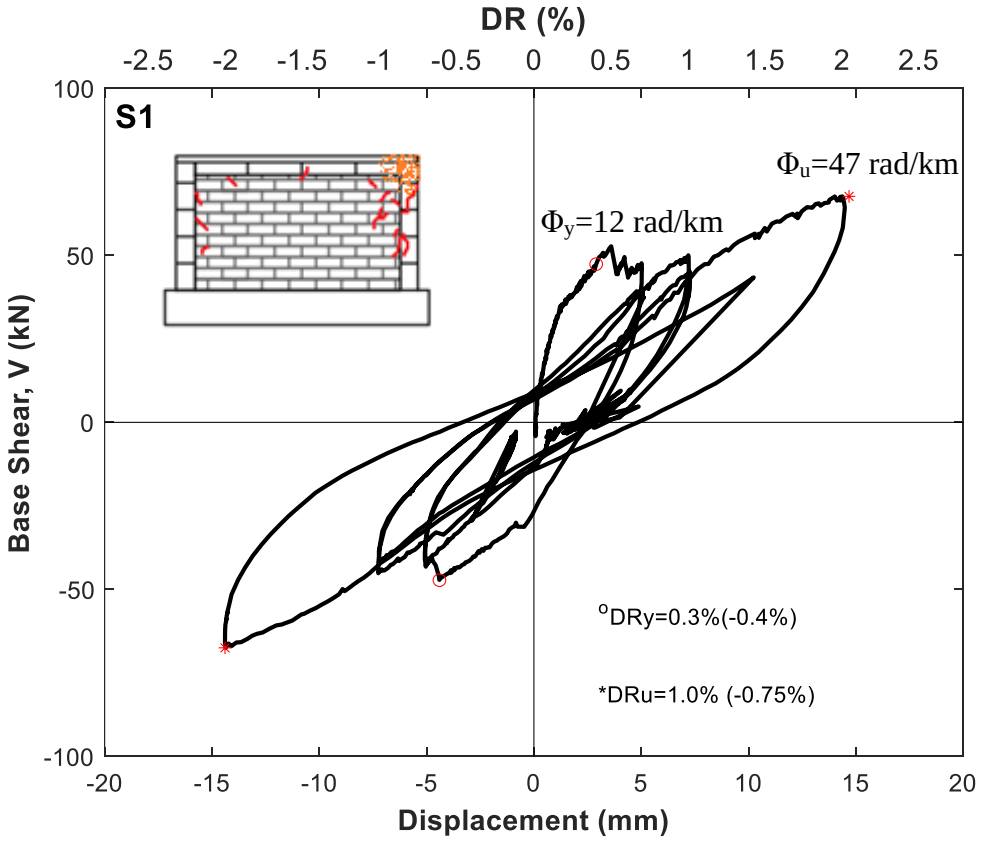

a) Base shear-displacement curve

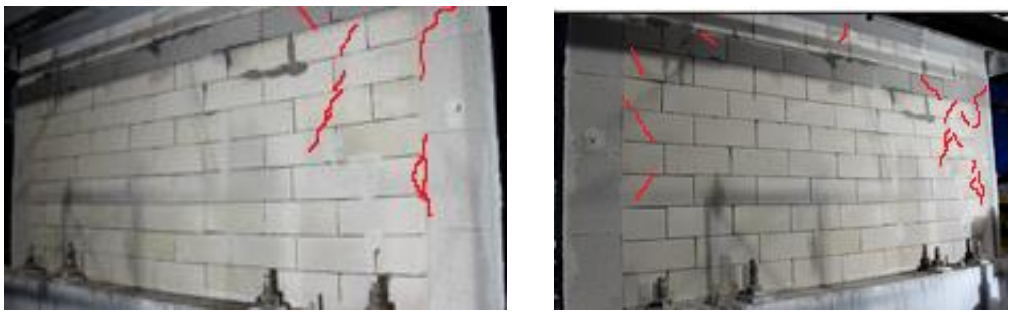

S1: DR=0.5% **S1: DR=1%**

b) Cracks on test specimen

Figure 4.1. S1 test results

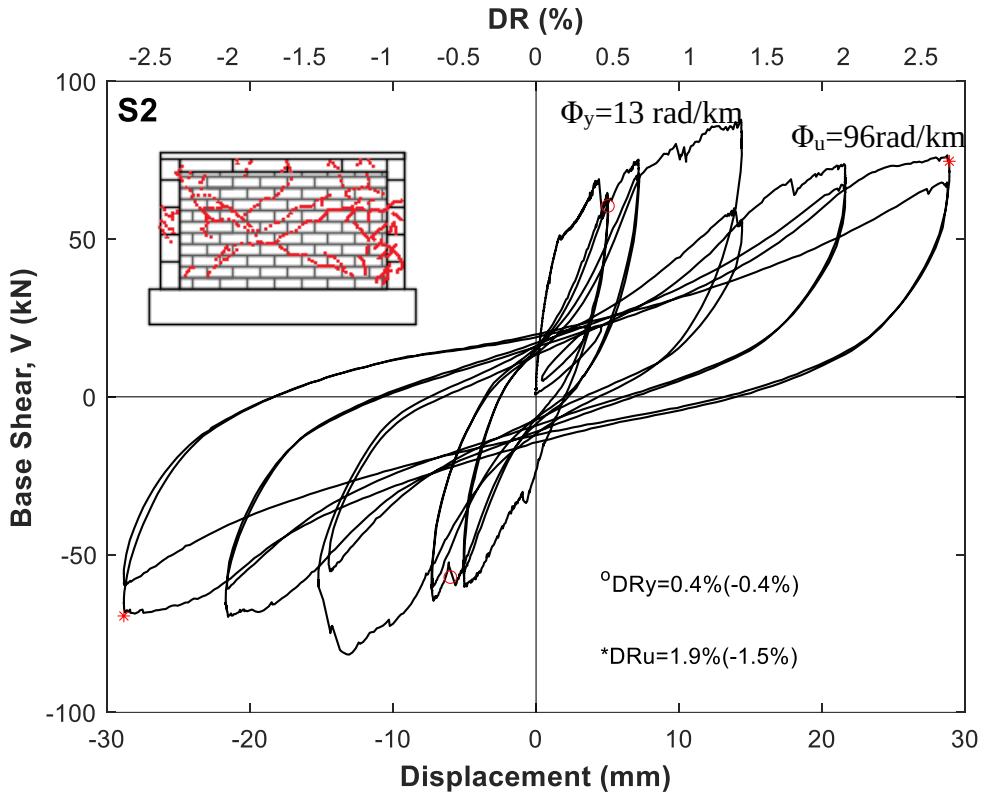

a) Base shear-displacement curve

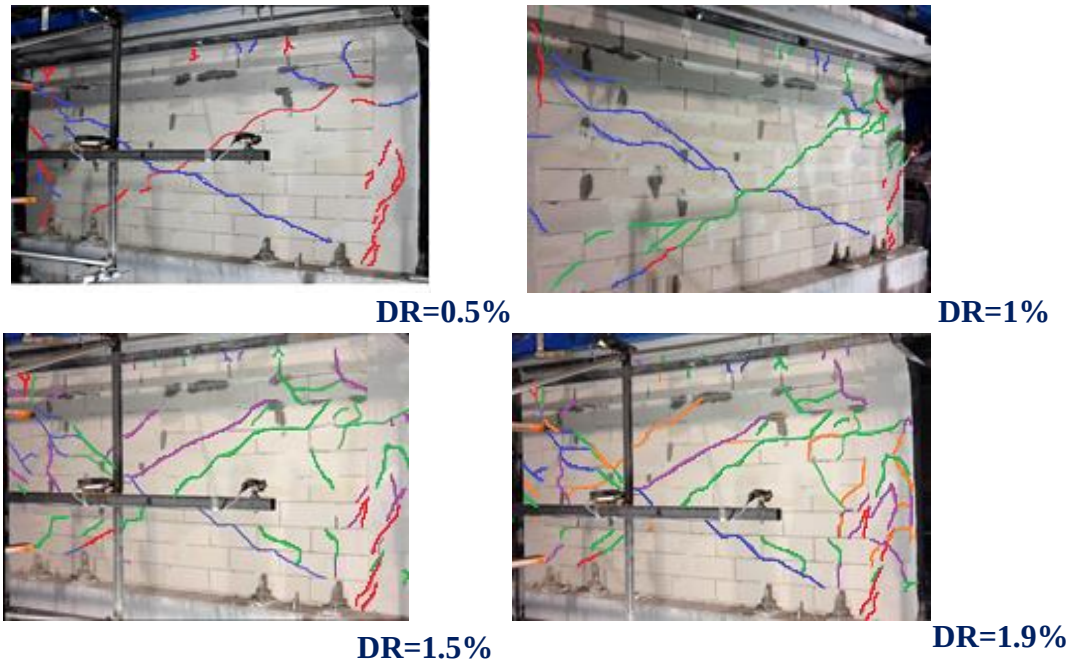

b) Cracks on test specimen

Figure 4.2. S2 test results

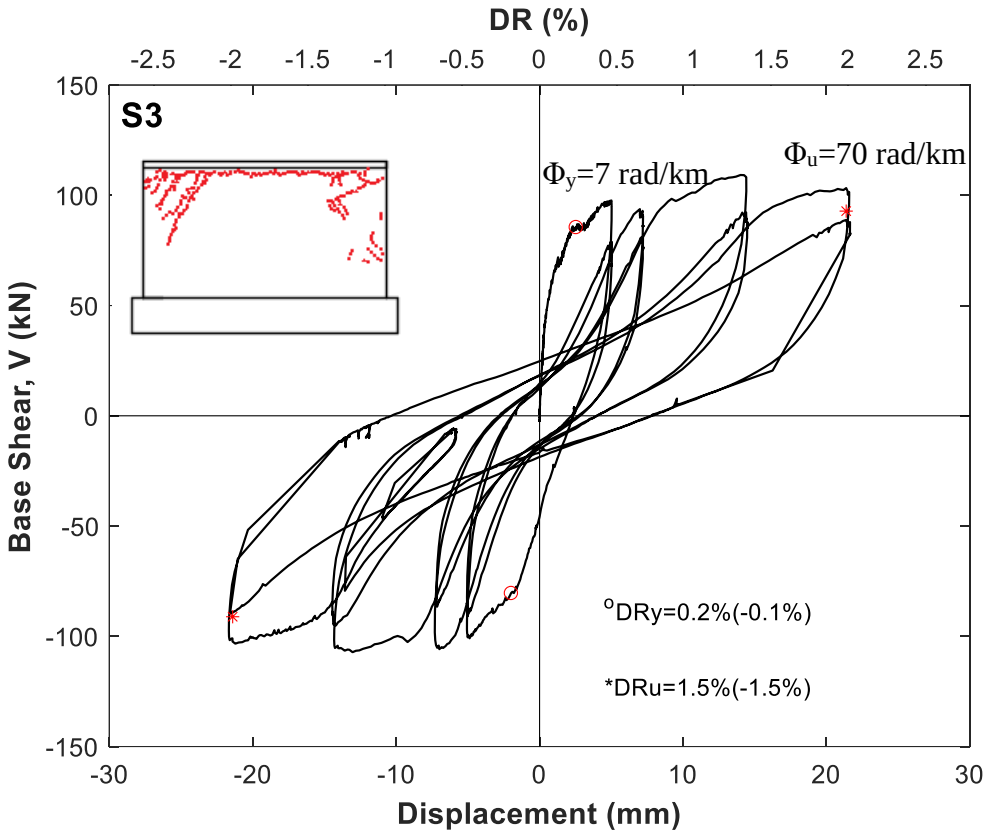

a) Base shear-displacement curve

DR=0.5%

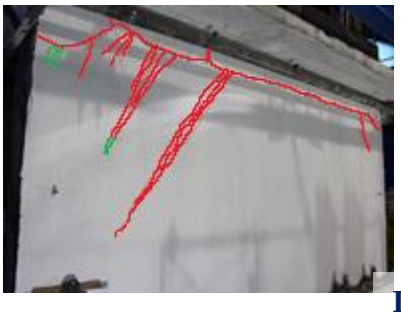

DR=1 %

DR=1.5%

b) Cracks on test specimen

Figure 4.3. S3 test results

4.1.2 OOP Loading (S4 Specimen)

In this part of the study, the infill wall was tested under an out-of-plane loading direction with the airbags provided in the laboratory. The load-displacement relation of specimen S4 is presented in Figure 4.4.

When the S4 specimen was tested under only out-of-plane loading, the deformed shape of the wall became bulged in the transverse direction in the middle of the wall. During the beginning of the loading, tiny, inclined cracks propagated on the front face of the wall.

Moreover, there were cracks on the back side of the wall where the airbag covers. The horizontal cracks were close to the top of the middle due to the presence of a gap between the top of the wall and the reinforced concrete beam. The yield line theory satisfied the deformed shape of the damaged rectangular wall, which at fixed supports of vertical and horizontal cracks. The out-of-plane load continued to increase up to the failure of the wall, which is measured as 57.5 kN as the maximum applied out-of-plane load. The corresponding ultimate displacement was obtained as 30.7 mm. Moreover, the displacement ductility is calculated as 4.7. The failure mechanism was formed by exceeding the moment capacity along the horizontal yield line at half the wall height level.

4.1.3 Combined IP+OOP Loading (S5 and S6 Specimen)

In the case of combined in-plane and out-of-plane loading, the out-of-plane load is applied up to a certain level of the maximum carrying capacity of OOP loading, which is 1/3 and 1/6, respectively, for S5 and S6 tests. Then, in-plane loading is applied while maintaining the out-of-plane load level. The comparison of the S5 and S6 test results shows the out-of-plane influence on the drift capacity due to different OOP load levels. While applying in-plane loading, the initial cracks are observed at the same drift ratio in S5 and S6 tests, which is 0.05%. Diagonal cracks at the corners and horizontal cracks at beam-wall interfaces were observed.

The yield displacement occurred in the S5 specimen at a 0.13 % drift ratio level. The maximum base shear of 84 kN (corresponding to 0.4% drift ratio) was the point of the observation of strength drop. The failure mode of the wall can be described as OOP failure due to the loss of contact at the upper boundary combined with shear separation observed at the CLIP interface due to high shear demand.

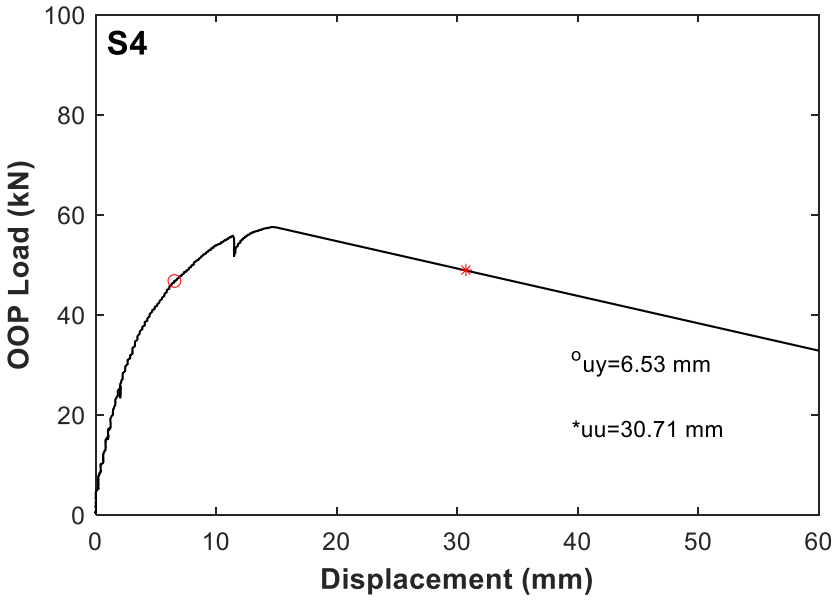

a) OOP Load-displacement curve

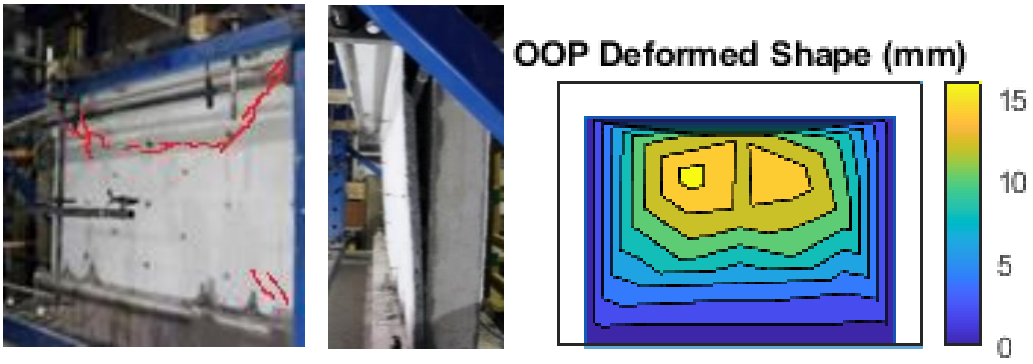

b) Cracks on test specimen at the maximum load level

Figure 4.4. S4 test results

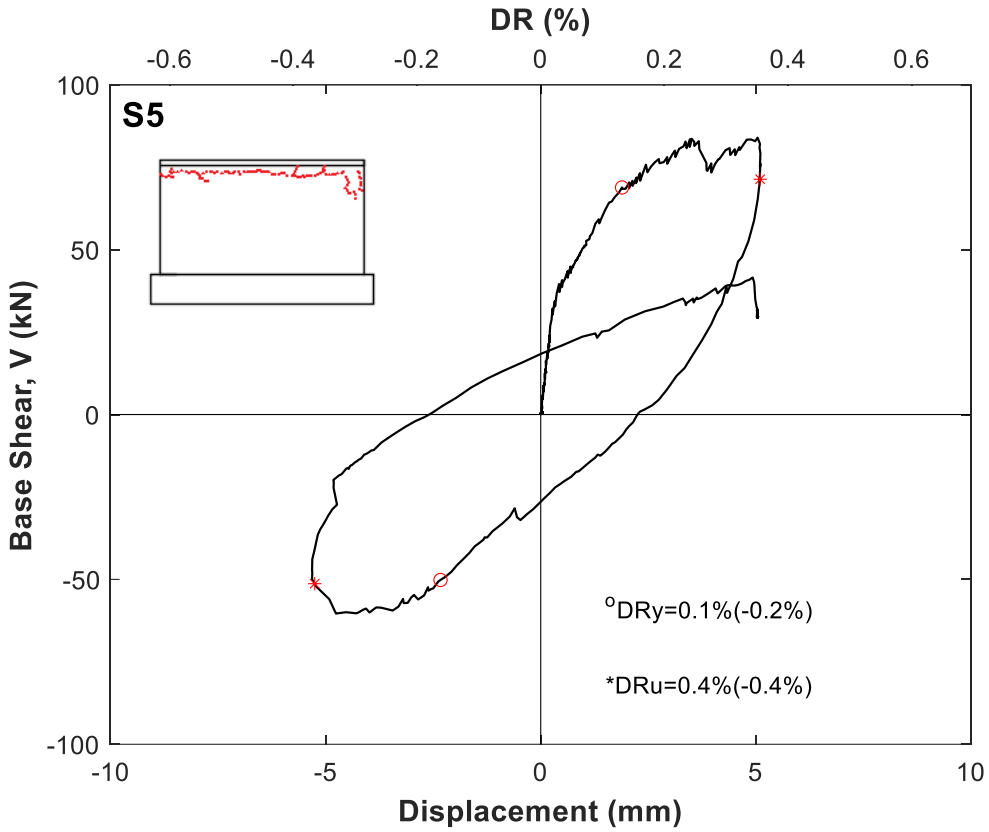

a) Base shear-displacement curve

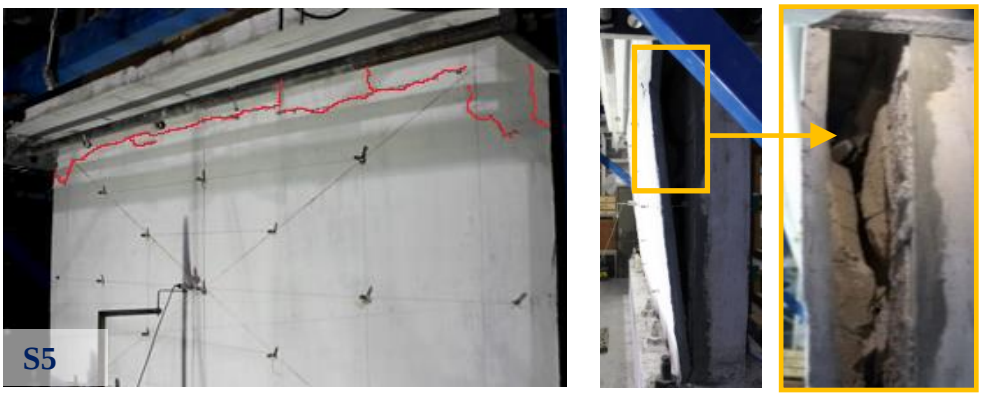

b) Cracks on test specimen at DR=0.4%

Figure 4.5. S5 test results

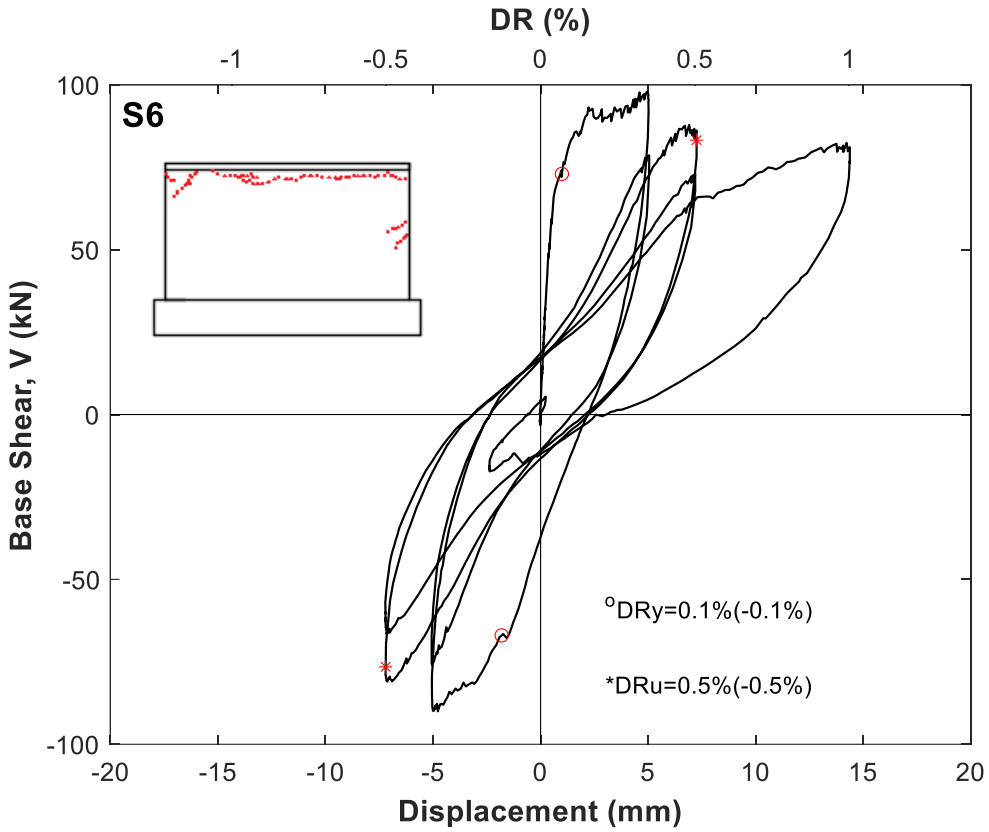

a) Base shear-displacement curve

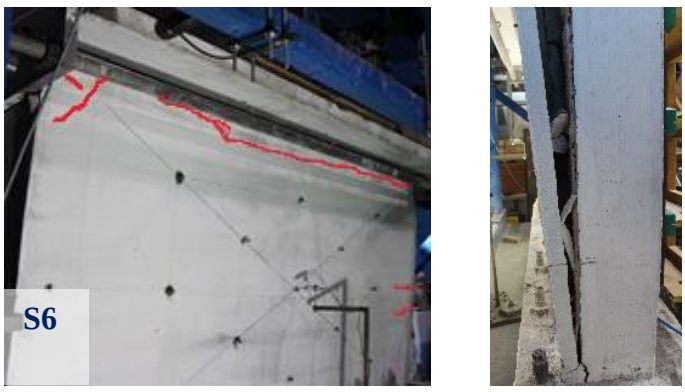

b) Cracks on test specimen at DR=0.5 %

Figure 4.6. S6 test results

The maximum base shear of the S6 specimen was approximately 15% greater than the maximum load of S5, recorded as 97.8 kN. The drift ratio at this level was calculated as 0.35%. Moreover, the ultimate drift ratio was increased to 0.5% when the load level in the out-of-plane direction decreased to 1/6 with a decrease of 50%. The increase in the drift capacity of the two systems was 25% when S5 and S6 were considered. The observed failure modes for specimens S5 and S6 were generally similar and can be attributed to the damage at the top boundary due to combined OOP loads and IP deformation demands.

4.2 Type 2 Wall Experiments

According to Type 1 Wall test results, it was observed that the most critical damage occurred in AAC infill walls with insulation panels under the combined IP and OOP loading. Therefore, this part develops and investigates the Type 2 wall system under combined IP and OOP loading.

4.2.1 OOP Loading (S7 Specimen)

In the Type 2 wall system, 100 mm thickness AAC blocks were positioned flush to the column surfaces with extraction. Then, minepor cementitious insulation plates were covered on the infill wall and reinforced concrete beams and columns. While pure out-of-plane loading was applied on the S7 specimen, the maximum load-carrying capacity was measured at 43.2 kN. The crack pattern of the wall is shown in Figure 4.7 b and is like the yield line theory of a two-way mechanism having simple supports at each side of the frame (bottom and sides). If out-of-plane loading test results are compared for the Type 1 and Type 2 systems, the yield and ultimate displacement values of Type 2 are less than those of Type 1.

The out-of-plane displacements are recorded from the LVDT measurements at locations, as shown in Figure 4.7. Using these records, the deformed shape of the infill wall in the out-of-plane direction was plotted in 2D surface.

4.2.2 Combined IP+OOP Loading (S8 Specimen)

In the next part, the maximum load level of S7 was determined, and 1/3 of the load level was applied as the constant OOP load before including the in-plane loading. The first cracks were observed at 0.03 % drift ratio in the S8 Specimen. The yield point of the specimen was at about 0.2 % drift ratio. The load increased slightly with the increasing horizontal displacements up to a maximum base shear of 97.6 kN (at the level of 0.32 % drift ratio). A strength drop of 15 % was observed at a 0.4 % drift ratio due to the OOP failure of the wall because of seating loss at the infill wall-beam interface.

The base shear versus displacement curve is plotted in Figure 4.8.a.

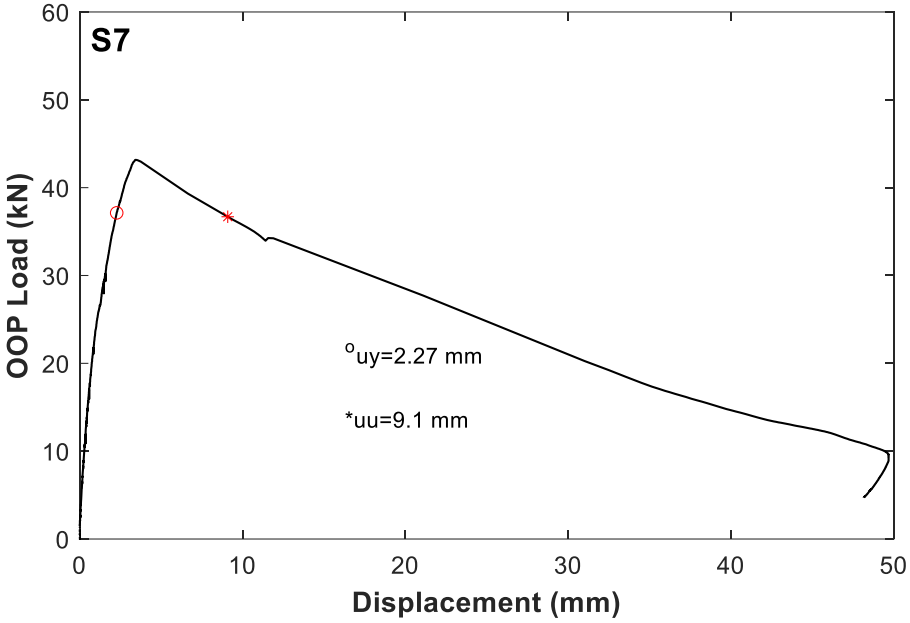

a) OOP Load-displacement curve

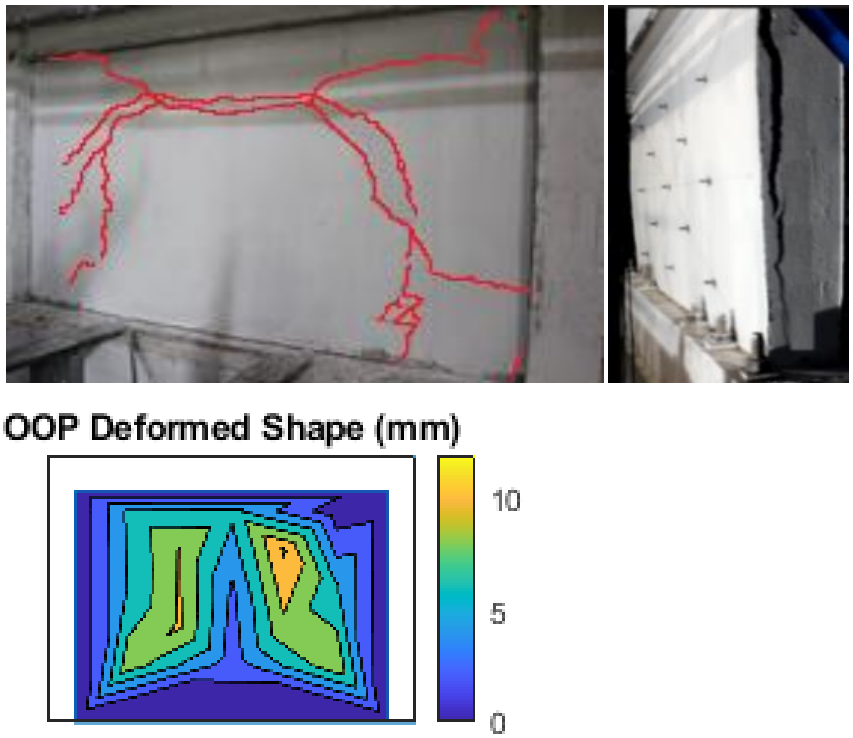

b) Cracks on test specimen at the maximum load level

Figure 4.7 S7 test results

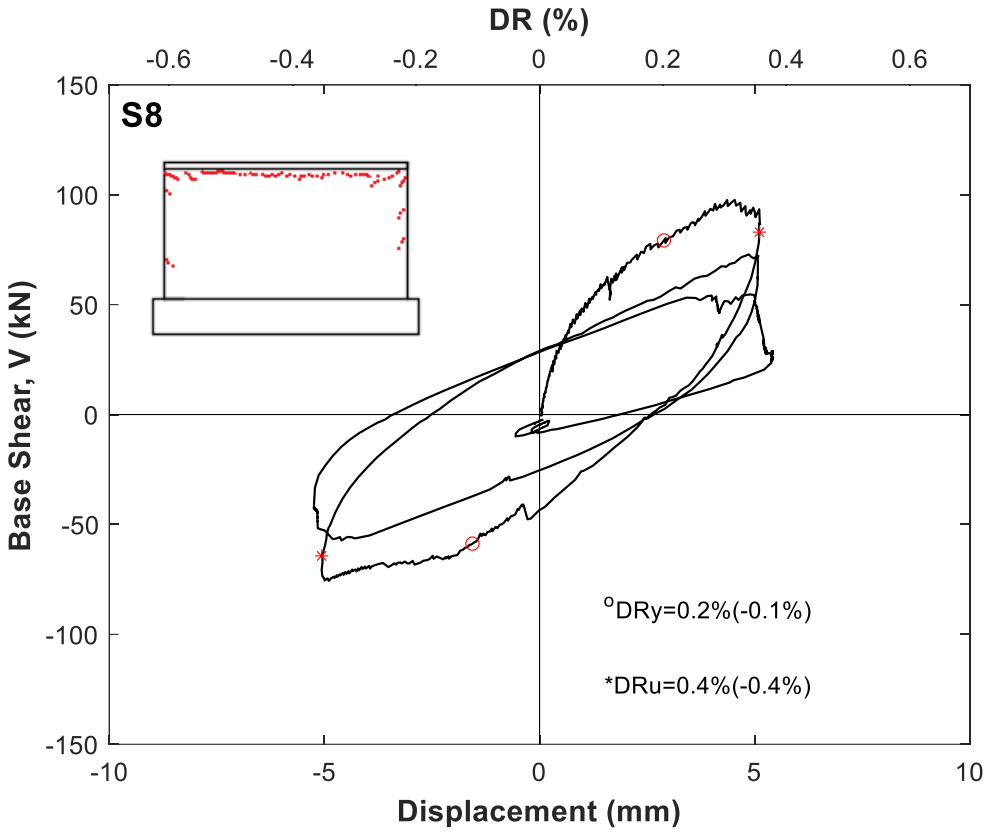

a) Base shear-displacement curve

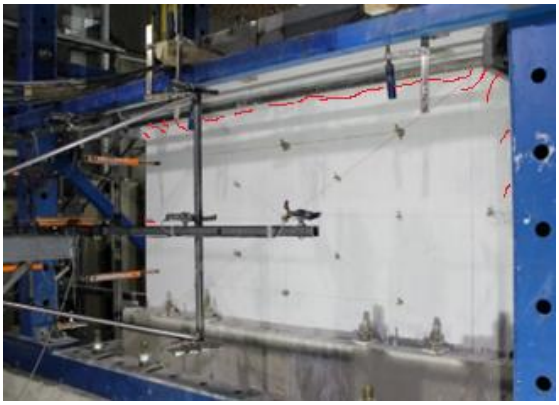

b) Cracks on test specimen at DR=0.4 %

Figure 4.8 S8 test results

4.3 Discussion of Results

The results of each test are summarized in Table 4.1 in terms of maximum force, yield and ultimate displacements, drift ratios, displacement ductility, and cumulative dissipated energy.

In Figure 4.9, the response of Type 1 systems under in-plane loading effect is compared for S1, S2, and S3 specimens to observe the effect of bed joint mortar strength and plaster. The vertical axis of the graphs is the normalized load obtained by dividing the base shear values by the maximum lateral load carrying amount. It is evident that as the bed joint strength increases, the drift ratio of the system also increases. The S1 specimen had insufficient mortar strength because the early testing age cannot give a chance to gain the proper strength. As a result, the lowest lateral load-carrying capacity was observed in the S1 test.

The failure behavior of the infill wall will be similar to each other in the case of the higher compressive strength of the AAC mortar than the AAC block's strength of 2.45 MPa. Except for S1 material strengths, the AAC mortar compressive strengths are greater than the AAC block. The crack propagation photos show where the failure is because of the failure of the AAC block itself, as in Figure 4.5 b on the right side.

In addition, the presence of plaster results in an increase in lateral strength since the S3 test was 20 % greater than the S2 strength. However, the plaster decreases the ductility of the system. The ultimate drift ratio decreased to 1.5 % in the S3 test, while it was 1.9% in the S2 test.

Table 4.1. Summary of test results

System	System	Loading	Yield Force (kN)	Max force (kN)	Δ_y (mm)	Δ_u (mm)	DR_y (%)	DR_u (%)	μΔ	$E_{Dis.}$ (kN.m)
Type 1	**S1**	IP	47.35	67.64	4.14	14.68	0.3% (-0.4%)	1.0% (-0.75%)	3.33 (1.25)	2.207
	S2	IP	61.48	87.83	5.02	27.17	0.4% (-0.4%)	1.9%(-1.5%)	4.75 (3.75)	10.262
	S3	IP	76.45	109.22	2.51	21.38	0.2% (-0.1%)	1.5% (-1.5%)	7.5 (15)	8.548
	S4	OOP	40.27	57.53	6.53	30.71	-	-	4.7	
	S5	OOP1/3 +IP	58.78	83.97	1.87	5.1	0.1% (-0.2%)	0.4% (-0.4 %)	4.0 (2.0)	0.699
	S6	OOP1/6 +IP	68.52	97.89	0.98	7.25	0.1% (-0.1%)	0.5% (-0.5%)	5.0 (5.0)	2.569
Type 2	**S7**	OOP	30.21	43.16	2.27	9.08	-	-	4	
	S8	OOP 1/3 +IP	68.34	97.63	2.88	5.11	0.2% (-0.1%)	0.4% (-0.4%)	2.0 (4.0)	1.354

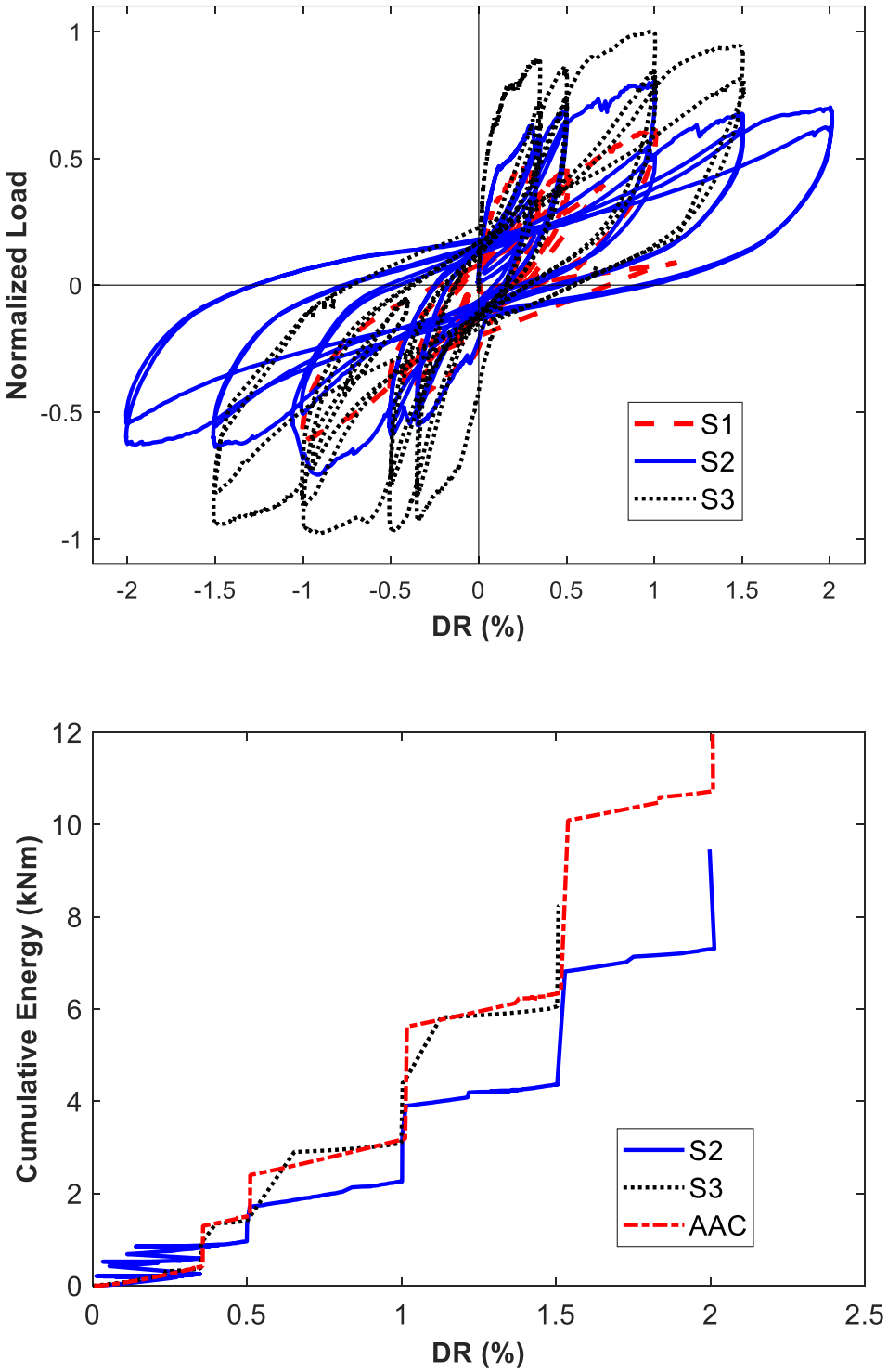

Figure 4.9. Effect of plaster on a) Behavior of Type 1 wall under in plane loading, b) cumulative energy dissipation versus drift ratio

The cumulative dissipated energy plots are prepared in Figure 4.9 b calculated from the area under the force-displacement graph for these specimens. The highest energy dissipation was observed in the specimen with plaster, and the lowest dissipation was observed in the specimen with the low bed joint strength. This result emphasized the importance of plaster and proper selection of bed joint strength for the seismic behavior of AAC-infilled frames one more time.

Table 4.2. Bare Frame (BF) and AAC infill wall results of studies of Binici et al. (2019)

Specimen	**Loading**	**Compressive Strength (MPa)**		**DR_y**	**DR_u**	**μΔ**	**Φu (rad/m)**
		Concrete	Plaster				
BF	IP	27.85	-	0.5% (-0.5 %)	3 % (-3 %)	6 (6)	
AAC-IP	IP	24.9	1.05	0.5 % (-0.5 %)	2% (-2.5 %)	4 (5)	0.43
AAC-OP1	OOP	28.2	1.1	u_y= 4.1 mm	u_u= 29.7 mm	7.2	
AAC-OP2	OOP 1/3 +IP	28.2	1.15	1% (-0.6 %)	1.3% (-1.3 %)	1.3 (2.2)	

The influence of out-of-plane load level on the lateral load carrying capacity of the system under combined IP+OOP conditions is investigated in Figure 4.10 by S3, S5, and S6 test results. The normalized lateral is computed in the vertical axis of the graph. It can be observed that the drift capacity was about 1.5% under pure IP, whereas it dropped to about 0.4 to 0.5% in the presence of combined IP and OOP demands. This result proves the reducing effect of OOP on the drift capacity of Type 1 infilled frames. As OOP force increases, the results show that OOP deformations

are more pronounced, reducing IP drift capacity

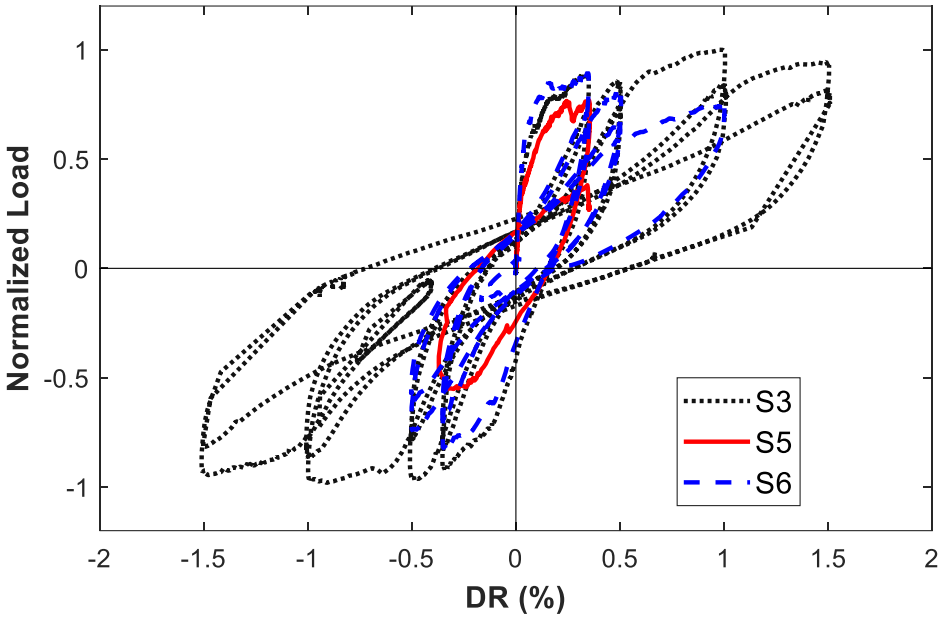

Figure 4.10. Effect of OOP Load Level for Type 1 Specimens

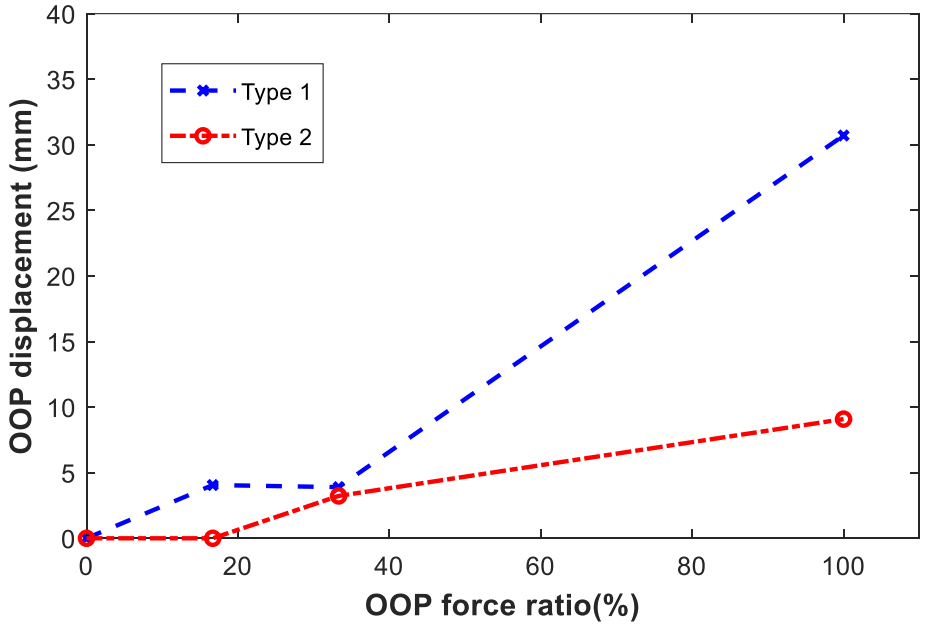

Figure 4.11. OOP displacement-OOP Load Level

The influence of out-of-plane load level on the lateral load-carrying capacity of the system under a testing program with similar details presented in this study was previously conducted by Binici et al. (2017). In that study, the AAC blocks were flush with the columns and beams' faces without additional insulation material. The study aimed to develop a new system with slider connections to provide out-of-plane support under the effect of in-plane induced forces.

In Table 4.2, four of the specimen details and key performance results are provided. The results of the bare frame (BF), AAC infill walled frame (AAC) with IP, OOP, and IP+OOP are compared herein with the companion Type 1 and Type 2 insulated wall systems.

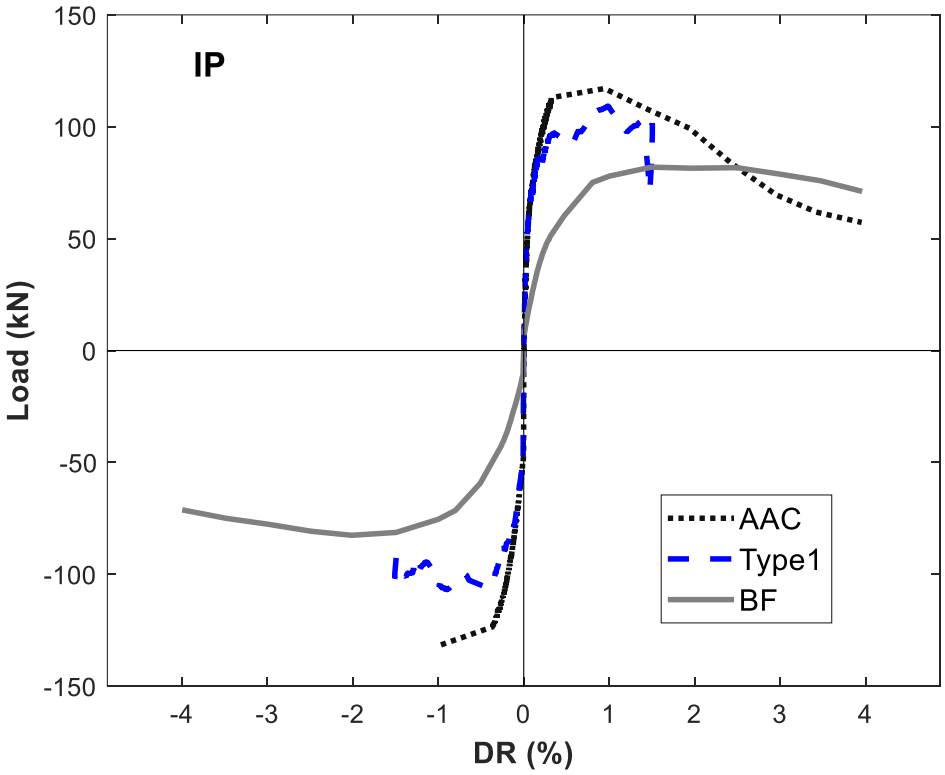

Figure 4.12. Comparison of various system behavior under IP loading

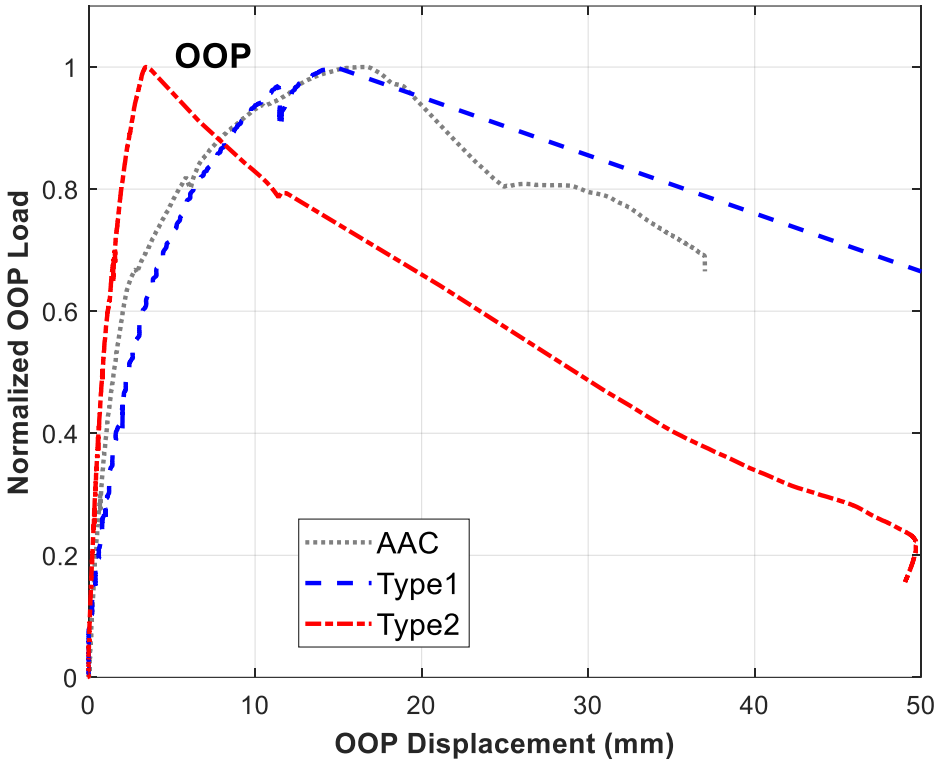

Figure 4.13. Comparison of various system behavior under OOP loading

Under IP loading, the AAC and the corresponding Type 1 specimen had a similar envelope curve of base shear-top displacement up to the peak strength. The AAC specimen's load-carrying capacity was slightly higher than Type 1 (about 7 %). In both systems, the infill had an approximately 25% increase in the load-carrying capacity compared to the bare frame. The bare frame's yield and ultimate drift ratios were 0.5% and 3%, respectively. The yield drift ratio was similar for the AAC and Type 1 infilled frames. However, the ultimate drift ratio was about 2% for specimen AAC, whereas it was about 1.5% for Type 1. This difference can be attributed to the presence of the infill wall eccentricity reducing the contact with the boundary columns. Hence, the Type 1 system exhibited a smaller drift capacity than the case with the infill wall placed inside the frame members (Figure 4.12).

In comparing infill walls under pure out-of-plane loading, it was observed that the Type 1 system (eccentric location of AAC blocks) and AAC block positioned centrally, as in the study of Binici et al., behave similarly. Type 2 wall was found to become more brittle than the others. In addition, the initial stiffness of Type 2 was the greatest, whereas the yield displacement was the smallest.

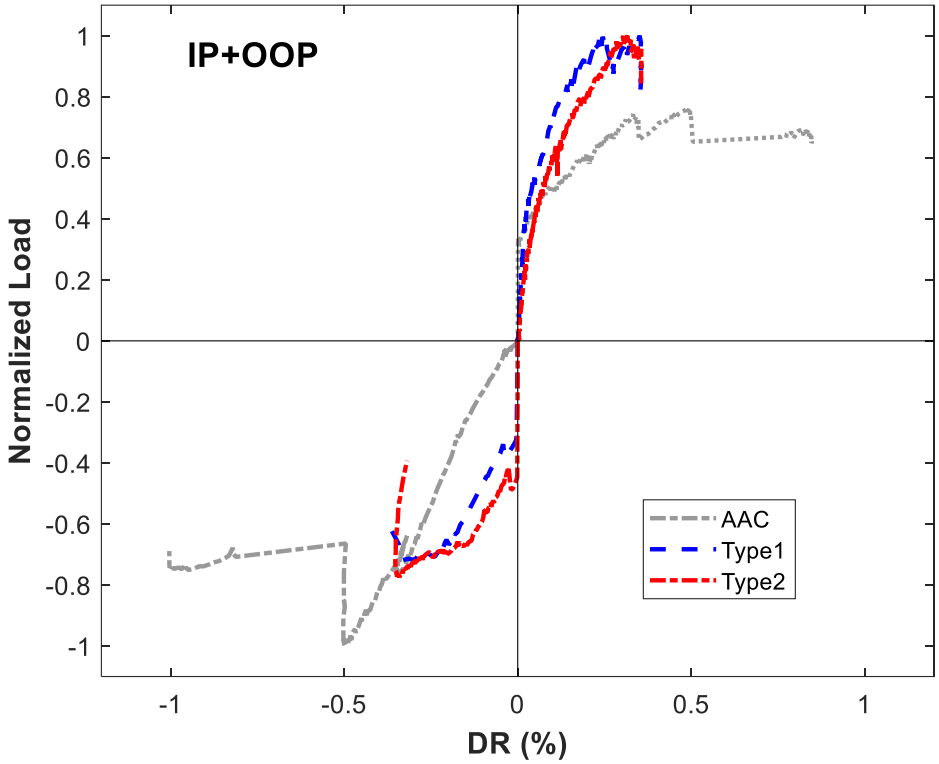

Figure 4.14. Comparison of various system behavior under IP+OOP loading

The lateral load-displacement curves of the AAC and companion Type 1 Type 2 specimens are compared for IP+OOP loading in Figure 4.14. Both Type 1 and Type 2 behaved in a more brittle manner with a drift capacity reduction of about 60%. This result shows that both Type 1 and Type 2 walls are quite vulnerable to the combined in-plane and out-of-plane seismic demands.

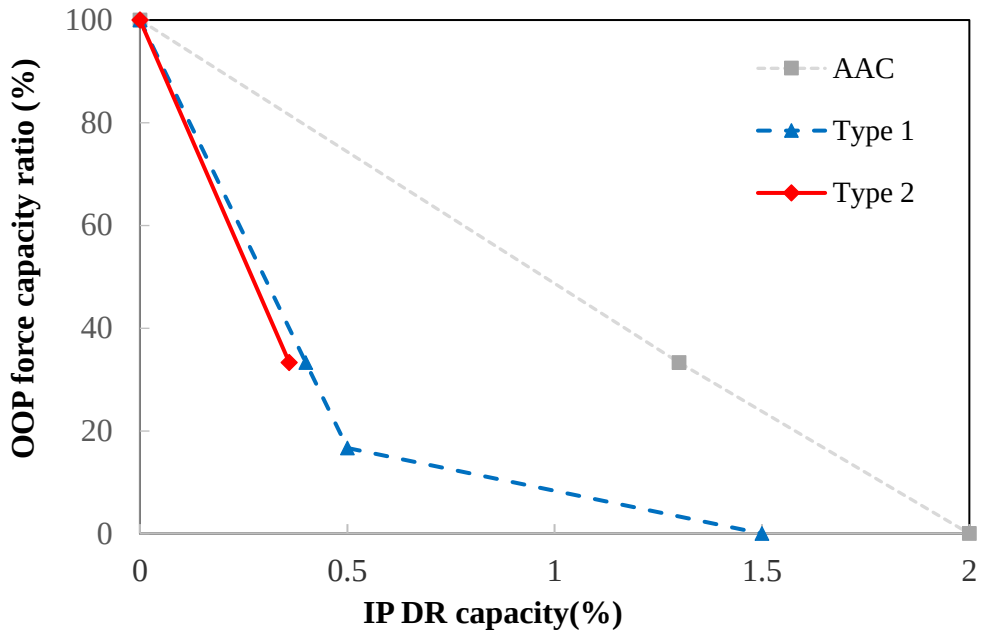

Figure 4.15. OOP force ratio- in-plane DR capacity

The effect of out-of-plane force ratio on the performance of in-plane drift capacity is investigated in Figure 4.15. It is obvious that lateral deformation capacity significantly reduces as the level of OOP load increases. According to the test results of AAC, a 0.4% drift ratio is found to be a safe capacity for fragile components. Unfortunately, none of the specimens can satisfy a 2% drift ratio, which is the assumed value in the design codes.

It is suggested that design engineers should first compute OOP loads by using floor accelerations and find the drift ratio (DR) capacity from limited to shown in Figure 4.15. Afterwards, the structural system should be designed for this DR level by using appropriate lateral force resisting system.

CHAPTER 5

NUMERICAL SIMULATIONS

5.1 Modeling Parameters

The response of the infill AAC wall reinforced concrete frame with CLIP insulation materials is simulated in this chapter. A 3-dimensional model with 6 degrees of freedom (dofs) model is required to investigate the behavior of the wall under in and out of plane loading directions. The frame set-up is re-shown in Figure 5.1 and Figure 5.2 for Type 1 and Type 2 plan views.

In Type 1 walls, the location of the AAC block is eccentric. While determining the material properties of the infill, the total thickness of the block and plaster is considered for calculating the effective strength of the wall, whereas the thickness inside the frame is taken for the calculation of the stiffness of the infill. The portion inside the frame is effective for the strut action under in-plane loading.

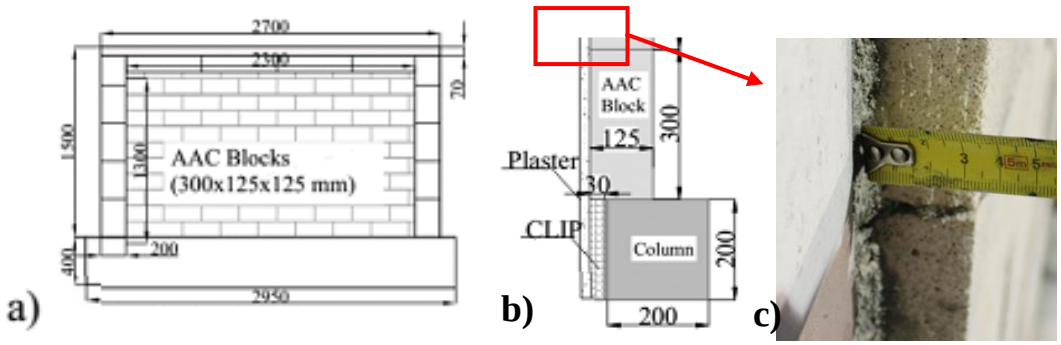

Figure 5.1. Modeling properties of Type 1 wall, a) Frame set-up b) plan view c) detail

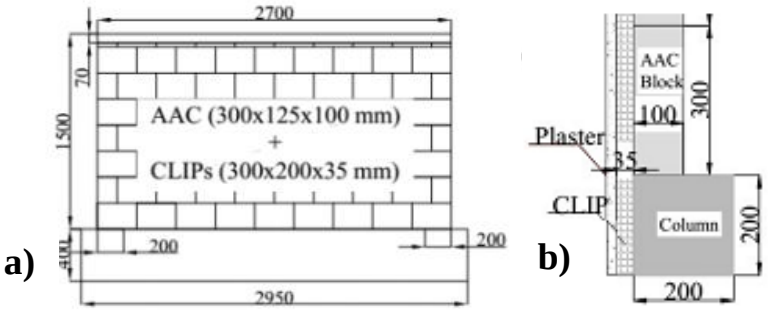

Figure 5.2. Modeling properties of Type 2 wall, a) Frame set-up b) plan view

5.1.1 Material

5.1.1.1 Unconfined Concrete Model

The unconfined concrete of columns is modeled according to the Hognestad concrete model, as shown in Figure 5.3. Concrete02 material model is used in the OpenSees model. The compressive strength of unconfined concrete is 27.9 MPa, and the modulus of elasticity is 25514 MPa.

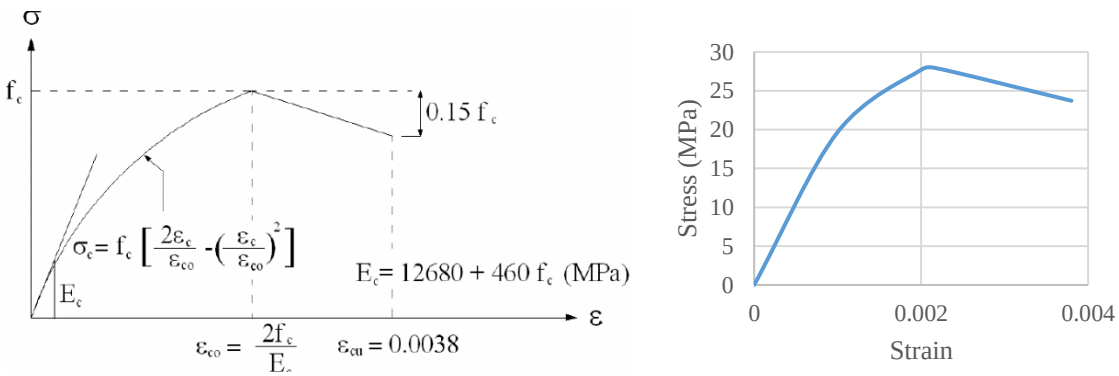

Figure 5.3. Hognestad concrete model for unconfined concrete

5.1.1.2 Confined Concrete Model

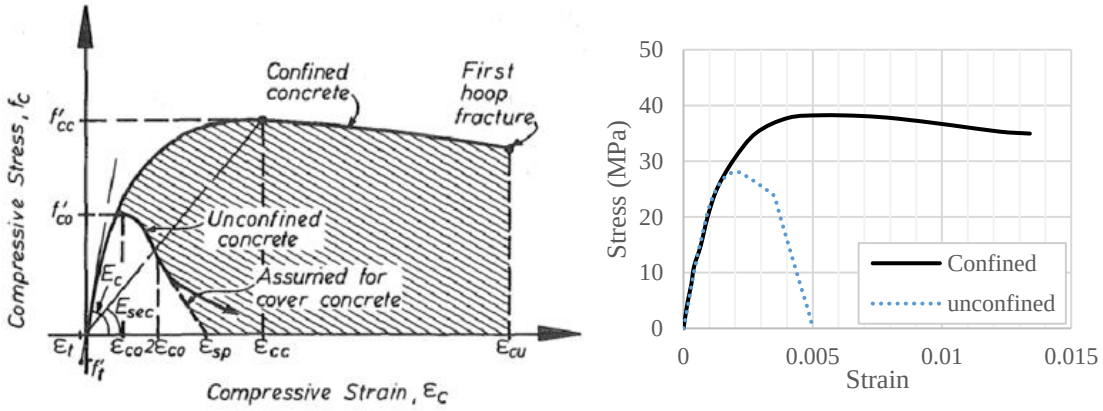

Figure 5.4. Mander's concrete model for confined concrete

The confined concrete properties are calculated using the Xtract software program considering Mander's concrete model. The compressive strength of concrete is 27.9 MPa. The dimensions of the column are 200x200 mm. There are eight deformed bars with 8 mm diameter having a yield strength of 425 MPa. Stirrups of the columns were prepared from 6 mm diameter plain bars with a spacing of 100 mm in the mid-height and 50 mm at the column ends (within 300 mm from the ends), having a yield strength of 448 MPa. The confined compressive strength of concrete is calculated as 38.09 MPa.

The confined concrete for the beam is calculated as 32.12 MPa. The transverse reinforcement spacing in the confined and middle regions of the beam was 50 mm and 100 mm. The material properties of the 6 mm and 8 mm bars used for the flanged beam were the same as those used in the columns.

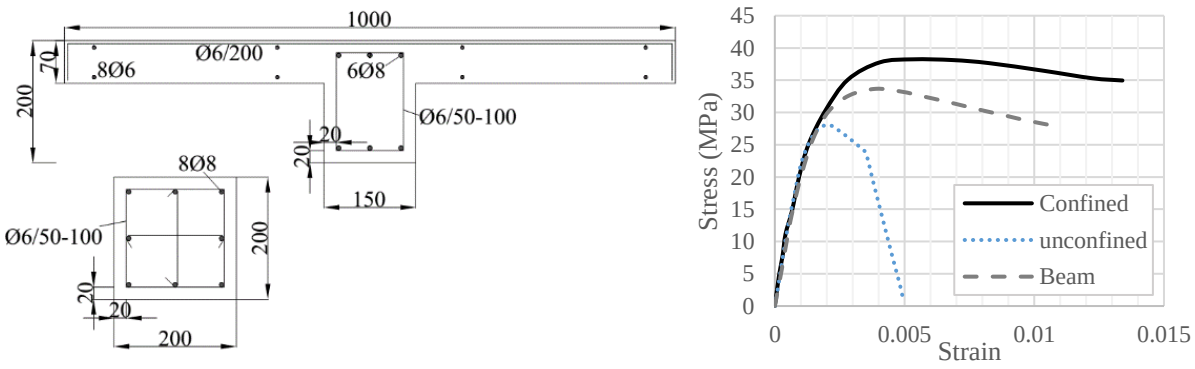

Figure 5.5. Cross sections of column and flanged beam

5.1.1.3 Steel Model

The property of steel is modeled according to the model of Guiffre-Menegotto-Pinto, Steel02 command in OpenSees. The yield strength is 448 MPa. The modulus of elasticity is 200 GPa. The strain hardening ratio is selected as 0.005. Moreover, the recommended values (strain hardening ratio=0.005, R0=15, cR1=0.925, cR2=0.15) of R0, cR1 and cR2 is used.

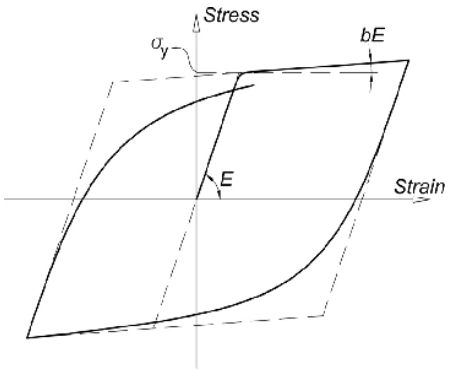

Figure 5.6. Modified Giuffré–Menegotto–Pinto uniaxial material constitutive model for structural steel

5.1.1.4 Infill Material Model

Infill material is modeled using horizontal, vertical, and diagonal struts. The behavior of the infill is demonstrated using several materials. These are Concrete01 model with zero tensile strength, concrete06, and hysteretic material. The parameters of strength and strain of the infills are determined according to the compressive strength test of three mortar cubes of 50 mm test specimens, ASTM C109.

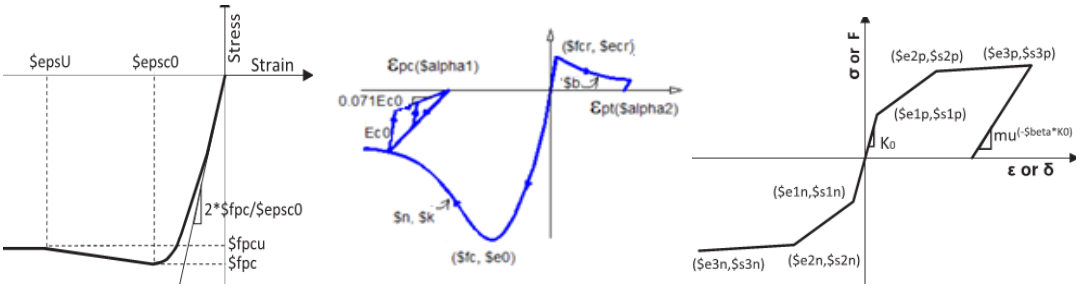

a) **b)** **c)**

Figure 5.7. Different Material properties of infill strut a) Concrete01 model b) Concrete06 model c) Hysteretic Material model

5.1.2 Section

A fiber section has a general geometric configuration formed by subregions of simpler, regular shapes (e.g., quadrilateral, circular, and triangular regions) called patches.

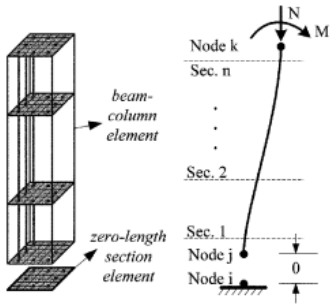

Figure 5.8. Fiber-based modeling of strain penetration effect (Zhao and Sritharan, 2007)

5.1.3 Element

The model system consists of 2 elements for columns, 1 element for the beam of reinforced concrete frame, and 2 vertical, 2 horizontal struts, and 4 diagonal struts are employed to behave as the infill wall, as shown in Figure 5.9. Each strut is represented by two beam-column elements. Four nodes at the midspan are free in the in-plane loading direction but move together in the out-of-plane loading direction restrained. The masonry's compressive strength and the struts' width affect the infill wall's resistance under IP, OOP, and combined IP and OOP load applications. Columns and beams of the frame are modeled using forced-based beam-column elements.

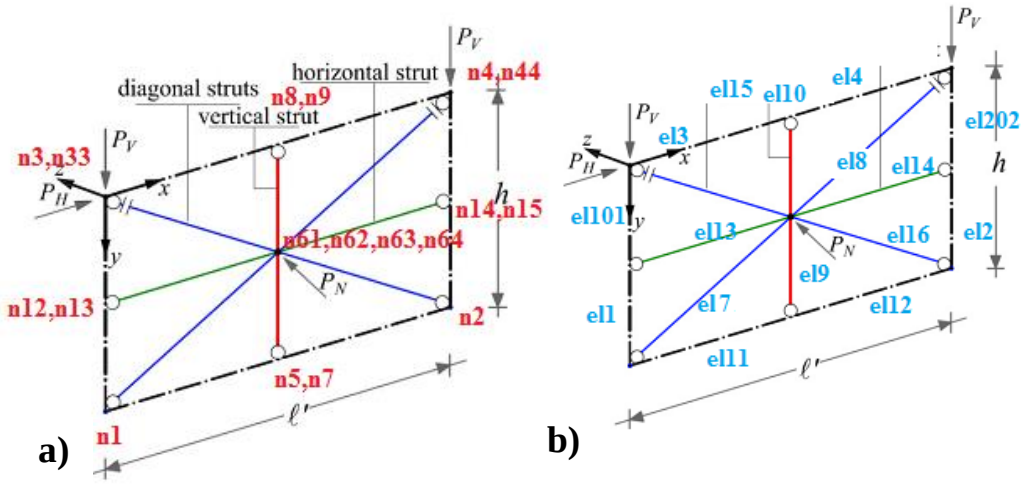

Figure 5.9. Modeling system a) Node Labeling b) Element Labeling

Horizontal, vertical, and diagonal struts are modeled using displacement-based beam-column elements. Zero-length elements are introduced to present hinges on the top of the frame to simulate the loss of contact between the frame and infill wall during in-plane loading. The diagonal struts are connected with these gap elements, allowing compressive stress transfer but have zero tensile strength.

5.2 Numerical Results and Experimental Validation

In this part, the numerical results of analyses are presented and compared with the experimental results. It is composed of 3 sections in which Type 1 and Type 2 wall systems are investigated with the presence of plaster or not for Type 1 walls.

Different load applications are studied in models: pure in-plane loading, only out-of-plane loading, and the combined effect on the behavior of the infill wall under out-of-plane loading and in-plane loading simultaneously. The parameters of struts used in each model are summarized in Table 5.1, and the calculation is explained in the chapter.

Table 5.1. Strut properties for Models

Model	Wall	Load	w_{dia} (mm)	t_{dia} (mm)	w_{ver} (mm)	t_{ver} (mm)	w_{hor} (mm)	t_{hor} (mm)
Model 1	Type-1 no pls	IP	880	90	686	90	292	90
Model 2	Type-1	IP	310	90	575	90	325	90
Model 3	Type-1	OOP	311	135	575	135	325	135
Model 4	Type-1	IP+OOP 1/3	296	85	575	85	325	85
Model 5	Type-1	IP+OOP 1/6	299	85	575	85	325	85
Model 6	Type-2	OOP	316	142.5	575	142.5	325	142.5
Model 7	Type-2	IP+OOP 1/3	295	100	575	100	325	100

5.2.1 Type 1 Wall without plaster

Only in-plane loading is applied in the first model of the Type 1 wall without plaster. As described in the previous part, the concrete frame components of columns and beams are modeled using forced-based beam-column elements. The strut widths are determined according to the study of Trapani et al. (2018). The diagonal strut's width is one-third of the diagonal length inside the frame.

$$w_d = {}^{a}/_{3} \tag{5.1}$$

$$w_v = l - {}^{w_d}/_{\sin\theta} \tag{5.2}$$

$$w_h = h - {}^{w_d}/_{\cos\theta} \tag{5.3}$$

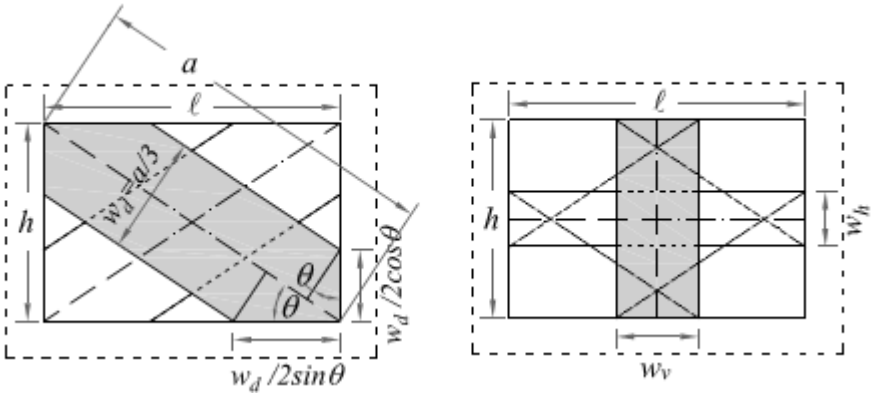

Figure 5.10. Diagonal, horizontal and horizontal strut widths (Trapani, 2018)

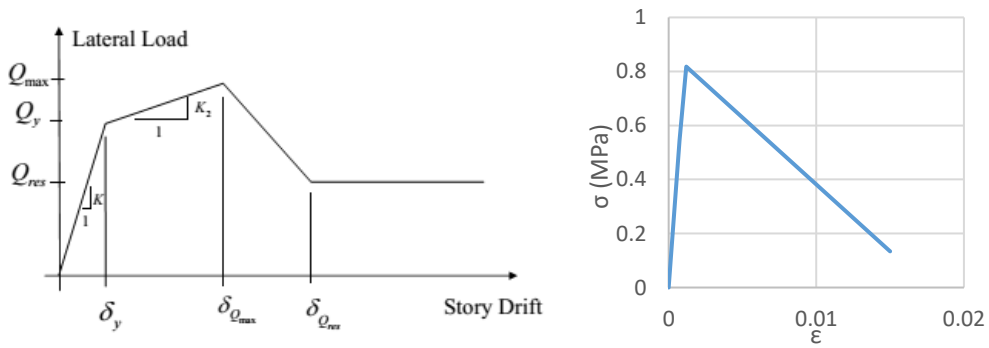

Figure 5.11. Material property of strut (Shing and Stavridis, 2014)

After determining strut widths, the material properties of the struts are calculated by following the procedure in Shing and Stavridis (2014). The compressive strength of the strut is obtained as 0.78 MPa for the in-plane loading model infill wall without plaster. The stress-strain graph is given in Figure 5.11. The thickness of the struts is considered as the thickness of the infill wall inside the frame. Therefore, due to the 35 mm contrusion in Type 1 walls (Figure 5.1.c), the 125 mm AAC wall thickness reduces to 90 mm in the model. The results of the analyses are compared with the test in terms of the base shear–top displacement graph shown in Figure 5.12. It is observed that the initial stiffness of each graph coincides. The maximum shear capacity is very similar, with a difference of less than 4%.

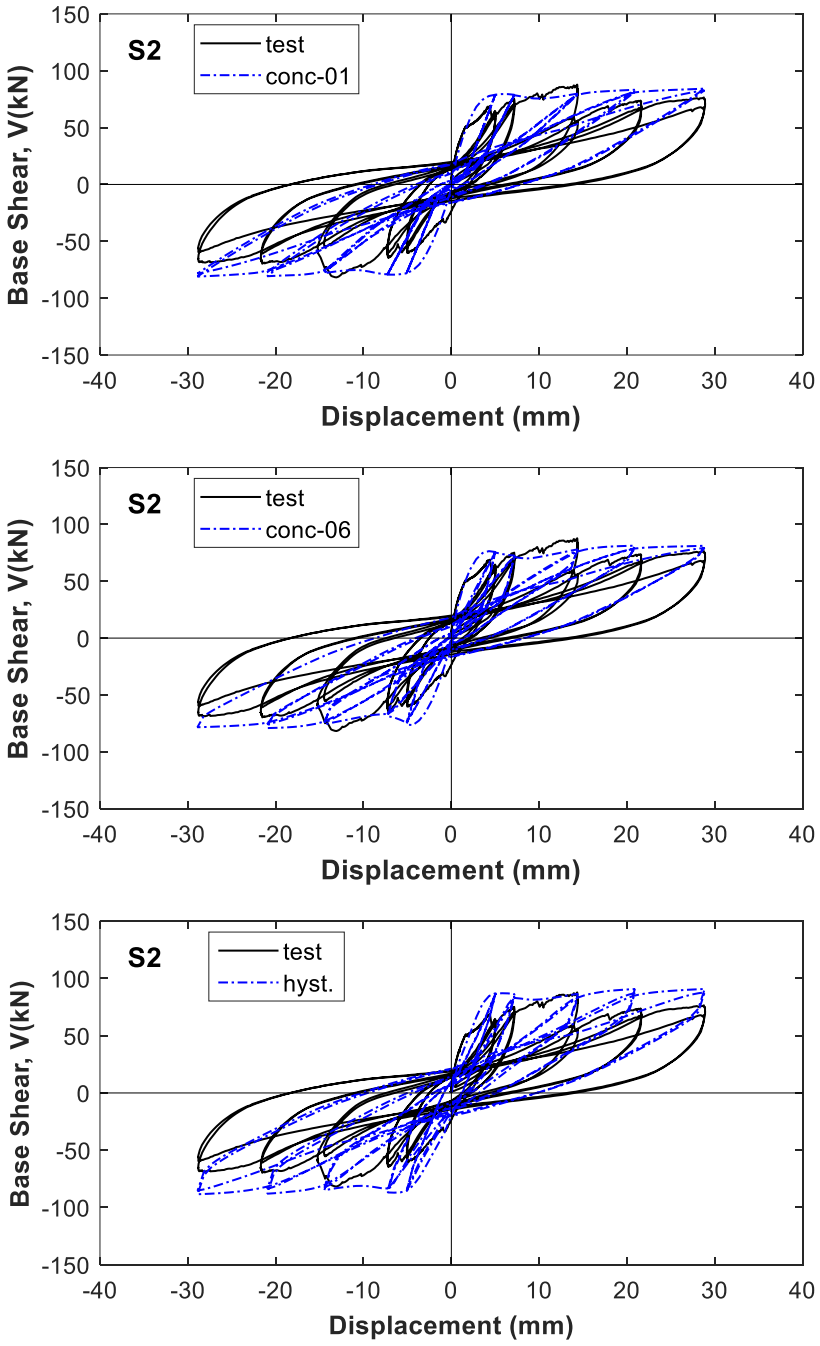

Figure 5.12. Verification of Model 1 Analysis with test (IP loading without plaster)

5.2.2 Type 1 Wall with plaster

The following tests include plaster on the surface of the walls on both sides, front and back, with a total thickness of 20 mm. The presence of plaster affects the strength and stiffness of the struts. The effective material properties of diagonal compression struts are calculated according to Binici & Ozcebe's (2008) study. In this study, the area of the composite strut (A_{st}) is composed of the strut thickness (t_{st}), which is the total thickness of infill (t_{in}) and plaster (t_p) multiplied by the effective width of the infill strut (w_s) from El-Dakhakhi et al. based on the work by Saneinejad and Hobbs.

$$A_{st} = w_s t_{st} \tag{5.4}$$

$$t_{st} = t_p + t_{in} \tag{5.5}$$

$$w_s = \frac{(1-\alpha)\alpha h}{\cos\theta} \tag{5.6}$$

$$\alpha = \sqrt{\frac{2\,(M_{pj}+0.2\,M_{pc})}{h^2 t_{st} f_{mc}}} \tag{5.7}$$

where

α is a parameter calculated as in Equation 5.7.

M_{pj}: Min (M_{pc}, M_{pb}), is the minimum of moment capacity of beam or column

M_{pc}: Column moment capacity

h: height of the infill wall

f_{mc}: Plaster composite infill compressive strength

θ: inclination angle of strut

The ultimate strength (f_{us}) of the strut is computed by dividing the ultimate diagonal compressive strength by the area of the composite strut. The minimum of the sliding shear (V_{ss}) and corner crushing (V_{cc}) capacities is chosen as the ultimate strength.

$$f_{us} = {V_{us}}/{A_{st}} \tag{5.8}$$

$$V_{us} = \min(V_{ss}, V_{cc}) \quad (5.9)$$

$$V_{ss} = f_{mv} L\, t_{st} \quad (5.10)$$

$$V_{cc} = 250 f_{mc} t_{st} \quad (5.11)$$

where

f_{mv}: Plaster shear strength at bed joint

L: Infill wall width

$$f_{mc} = \frac{f_{in} t_{in} + f_m t_p}{t_{st}} \quad (5.12)$$

$$E_{sm} = \frac{E_{in} t_{in} + E_m t_p}{t_{st}} \quad (5.13)$$

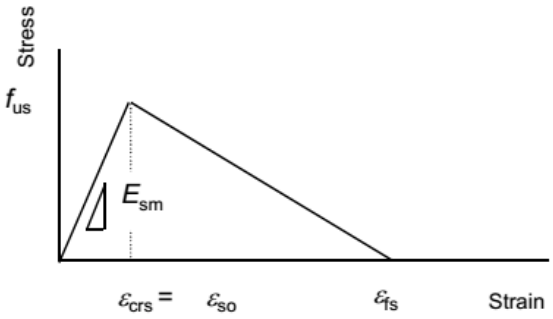

Figure 5.13. Infill strut stress-strain model

The elastic modulus of AAC infill is calculated as

$$E_{AAC} = 887.8 {f_{AAC}}^{0.6} \quad (5.14)$$

According to Masonry Standards Joint Committee (MSJC, 2011) study.

The following models, including plaster and different types of loadings, are investigated separately. Then the combination of out-of-plane loading and in-plane loading with different levels of out-of-plane loads.

Table 5.2. Parameter for the calculation of effective strut material properties

t_p (mm)	t_{in} (mm)	h (mm)	L (mm)	cosθ	M_{pb} (kNm)	M_{pc} (kNm)	M_{pj} (kNm)
20	125	1300	2300	0.87	28	27.8	27.8

Table 5.3. Summary of strut parameters with presence of plaster- Type 1

	t_{st} (mm)	f_c (MPa)	E_{sm} (MPa)	α	w_s (mm)	A_{st} (mm^2)
Model 2	145	3.16	3109	0.294	310	44900
Model 3	135	3.40	2775	0.293	310	41795
Model4	145	4.75	4162	0.240	272	39438
Model 5	145	4.05	3754	0.259	287	41594

Table 5.4. Summary of calculation the effective strut width

	V_{ss} (kN)	V_{cc} (kN)	V_{us} (kN)	f_{us} (MPa)	ε_{crs}	a (mm)
Model 2	184	115	115	2.55	0.00082	305
Model 3	242	115	115	2.74	0.0010	311
Model 4	292	172	172	4.36	0.0010	296
Model 5	250	147	147	3.53	0.0009	299

The width of the vertical and horizontal struts is chosen as L/4 from past experiences. The length of the frame is 2300 mm, and the height is 1300 mm. As a result, the vertical strut width is 575 mm, and the horizontal strut width is 325 mm. The thickness of the infill is taken as 90 mm, which is inside the frame. The diagonal strut width is calculated from the formula as shown in below:

$$\lambda_1 = \left(\frac{E_{me} t_{in} \sin 2\theta}{4 E_{fe} I_{col} h_{in}}\right)^{0.25} \tag{5.15}$$

$$a = 0.175(\lambda_1 \, h_{col})^{-0.4} r_{inf} \tag{5.16}$$

$$r_{inf} = \sqrt{l^2 + h^2} \tag{5.17}$$

5.2.2.1 In plane Loading Model with Plaster

In the Type 1 system, the thickness of the AAC is 125 mm, but the 90 mm is inside the concrete frame, as shown in Figure 5.14, where the in-plane loading has a role in the performance of the wall. Moreover, a total of 20 mm plaster is applied on both sides of the wall with 2 layers of fiber-reinforced mesh between the two plaster layers. The compressive strength of the AAC block is 2.45 MPa. The compressive strength of the plaster is obtained from the cubic test specimens (50 mm dimensions) taken on the experiment day. The composite material properties of the AAC plus plaster are calculated according to Binici and Ozcebe's study (2008).

a) Model 2 b) Model 4 c) Model 5

Figure 5.14. Infill extrusion detail for Type 1

The analysis model for in-plane loading with given material properties results fits the test behavior and can be investigated in Figure 5.15 using conc01, conc06, and hysteretic material properties for the infills. The test result's initial stiffnesses, maximum load, and displacement is similar to the analysis results. The only

difference is observed on the descending portion of the last loop of force displacement. The unloading part of the analysis results shows less dissipated energy when compared with the test result.

5.2.2.3 Out-of-Plane (OOP) Loading

In the third model, pure out-of-plane loading is considered. The thickness of the infill struts is taken as the summation of the AAC infill wall and plaster since the out-of-plane loading is applied to the system using the airbags. The total thickness resists the applied load. The diagonal strut width is calculated from the formula, and 575 mm and 325 mm are the vertical and horizontal struts' thicknesses, respectively, corresponding to ¼ of the frame dimension.

The evaluation of the analysis result and experiment is shown in Figure 5.16. It is observed that the maximum load capacity of the conc06 analysis model is relatively less than the others, 5% less than the test load capacity. However, the conc01 analysis result is 4% higher for the determination of the maximum load capacity of the test.

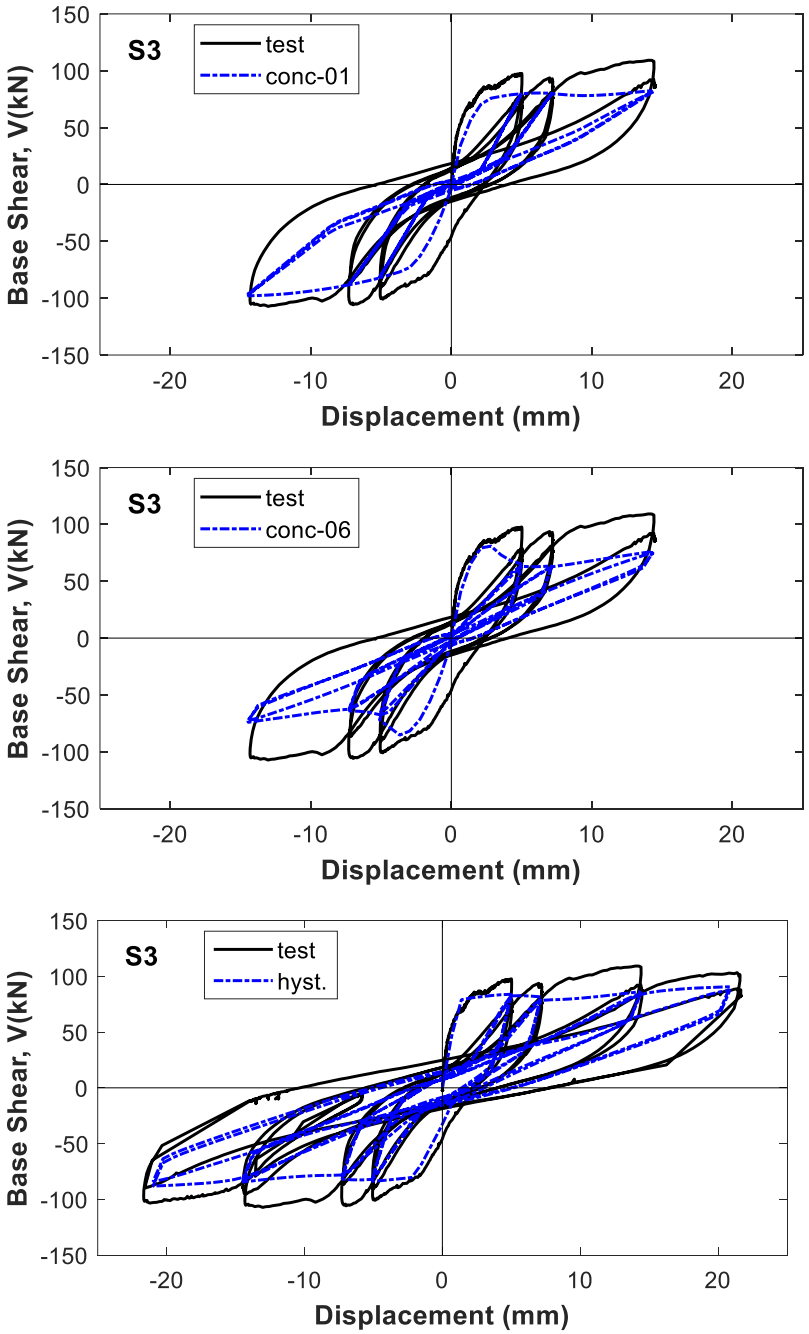

Figure 5.15. Verification of Model 2 Analysis with test

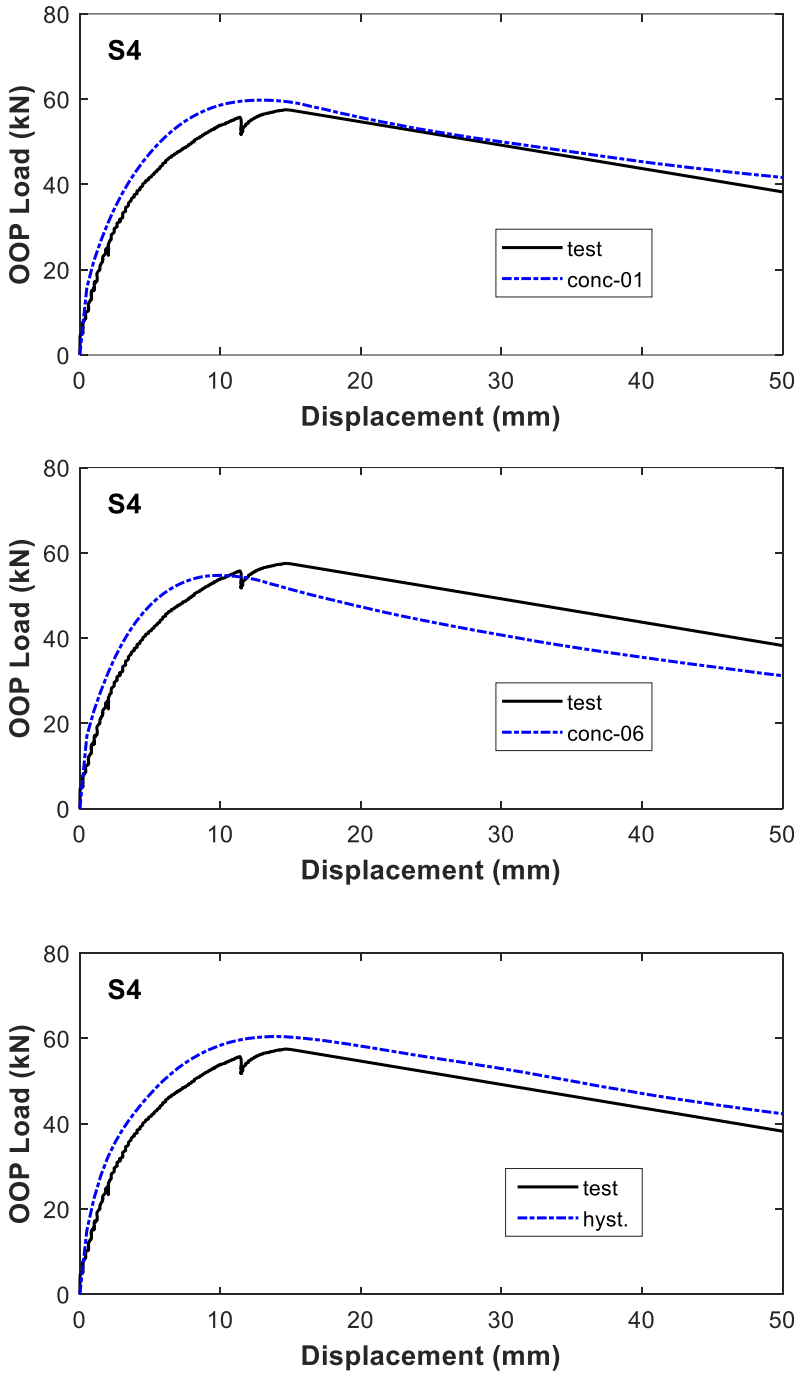

Figure 5.16. Verification of Model 3 Analysis with test (OOP loading with plaster)

5.2.2.4 IP+OOP (1/3 Capacity) Combined Loading

In this model, firstly, 2 tons of out-of-plane loading is applied on the wall, which is one-third of the maximum load capacity of the infill, then the in-plane loading takes place. The dimensions of the infill walls are calculated using the total thicknesses. The compressive strength of the struts is determined. However, in the analysis, the used thickness of the struts is 85 mm for the stiffness calculations.

The analysis results fit the initial stiffness and maximum base shear test behavior. Unfortunately, the analysis shows a convergence problem and exits from the complier in the unloading part of the cyclic analysis. The descending part of the force-displacement graph cannot be completed. In Figure 5.17, the analysis result of the active part is compared with the test behavior.

5.2.2.5 IP+OOP (1/6 Capacity) Combined Loading

In Model 5, the combined in-plane and out-of-plane loading is applied to the Type 1 wall, with the out-of-plane load level of 1/6 of the capacity corresponding to 1 ton. The properties of materials used are listed in Table 5.3 and Table 5.4.

The analysis results of Model 5 are verified with test results in Figure 5.18. The results coincide with each other for each infill material property. The best fit is observed when the hysteretic material is chosen for the infill material. The convergence problem, as in Model 4, has yet to be experienced again. Moreover, the descending portion of the unloading curve fits the test behavior. The maximum base shear is calculated to be 5% less than the test result.

The conc01 material model fits the maximum load capacity of the test with only a 1% difference. However, the unloading part of the last cycle shows a smaller dissipated energy than the test result. Nevertheless, each alternative of infill material properties shows accurate and acceptable results.

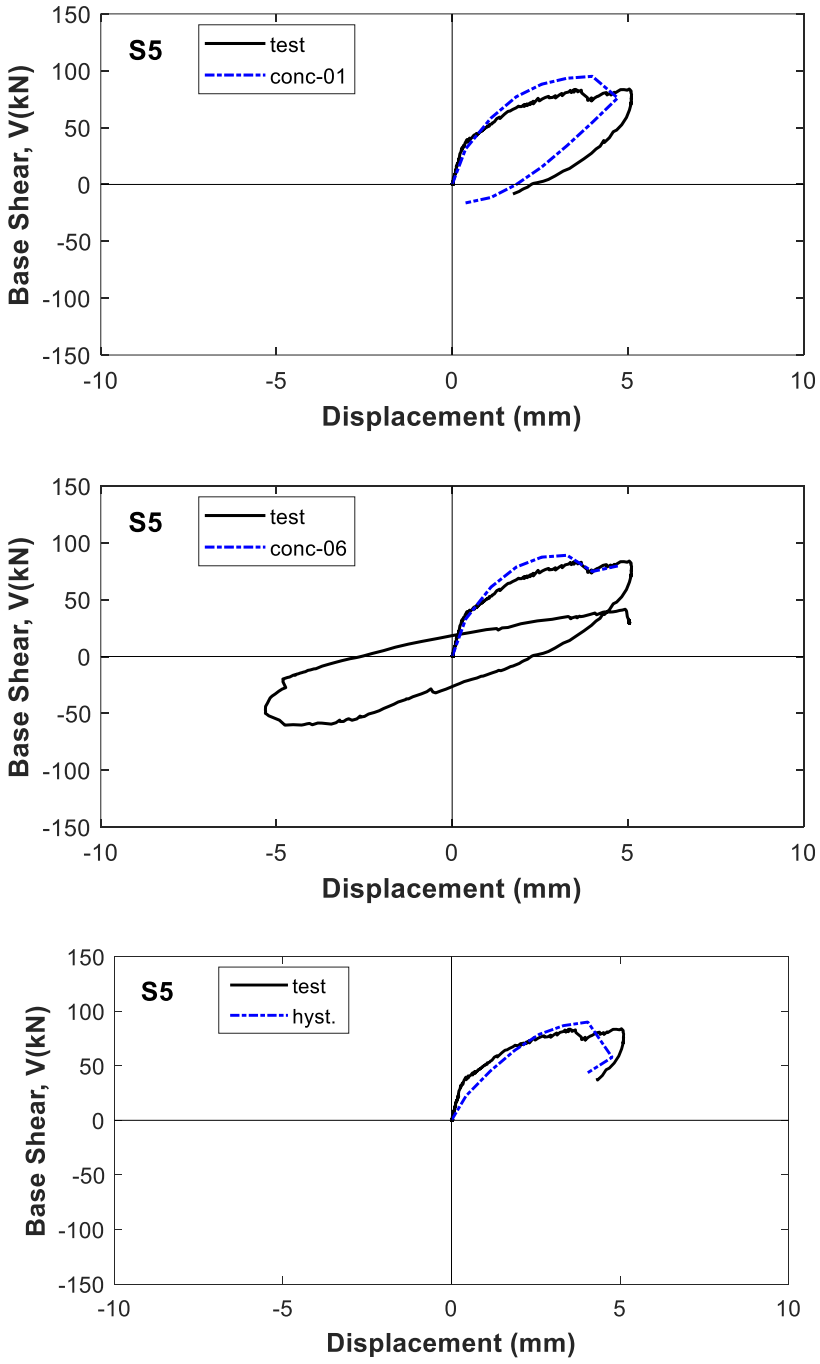

Figure 5.17. Verification of Model 4 Analysis with test

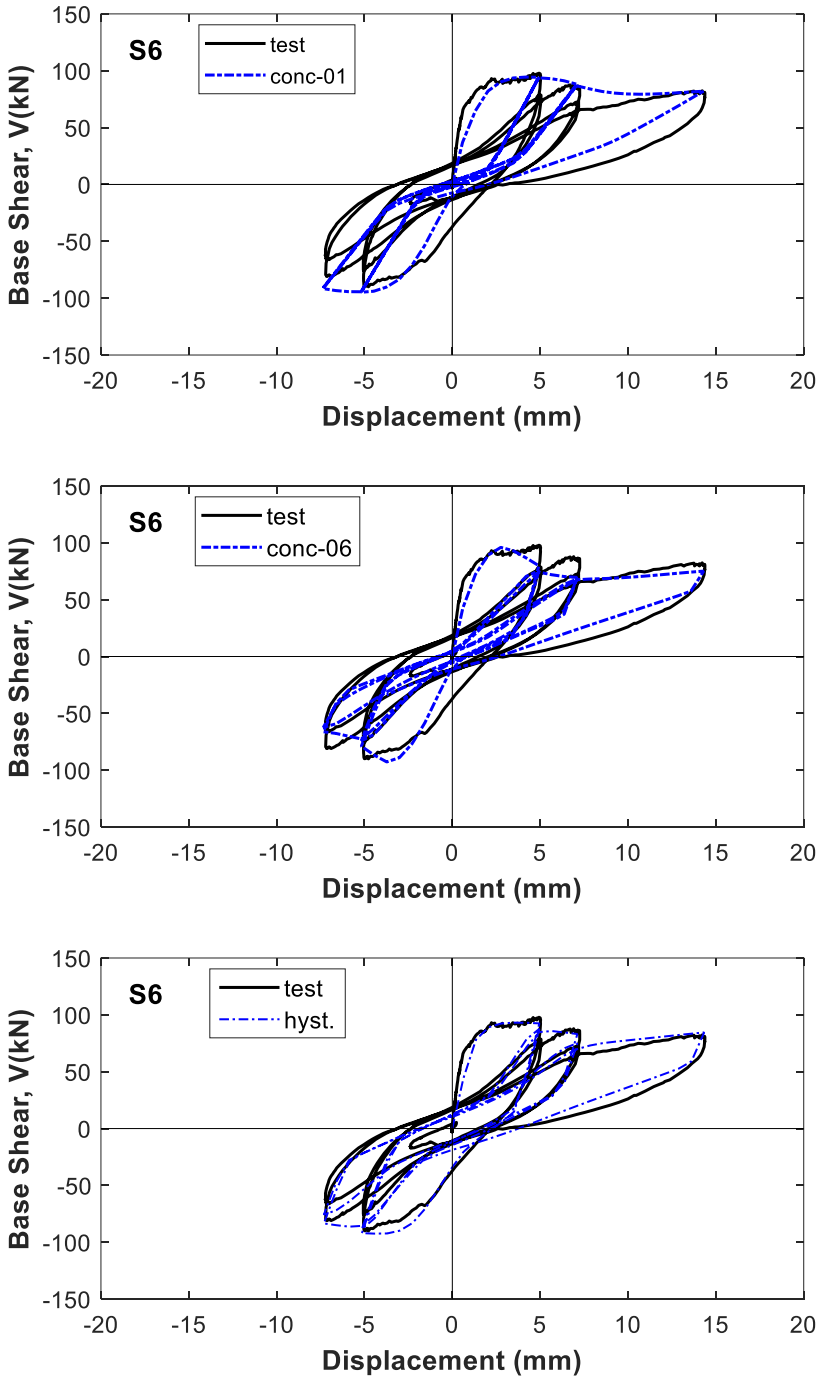

Figure 5.18. Verification of Model 5 Analysis with test

5.2.3 Type 2 Wall with plaster

The next part investigates the behavior of Type 2 walls under different loading conditions. The AAC block has a thickness of 100 mm and is positioned flat surface inside the frame. Then, 35 mm (CLIP) cementitious lightweight insulation panels are applied on the surface of the infill wall and frame. Plaster applied on both surfaces of the wall with 2 layers. The strut parameters are calculated like Binici and Ozcebe's (2008) study with modifications. The total thickness of the wall is the summation of infill, CLIP, and plaster thicknesses.

$$t_{st} = t_p + t_{in} + t_{clip} \tag{5.18}$$

$$f_{mc} = \frac{f_{in}t_{in} + f_m t_p + f_{clip}t_{clip}}{t_{st}} \tag{5.19}$$

$$E_{sm} = \frac{E_{in}t_{in} + E_m t_p + E_{clip}t_{clip}}{t_{st}} \tag{5.20}$$

The compressive strength is 0.42 MPa, and the modulus of elasticity is 1000 MPa for the CLIP material, according to the technical approval document of the Turkish Standards Institute (TSE/UTO/14-029).

The calculated strut parameters are listed in Table 5.5- Table 5.7.

Table 5.5. Parameter for the calculation of effective strut material properties

t_p (mm)	t_{in} (mm)	h (mm)	L (mm)	cosθ	M_{pb} (kNm)	M_{pc} (kNm)	M_{pj} (kNm)
20	100	1300	2300	0.87	28	27.8	27.8

Table 5.6. Summary of strut parameters with presence of plaster- Type 2

	t_{st} (mm)	f_c (MPa)	E_{sm} (MPa)	α	w_s (mm)	A_{st} (mm^2)
Model 6	142.5	2.22	1998.51	0.348	339	48307.6
Model 7	155	3.8	3685	0.255	284	44002

Table 5.7. Summary of calculation the effective strut width

	V_{ss} (kN)	V_{cc} (kN)	V_{us} (kN)	f_{us} (MPa)	ε_{crs}	a (mm)
Model 6	181	79	79	1.64	0.0008	316
Model 7	289	147	147	3.35	0.0009	295

Two different loading conditions are investigated for Type-2 infill walls. In Model 6, the only out-of-plane loading is tested. In Model-7, the combined in-plane and out-of-plane load application test is evaluated with analytical results.

5.2.3.1 OOP Loading

In this part, the test verification with an analytical model named Model 6 is described to understand the behavior of the Type 2 wall system under the effect of pure out-of-plane loading with the help of airbags. Since out-of-plane loading is applied, the total thickness of the wall including the plaster, CLIP, and AAC wall, is calculated as the thickness of struts. The out-of-plane applied load versus mid-displacement graph is drawn in Figure 5.19. The maximum load levels fit each other. The stiffness of the two graphs coincides up to 30 kN load level; then, the analysis model stiffness decreases when compared with the test result.

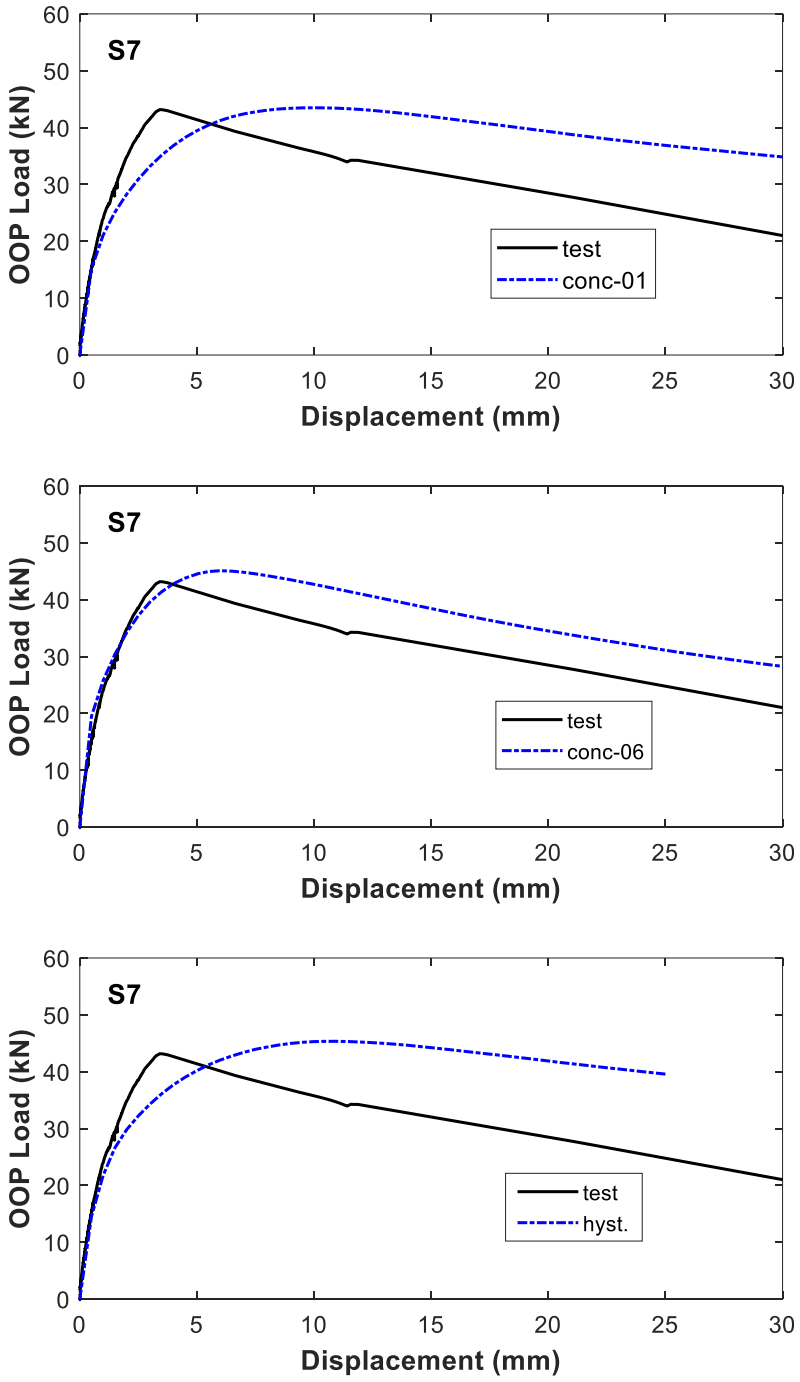

Figure 5.19. Verification of Model 6 Analysis with test (OOP)-Type2

The maximum load-carrying capacity of the wall is calculated as 43.5, 45.1, and 45.34 kN respectively, for conc01, conc06, and hysteretic material properties. The test result is 46.16 kN. The best fit is observed in the conc06 analysis model.

5.2.3.2 IP+OOP (1/3 Capacity) Combined Loading

The last analysis model verifies the Type-2 wall under the combined out-of-plane and in-plane loading test. The thicknesses of the struts are considered as 100 mm in the model for the stiffness, whereas the effective compressive strength of struts is calculated by taking the properties of AAC block, CLIP, and plaster into consideration. The thickness of the wall inside the frame plays a role in the performance of the in-plane loading.

The comparison of the test result and analysis result is shown in Figure 5.20. The initial stiffnesses of each graph coincide. However, the maximum base shear is approximately 10% less than the test result. The best fit is observed for the hysteretic material analysis results.

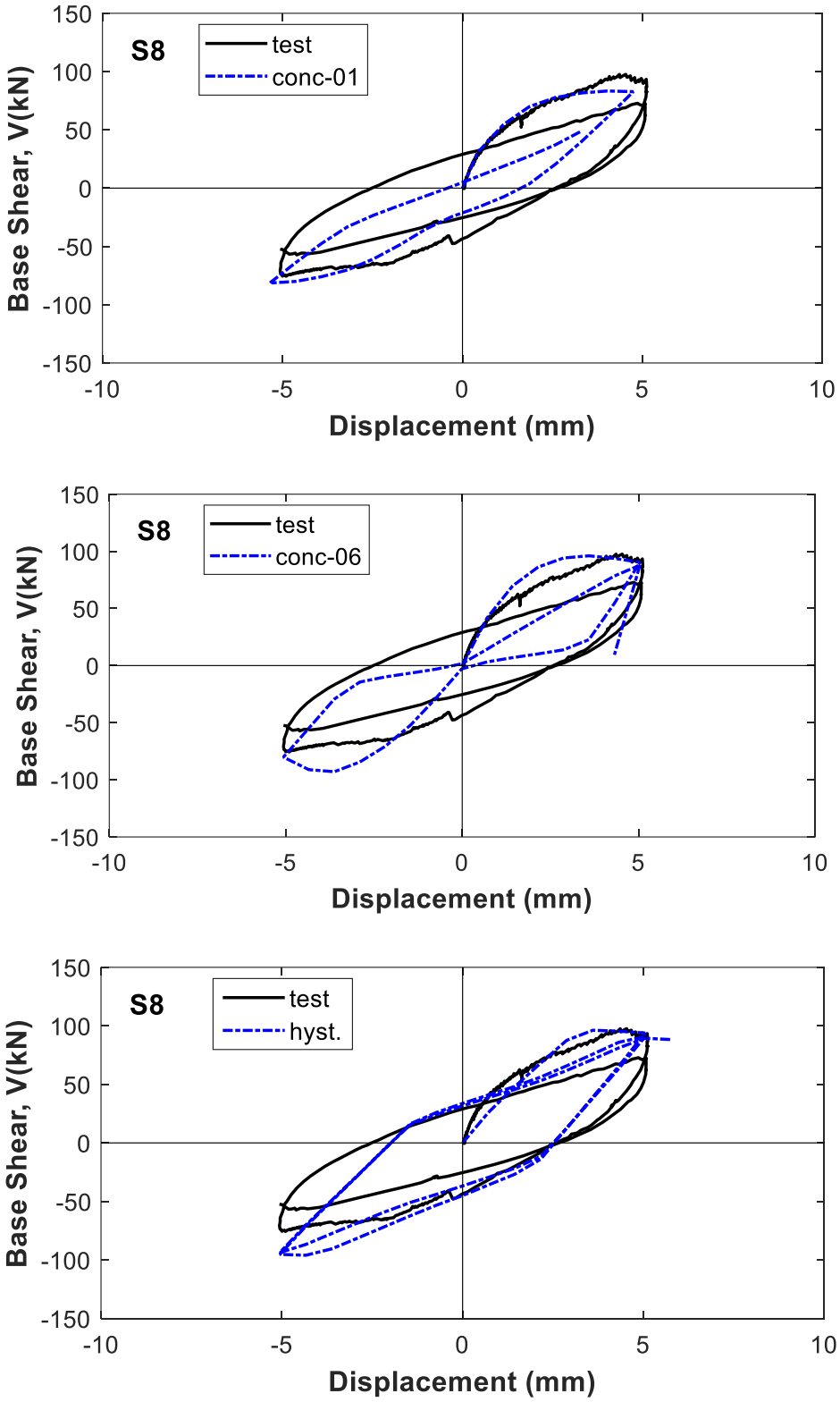

Figure 5.20. Verification of Model 7 Analysis with test

According to the comparisons of modeling load-displacement behavior of the wall types under different loading conditions with the experimental test results, it is obvious that modeling parameters are successful in the simulation of the laboratory test behavior. Type 1 and Type 2 walls were modeled for in-plane loading and the combined effect of in-plane and out-of-plane loading cases.

CHAPTER 6

CONCLUSIONS

6.1 Summary

This study mainly focused on the performance of autoclaved aerated concrete (AAC) blocks infill walls with insulated panels of minepor under different types of loadings of in-plane and out-of-plane loading, and a combination of two loads simultaneously. Two different types of walls were prepared by adjusting the location of AAC blocks and cementitious lightweight insulated panels. In the Type 1 wall, the AAC blocks were positioned eccentrically to the reinforced concrete (RC) frame, and then the RC frame were covered with minepor insulation plates. In the second wall system in Type 2, the AAC blocks were in line with the center of the RC frame. Then, Minepor plates were covered on the entire surface of the AAC blocks and RC frame. The seismic performance of AAC infill walls with Type 1 and Type 2 walls was examined within the scope of this dissertation. In that spirit, an experimental study was conducted at the Structural and Earthquake Engineering Laboratory of Middle East Technical University. Eight reinforced concrete frame infill walls were tested to obtain the experimental data required to assess loading types. Some of the frames were tested under reversed cyclic lateral loadings, and in other cases, the out-of-plane loading was applied to the specimens using an airbag system. Moreover, the combined effect of in-plane and out-plane loadings was applied simultaneously in the other tests. The test results regarding strength, ductility, drift ratios, and dissipated energy level were investigated and compared.

A numerical model of the infilled frame specimens was generated and performed using OpenSees software with three-dimensional modeling. Comparing the analytical and experimental test results is crucial for evaluating and verifying the

models' reliability. By comparing the ultimate strength, initial stiffness, and drift capacities, it provides insights into how accurately the numerical model represents the real-world behavior of the specimens. Such comparisons are valuable for assessing the model's effectiveness and improving future design and analysis methods.

6.2 Conclusions

In the light of the conducted study, the following conclusions can be summarized:

- Interaction between in-plane (IP) and out-of-plane (OOP) responses was found to be important, similar to previous studies estimating the performance and capacity of infilled RC frames.
- The level of out-of-plane loading adversely affected the ultimate drift ratio of in-plane loading. The drift capacity was about 1.5% under pure IP loading, whereas it reduced to about 0.4% under combined IP and OOP demands under 1/3 of out-of-plane load level capacity.
- It is interesting to note that plaster's presence in the system affected the load-carrying capacity positively. The compressive strengths of the plaster played a significant role in determining the deformation capacity and maximum load. This suggests that the plaster enhances the overall structural integrity and contributes to the system's ability to withstand deformation and carry higher loads.
- Complete installation of insulation material to the wall surface (Type 2) resulted in slightly lower deformation and load-carrying capacity than the Type 1 under the out-of-plane loading. Cementitious lightweight insulation panels (CLIPs) were found to accelerate the formation of weak interfaces, resulting in premature OOP failures.
- Mineral-based CLIPs bonded to AAC infill walls had a lower deformation capacity than plain AAC walls under pure in-plane loading and combined in-plane and out-of-plane loading.

- CLIPs can be used as supplementary insulation with eccentric infill wall arrangements if designed as fragile components with limited drift capacity (around 0.4% under combined IP and OOP loading). This can be achieved by using stiff lateral force-resisting elements.
- Based on the information gathered from the results of this study, it is not recommended to use either Type 1 or Type 2 with existing drift limits in the Turkish Earthquake Code.
- It is suggested to check the combined in-plane and out-of-plane capacity of infill walls and limit inter-story drift demands based on the developed interaction limits of OOP capacity and IP drift capacity for design purposes.

6.3 Recommendations for Future Research

The current study does not consider the presence of openings in the infill wall system with insulated panels. However, it might be beneficial for researchers to investigate Type 1 wall systems with various dimensions of openings. This expanded analysis could provide valuable insights into the performance and behavior of such systems under different loading conditions.

The aspect ratio of the infill wall system can be explored by studying different frame specimen sizes, but this falls outside the scope of the current research. It is understandable to focus on specific aspects and limitations within a study.

It is suggested to continue with new test programs that incorporate sliding anchors or innovative systems to protect Type 1 or Type 2 CLIP+AAC systems for seismic behavior improvement.

It is suggested to conduct nonlinear dynamic analysis on building models by using the modeling approach suggested in Chapter 5 calibrated with test results. In this way, it will be possible to observe the expected actual dynamic performance.

With proper insulation, green buildings play a crucial role in reducing energy consumption and minimizing environmental impact. Developing new techniques for applying insulated panels can further enhance the energy efficiency of buildings. Some possible areas of improvement include developing more efficient installation methods, using innovative insulation materials, and optimizing the design and construction process to minimize thermal bridging. By continuously advancing these techniques, we can create greener and more sustainable buildings for the future.

REFERENCES

Abrams DP, Angel R, Uzarski J. (1996). Out-of-plane strength of unreinforced masonryinfill panels. Earthq Spect, 12(4):825–44.

ACI Committee 523 (2009). Guide for design and construction with autoclaved aerated concrete panels. ACI 5223.4R-09, Farmington Hills, USA.

Angel R. Behavior of reinforced concrete frames with masonry infill walls (1994). PhD thesis. Illinois: University Illinois at Urbana-Champaingn

Asteris PG, Antoniou ST, Sophianopoulos DS, Chrysostomou CZ. (2011). Mathematical macromodeling of infilled frames: state of the art. J Struct Eng. 2011; 137(12), 1508-17.

Asteris PG, Cavaleri L, Trapani FD, Tsaris AK. (2017). Numerical modelling of out-of plane response of infilled frames: state of the art and future challenges for the equivalent strut macromodels. Eng Struct, 2017; 132: 110–22.

Artino, A., Evola, G., Margani, G., & Marino, E. M. (2019). Seismic and energy retrofit of apartment buildings through autoclaved aerated concrete (AAC) blocks infill walls. *Sustainability (Switzerland)*, *11*(14). https://doi.org/10.3390/su11143939

Binici B., Ozcebe G. (2005). Analysis of infilled reinforced concrete frames strengthened with frps. *Advances in Earthquake Eng. for urban risk reduction*. Springer, Netherlands, 455-470.

Binici B., Ozcebe G. & Ozcelik R. (2007). Analysis and design of FRP composites for seismic retrofit of infill walls in reinforced concrete frames. *Composites Part B: Engineering* 38 (5–6): 575–83. https://doi.org/10.1016/j.compositesb.2006.08.007.

Binici B., Demirel I.O., Aldemir A., Canbay E., Yakut A. (2017). Behaviour of AAC infilled RC frames under in plane and out of plane seismic demands. In: Proc Aust Earthquake Eng Soc Conf, Canberra, Australia.

Binici, B., Canbay, E., Aldemir, A., Demirel, I. O., Uzgan, U., Eryurtlu, Z., Bulbul, K., & Yakut, A. (2019). Seismic behavior and improvement of autoclaved aerated concrete infill walls. *Engineering Structures*, *193*, 68–81. https://doi.org/10.1016/j.engstruct.2019.05.032

Bommer, J.J., Scott, S.G. and Sarma, S.K. (2000). Hazard-consistent earthquake scenarios. Soil Dynamics and Earthquake Engineering, Vol. 19, pp. 219–231

Calvi GM, Bolognini D (1999) Seismic response of reinforced concrete frames infilled with weakly rein-forced masonry panels. J Earthq Eng 5:153–185.

Carrigan S, Hartner M, Hofmann M, Kornadt O, Schoch T (2018). Performance of Multipor WI as exterior insulation. ce papers. 2018;2:73–7.

CEN [2004b] Eurocode 8 – Design of structures for earthquake resistance – part 1: general rules, seismic actions and rules for buildings, EN 1998-1:2004, Brussels, Belgium.

Costa, A. A., Penna, A., & Magenes, G. (2011). Seismic performance of Autoclaved Aerated Concrete (AAC) masonry: From experimental testing of the in-plane capacity of walls to building response simulation. *Journal of Earthquake Engineering*, *15*(1), 1–31. https://doi.org/10.1080/13632461003642413.

Demirel İ.O., Yakut A. & Binici B. (2018). Dolgu duvarların düzlem dışı yönde hava yastığı ile deneyi. *Anadolu Üniversitesi Bilim ve Teknoloji Dergisi -B Teorik Bilimler*, 6, 133–140. https://doi.org/10.20290/aubtdb.489940.

Demirel İ.O., (2023). Infilled reinforced concrete frame performance under seismic actions, Doctor of Philosophy Thesis, Middle East Technical University.

El-Dakhakhni W.W., Elgaaly M., and Hamid A.A. (2003). Three-strut model for concrete masonry infilled steel frames, *ASCE, Journal of Structural Engineering*, 129(2), 177-185.

Erdem, I., Akyuz, U., Ersoy, U., & Ozcebe, G. (2006). An experimental study on two different strengthening techniques for RC frames, *Engineering Structures* 28, 1843–1851.

FEMA (2000). Prestandard and commentary for the seismic rehabilitation of buildings. FEMA-356, Washington, DC.

FEMA (1998). Evaluation of earthquake damaged concrete and masonry wall buildings: basic procedures manual. FEMA-306, Washington, DC.

Ferretti D, Michelini E, Rosati G.(2015) Mechanical characterization of autoclaved aerated concrete masonry subjected to in-plane loading: experimental investigation and FE modeling. Constr Build Materials; 98: 353–65.

Fiore, A., Netti, A., & Monaco, P. (2012). The influence of masonry infill on the seismic behaviour of RC frame buildings. *Engineering Structures*, *44*, 133–145. https://doi.org/10.1016/j.engstruct.2012.05.023

Gokmen, F., Binici, B., Aldemir, A., Taghipour, A., & Canbay, E. (2019). Seismic behavior of autoclaved aerated concrete low rise buildings with reinforced wall panels. *Bulletin of Earthquake Engineering*, *17*(7), 3933–3957. https://doi.org/10.1007/s10518-019-00630-3

Hashemi A, Mosalam KM (2006). Shake-table experiment on reinforced concrete structure containing masonry infill wall. Earthq Eng Struct Dyn;35:1827–52.

Hashemi A, Mosalam KM (2007). Seismic evaluation of reinforced concrete buildings including effects of masonry infill walls PEER Report. Berkeley: University of California.

Huang, Q., Guo, Z., & Kuang, J. S. (2016). Designing infilled reinforced concrete frames with the "strong frame-weak infill" principle. *Engineering Structures*, *123*, 341–353. https://doi.org/10.1016/j.engstruct.2016.05.024

Kadysiewski S, Mosalam KM (2009). Modeling of unreinforced masonry infill walls considering in-plane and out-of-plane interaction PEER Report 2008/102. Berkeley: University of California; January 2009.

Kałuza, M. (2017). Analysis of In-plane Deformation of Walls Made Using AAC Blocks Strengthened by GFRP Mesh. *Procedia Engineering*, *193*, 393–400. https://doi.org/10.1016/j.proeng.2017.06.229

Kasapgil, S. M., Binici, B., & Canbay, E. (2021). Seismic behavior of AAC infill walls insulated with cementitious lightweight panels in reinforced concrete frames. *Engineering Structures*, *248*. https://doi.org/10.1016/j.engstruct.2021.113215

Kent, D. C., and Park, R., (1971). Flexural members with confined concrete, *Journal of Structures Division*, ASCE, ST7(97), 1969–1990.

Kurt E.G., Binici B., Kurç Ö., Canbay E., Akpinar U., & Ozcebe G. (2011). Seismic performance of a deficient reinforced concrete test frame with infill walls. *Earthquake Spectra* 27 (3): 817–34. https://doi.org/10.1193/1.3609876.

Liu Y, Li G. Behavior of steel frames with and without AAC infilled walls subjected tostatic and cyclic horizontal loads (2004). In:13th World Conf Earthquake Eng, Vancouver, B.C.,Canada.

Liu, Y., Chen, G., Wang, Z., Chen, Z., Gao, Y., & Li, F. (2020). On the seismic performance of autoclaved aerated concrete self-insulation block walls. *Materials*, *13*(13), 1–13. https://doi.org/10.3390/ma13132942

Mazzoni, S., McKenna, H., Scott, M. H., and Fenves, G. L., (2009). OpenSees Manual, Pacific Earthquake Engineering Research Center, http://OpenSees.berkeley.edu.

Mehrabi AB, Shing PB, Schuller M, Noland J.(1996). Experimental evaluation of masonry infilled RC frames. J. Struct. Eng. 122(3), 228 –37.

Miccoli, L. (2018). Seismic performances of AAC masonry: a review of experimental and numerical approaches. *Mauerwerk*, *22*(5), 314–328. https://doi.org/10.1002/dama.201800023

Milanesi, R. R., Morandi, P., & Magenes, G. (2018). Local effects on RC frames induced by AAC masonry infills through FEM simulation of in-plane tests. *Bulletin of Earthquake Engineering*, *16*(9), 4053–4080. https://doi.org/10.1007/s10518-018-0353-5

Okuyucu D., (2011). Effect of frame aspect ratio on the seismic performance improvement of panel strengthening technique, Doctor of Philosophy Thesis, Middle East Technical University.

Ozcebe, G., Ersoy U., Tankut T., Akyuz U.& Erduran E. (2004). Rehabilitation of existing reinforced concrete structures using CFRP fabrics. *13th World Conference on Earthquake Engineering*, no. 1393.

Özgenoğlu M., (2015). Comparison of ASCE/SEI Standard (2010) and Modal Pushover Based Ground Motion Scaling Procedures for Pre-Tensioned Concrete Bridges, Master of Science Thesis, Middle East Technical University.

Özcan, O., Binici, B. and Özcebe, G., (2008).Improving Seismic Performance of Deficient Reinforced Concrete Columns Using Carbon Fiber-Reinforced Polymers, Engineering Structures, Volume 30, pp. 1632-1646.

Pantò, B., Silva, L., Vasconcelos, G., & Lourenço, P. B. (2019). Macro-modelling approach for assessment of out-of-plane behavior of brick masonry infill walls. *Engineering Structures*, *181*, 529–549. https://doi.org/10.1016/j.engstruct.2018.12.019

Penna A, Calvi GM, Magenes G, Costa AA (2008). Seismic performance of AAC infill and bearing walls with different reinforcement solutions. In: Proc 14th Int Brick Block masonry. Sydney, Australia.

Penna, A., Mandirola, M., Rota, M., & Magenes, G. (2015). Experimental assessment of the in-plane lateral capacity of autoclaved aerated concrete (AAC) masonry walls with flat-truss bed-joint reinforcement. *Construction and Building Materials*, *82*, 155–166. https://doi.org/10.1016/j.conbuildmat.2015.02.057

Priestley MJN, Bridgeman DO. (1974). Seismic resistance of brick masonry walls. BullNZ Natl Soc Earthq Eng 1974;7(4):167–87

Rosti, A., Penna, A., Rota, M., & Magenes, G. (2016). In-plane cyclic response of low-density AAC URM walls. *Materials and Structures/Materiaux et Constructions*, *49*(11), 4785–4798. https://doi.org/10.1617/s11527-016-0825-5

Saneinejad A., and Hobbs B. (1995). Inelastic design of infilled frames, *ASCE, Journal of Structural Engineering*, 121(4), 634-650.

Schwarz S, Hanaor A, Yankelevsky DZ.(2015). Experimental response of reinforced concrete frames with aac masonry infill walls to in-plane cyclic loading. Struct 2015;3:306 –19.

Shing, P. B., and Stavridis, A. (2014). "Analysis of seismic response of masonry-infilled RC frames through collapse." ACI Struct. J., 297, 1–20.

Sucuoglu, H., & Siddiqui, U. A. (2014). Pseudo-dynamic testing and analytical modeling of AAC infilled RC frames. *Journal of Earthquake Engineering*, *18*(8), 1281–1301. https://doi.org/10.1080/13632469.2014.932723

Sucuoglu, H., Lin, W.W., Binici B. & Ezzatfar P. (2014). Pseudo-dynamic testing, performance assessment, and modeling of deficient reinforced concrete frames. *ACI Structural Journal*, 2004; 111 (5): 1203-1212.

Tanner JE, Varela JL, Klingner RE, Brightman MJ, Cancino U. (2005). Seismic testing of autoclaved aerated concrete shearwalls: a comprehensive review. *ACI Struct J*, 2005; 102-S37: 374–82.

Timoshenko S, Woinowsh-Krieger S. Theory of plates and shells. McGraw-Hill;1959.

Todorovic, L. (2019). Out of plane seismic performance of AAC infill walls with openings. Master of Science Thesis, Middle East Technical University and Istituto Universitario di Studi Superiori di Pavia.

Todorovic, L., Demirel, I. O. & Binici B. (2020). Effect of openings on the seismic response of AAC infilled frames and an innovative method to improve performance. *International Journal of Masonry Research and Innovation*, 5(2), 226–247. https://doi.org/10.1504/ijmri.2020.106333

Tomaževič, M., & Gams, M. (2012). Shaking table study and modelling of seismic behaviour of confined AAC masonry buildings. *Bulletin of Earthquake Engineering*, *10*(3), 863–893. https://doi.org/10.1007/s10518-011-9331-x

Trapani, F. D., Shing, P. B., & Cavaleri, L. (2018). Macroelement model for in-plane and out-of-plane responses of masonry infills in frame structures. *J. Struct. Eng, 144*(2), 04017198th ser., 1-13.

Turgay T., Durmus M.C., Binici B. & Ozcebe G. (2014). Evaluation of the predictive models for stiffness, strength and deformation capacity of RC fanes with masonry infill walls. *Journal of Structural Engineering* 140 (10): 06014003. https://doi.org/10.1061/(asce)st.1943- 541x.0001069.

Turkish Earthquake Code (TEC2007). Specifications for the buildings to be constructed in disaster areas, Ministry of Public Works and Settlement, Ankara, Turkey; 2007.

Turkish Earthquake Code (TEC2019), Ministry of Public Works and Settlement, Ankara, Turkey; 2019.

Turkish Standards Institution (2019). Mineral-based cementitious heat insulation plates. National Technical Approval, Aerated Concrete Thermal Insulation Board, TSI/NTA 14-029.

Turnsek V, Sheppard P (1980) The shear and flexural resistance of masonry walls. In: Proceedings of international research conference on earthquake engineering, Skopje,pp 517–573.

Varela, J. L., Tanner, J. E., & Klingner, R. E. (2006). Development of seismic force reduction and displacement amplification factors for autoclaved aerated concrete structures. *Earthquake Spectra*, *22*(1), 267–286. https://doi.org/10.1193/1.2166034

Vecchio FJ, Collins MP (1986) The modified compression-field theory for reinforced concrete elementssubjected to shear. ACI Struct J 83:219–23

Zhenggang C, Peng D, Feng F, Ming F (2017). Cyclic testing and parametric analyses of the fabricated steel frames infilled with autoclaved aerated concrete panels. Adv Struct Eng, 2017; 20(4): 629–40.

Zovkic, J., Sigmund, V., & Guljas, I. (2013). Cyclic testing of a single bay reinforced concrete frames with various types of masonry infill. *Earthquake Engineering and Structural Dynamics*, *42*(8), 1131–1149. https://doi.org/10.1002/eqe.2263

APPENDICES

A. Material properties of test samples of AAC mortar, CLIP adhesive and plaster

1) **S1 (IP model- Type 1 wall)** Date of Experiment= 18.05.2018

Flexural Strength (Test Specimen 40*40*100mm, Loading Rate=0.26 kN/s)

	Sample	Weight (gr)	Bending force (kN)	Bending Stress (MPa)	Date of casting
AAC mortar	1	422	1.01	2.4	16.05.2018
	2	422.8	0.21	0.5	
	3	425	0.16	0.4	
CLIP Adhesive	1	396.3	0.82	1.9	16.05.2018
	2	402	0.81	1.9	
	3	398.8	0.95	2.2	
Plaster	1	No plaster exists			
	2				
	3				

Uniaxial Compressive Strengths of Halves (Loading Rate=1.5 kN/s)

	Sample	Compressive Force (kN)	Compressive Stress (MPa)
AAC mortar	1-1	2.89	1.8
	1-2	2.81	1.8
	2-1	2.81	1.8
	2-2	2.61	1.6
	3-1	2.71	1.7
	3-2	2.56	1.6
CLIP Adhesive	1-1	7.31	4.6
	1-2	7.88	4.9
	2-1	7.06	4.4
	2-2	8.03	5
	3-1	6.65	4.2
	3-2	6.39	4

Uniaxial Compressive Strengths of 50x50x50 mm Cubic Samples

	Sample	Weight (gr)	Compressive Force (kN)	Compressive Stress (MPa)	Date of casting
AAC mortar	1	209.2	2.61	1.04	16.5.2018
	2	209.8	2.92	1.17	
	3	210.3	3.02	1.21	
CLIP Adhesive	1	193.1	10.18	4.07	16.5.2018
	2	191.7	9.97	3.99	
	3	192.3	10.13	4.05	
Plaster	1	No plaster exists.			
	2				
	3				

2) **S2 (IP model- Type 1 wall)** Date of Experiment= 20.06.2018

Flexural Strength (Test Specimen 40*40*100mm, Loading Rate=0.26 kN/s)

	Sample	Weight (gr)	Bending force (kN)	Bending Stress (MPa)	Date of casting
AAC mortar	1	398.2	1.23	2.9	05.06.2018
	2	402.7	1.34	3.1	
	3	404.6	1.33	3.1	
CLIP Adhesive	1	402.9	1.39	3.3	05.06.2018
	2	398.7	1.38	3.2	
	3	398.2	1.56	3.7	
Plaster	1	No plaster exists			
	2				
	3				

Uniaxial Compressive Strengths of Halves (Loading Rate=1.5 kN/s)

	Sample	Compressive Force (kN)	Compressive Stress (MPa)
AAC mortar	1-1	14.99	9.4
	1-2	15.91	9.9
	2-1	13.09	8.2
	2-2	13.81	8.6
	3-1	14.68	9.2
	3-2	15.6	9.8
CLIP Adhesive	1-1	19.95	12.5
	1-2	21.3	13.3
	2-1	20.6	12.9
	2-2	19.49	12.2
	3-1	21.55	13.5
	3-2	20.8	13

Uniaxial Compressive Strengths of 50x50x50 mm Cubic Samples

	Sample	Weight (gr)	Compressive Force (kN)	Compressive Stress (MPa)	Date of casting
AAC mortar	1	195.1	18.72	7.49	05.06.2018
	2	196.7	19.03	7.61	
	3	197	17.8	7.12	
CLIP Adhesive	1	201.1	24.4	9.76	05.06.2018
	2	197.6	23.45	9.38	
	3	198.7	24.25	9.70	
Plaster	1	No plaster exists.			
	2				
	3				

3) **S3 (IP model- Type 1 wall)** Date of Experiment= 03.04.2018

Flexural Strength (Test Specimen 40*40*100mm, Loading Rate=0.26 kN/s)

	Sample	Weight (gr)	Bending force (kN)	Bending Stress (MPa)	Date of casting
AAC mortar	1	392.39	1.72	4.0	19.3.2018
	2	393.12	2.01	4.7	
	3	394.42	1.91	4.5	
CLIP Adhesive	1	377.89	1.22	2.9	19.3.2018
	2	381.02	1.25	2.9	
	3	374.18	1.54	3.6	
Plaster	1	406.23	1.58	3.7	20.3.2018
	2	401.97	1.41	3.3	
	3	399.6	1.54	3.6	

Uniaxial Compressive Strengths of Halves (Loading Rate=1.5 kN/s)

	Sample	Compressive Force (kN)	Compressive Stress (MPa)
AAC mortar	1-1	24.6	15.4
	1-2	25.7	16.1
	2-1	27.7	17.3
	2-2	27.85	17.4
	3-1	28.9	18.1
	3-2	26.8	16.8
CLIP Adhesive	1-1	14.73	9.2
	1-2	14.83	9.3
	2-1	15.91	9.9
	2-2	13.25	8.3
	3-1	16.01	10
	3-2	15.6	9.8
Plaster	1-1	16.06	10
	1-2	16.27	10.2
	2-1	15.65	9.8
	2-2	14.99	9.4
	3-1	15.75	9.8
	3-2	15.4	9.6

Uniaxial Compressive Strengths of 50x50x50 mm Cubic Samples

	Sample	Weight (gr)	Compressive Force (kN)	Compressive Stress (MPa)	Date of casting
AAC mortar	1	206.74	38.15	15.3	19.3.2018
	2	208.91	40.65	16.3	
	3	214.22	45.1	18.0	
CLIP Adhesive	1	180.99	21.75	8.7	19.3.2018
	2	182.8	23.7	9.5	
	3	179.66	22	8.8	
Plaster	1	189.13	20.55	8.2	20.3.2018
	2	189.98	18.21	7.3	
	3	189.7	18.21	7.3	

4) S4 (OOP model- Type 1 wall) Date of Experiment= 22.01.2018

Flexural Strength (Test Specimen 40*40*100mm, Loading Rate=0.26 kN/s)

	Sample	Weight (gr)	Bending force (kN)	Bending Stress (MPa)	Date of casting
AAC mortar	1	406	1.93	4.5	27.12.2017
	2	406	1.88	4.4	
	3	400	2.15	5	
Plaster	1	408	2.71	6.4	28.12.2017
	2	413	2.67	6.3	
	3	400	3.03	7.1	

Uniaxial Compressive Strengths of Halves (Loading Rate=1.5 kN/s)

	Sample	Compressive Force (kN)	Compressive Stress (MPa)
AAC mortar	1-1	18.7	11.7
	1-2	18.4	11.5
	2-1	20.2	12.6
	2-2	14.5	9.1
	3-1	18.4	11.5
	3-2	21.9	13.7
Plaster	1-1	26.2	16.3
	1-2	21.3	13.3
	2-1	31.9	19.9
	2-2	25.1	15.7
	3-1	28.4	17.7
	3-2	22.7	14.2

Uniaxial Compressive Strengths of 50x50x50 mm Cubic Samples

	Sample	Weight (gr)	Compressive Force (kN)	Compressive Stress (MPa)	Date of casting
AAC mortar	1	193	17.95	7.2	27.12.2017
	2	193	22	8.8	
	3	193	22.5	9.0	
CLIP Adhesive	1	194	32.6	13	27.12.2017
	2	191	33.45	13.4	
	3	196	38.05	15.2	
Plaster	1	200	34.2	13.7	28.12.2017
	2	200	39.4	15.7	
	3	200	40.8	16.3	

5) **S5 (IP+OOP Model- Type 1 wall)** Date of Experiment= 14.02.2018

Flexural Strength (Test Specimen 40*40*100mm, Loading Rate=0.26 kN/s)

	Sample	Weight (gr)	Bending force (kN)	Bending Stress (MPa)	Date of casting
AAC mortar	1	384.2	1.7	4	02.02.2018
	2	392.4	1.32	3.1	
	3	387.5	1.73	4	
CLIP Adhesive	1	393.6	1.21	2.8	5.2.2018
	2	390.6	1.27	3	
	3	393.2	1.18	2.8	
Plaster	1	415.6	1.68	3.9	5.2.2018
	2	416.3	1.65	3.9	
	3	421.1	1.67	3.9	

Uniaxial Compressive Strengths of Halves (Loading Rate=1.5 kN/s)

	Sample	Compressive Force (kN)	Compressive Stress (MPa)
AAC mortar	1-1	18.16	11.3
	1-2	17.8	11.1
	2-1	15.7	9.8
	2-2	14.48	9
	3-1	18.36	11.5
	3-2	18.06	11.3
CLIP Adhesive	1-1	15.91	9.9
	1-2	16.06	10
	2-1	14.48	9
	2-2	15.04	9.4
	3-1	14.88	9.3
	3-2	16.11	10.1
Plaster	1-1	26.85	16.8
	1-2	27.25	17
	2-1	27.45	17.2
	2-2	26.45	16.5
	3-1	28.25	17.7
	3-2	25.65	16

Uniaxial Compressive Strengths of 50x50x50 mm Cubic Samples

	Sample	Weight (gr)	Compressive Force (kN)	Compressive Stress (MPa)	Date of casting
AAC mortar	1	187.8	25.6	10.2	2.2.2018
	2	185.6	27	10.8	
	3	192.2	24.3	9.7	
CLIP Adhesive	1	192.5	26.5	10.6	5.2.2018
	2	191.6	25.5	10.2	
	3	192.2	27.55	11.0	
Plaster	1	221.5	52.2	20.9	5.2.2018
	2	215.8	49.1	19.6	
	3	224.4	46.9	18.8	
	4	218.3	42.15	16.9	

6) **S6 (IP+OOP Model- Type 1 wall)** Date of Experiment= 13.03.2018

Flexural Strength (Test Specimen 40*40*100mm, Loading Rate=0.26 kN/s)

	Sample	Weight (gr)	Bending force (kN)	Bending Stress (MPa)	Date of casting
AAC mortar	1	430.02	1.17	2.7	5.3.2018
	2	438.84	1.48	3.5	
	3	431.26	1.48	3.5	
CLIP Adhesive	1	380.8	1.09	2.6	5.3.2018
	2	382.02	1.07	2.5	
	3	378.21	1	2.3	
Plaster	1	415.68	1.29	3	6.3.2018
	2	422.89	1.59	3.7	
	3	417.08	1.49	3.5	

Uniaxial Compressive Strengths of Halves (Loading Rate=1.5 kN/s)

	Sample	Compressive Force (kN)	Compressive Stress (MPa)
AAC mortar	1-1	9.77	6.1
	1-2	10.33	6.5
	2-1	12.07	7.5
	2-2	9.46	5.9
	3-1	9.67	6
	3-2	9.36	5.9
CLIP Adhesive	1-1	10.08	6.3
	1-2	10.13	6.3
	2-1	11.61	7.3
	2-2	11.41	7.1
	3-1	9.41	5.9
	3-2	9.16	5.7
Plaster	1-1	19.18	12
	1-2	23.05	14.4
	2-1	25.15	15.7
	2-2	23.5	14.7
	3-1	21.7	13.6
	3-2	21.2	13.2

Uniaxial Compressive Strengths of 50x50x50 mm Cubic Samples

	Sample	Weight (gr)	Compressive Force (kN)	Compressive Stress (MPa)	Date of casting
AAC mortar	1	205.43	17.95	7.2	5.3.2018
	2	208.12	17.03	6.8	
	3	204.73	19.69	7.9	
CLIP Adhesive	1	187.86	17.29	6.9	5.3.2018
	2	184.4	17.54	7.0	
	3	184.19	17.95	7.2	
Plaster	1	204.9	33.65	13.5	6.3.2018
	2	205.23	35.7	14.3	
	3	206.73	35.75	14.3	

7) **S7 (OOP Model Type 2 Wall)** Date of Experiment= 29.05.2019

Flexural Strength (Test Specimen 40*40*100mm, Loading Rate=0.26 kN/s)

	Sample	Weight (gr)	Bending force (kN)	Bending Stress (MPa)	Date of casting
AAC mortar	1	347.29	0.98	2.3	20.5.2019
	2	345.78	0.97	2.3	
	3	341.04	1.1	2.6	
CLIP Adhesive	1	362.65	1.25	2.9	20.5.2019
	2	362.8	1.4	3.3	
	3	363.22	1.33	3.1	
Plaster	1	414.67	1.54	3.6	21.5.2019
	2	404.9	1.31	3.1	
	3	404.7	1.47	3.4	

Uniaxial Compressive Strengths of Halves (Loading Rate=1.5 kN/s)

	Sample	Compressive Force (kN)	Compressive Stress (MPa)
AAC mortar	1-1	12.23	7.6
	1-2	12.23	7.6
	2-1	12.48	7.8
	2-2	10.9	6.8
	3-1	10.49	6.6
	3-2	11.1	6.9
CLIP Adhesive	1-1	14.12	8.8
	1-2	16.47	10.3
	2-1	14.17	8.9
	2-2	13.35	8.3
	3-1	15.14	9.5
	3-2	13.76	8.6
Plaster	1-1	28.15	17.6
	1-2	28	17.5
	2-1	27.2	17
	2-2	29.05	18.2
	3-1	29.6	18.5
	3-2	27.3	17.1

Uniaxial Compressive Strengths of 50x50x50 mm Cubic Samples

	Sample	Weight (gr)	Compressive Force (kN)	Compressive Stress (MPa)	Date of casting
AAC mortar	1	171.06	18.26	7.3	20.5.2019
	2	169.79	14.63	5.9	
	3	171.3	17.85	7.1	
CLIP Adhesive	1	177.25	17.44	7.0	20.5.2019
	2	177.97	17.85	7.1	
	3	178.23	21.7	8.7	
Plaster	1	209.93	46.1	18.4	21.5.2019
	2	203.56	45.2	18.1	
	3	211.18	48	19.2	
	4	208.42	48.8	19.5	

8) **S8 (IP+OOP Model Type 2 wall)** Date of Experiment= 14.05.2019

Flexural Strength (Test Specimen 40*40*100mm, Loading Rate=0.26 kN/s)

	Sample	Weight (gr)	Bending force (kN)	Bending Stress (MPa)	Date of casting
AAC mortar	1	355.4	1.52	3.6	26.4.2019
	2	351.4	1.59	3.7	
	3	350.7	1.45	3.4	
CLIP Adhesive	1	351	1.36	3.2	26.4.2019
	2	352.9	1.43	3.4	
	3	355.8	1.52	3.6	
Plaster-1st layer	1	434.8	1.52	3.6	30.4.2019
	2	441.8	2.04	4.8	
	3	440.5	1.76	4.1	
Plaster-2nd layer	1	414.5	1.14	2.7	30.4.2019
	2	419	1.83	4.3	
	3	429.2	1.1	2.6	

Uniaxial Compressive Strengths of Halves (Loading Rate=1.5 kN/s)

	Sample	Compressive Force (kN)	Compressive Stress (MPa)
AAC mortar	1-1	16.37	10.2
	1-2	15.55	9.7
	2-1	14.94	9.3
	2-2	15.7	9.8
	3-1	15.45	9.7
	3-2	13.91	8.7
CLIP Adhesive	1-1	13.5	8.4
	1-2	12.74	8
	2-1	14.68	9.2
	2-2	16.57	10.4
	3-1	15.24	9.5
	3-2	13.91	8.7
Plaster 1st layer	1-1	31.5	19.7
	1-2	30.6	19.1
	2-1	29.95	18.7
	2-2	30.5	19.1
	3-1	31.35	19.6
	3-2	31.8	19.9
Plaster 2nd layer	1-1	26.9	16.8
	1-2	26.15	16.3
	2-1	25.7	16.1
	2-2	25.45	15.9
	3-1	24.9	15.6
	3-2	24.4	15.2

Uniaxial Compressive Strengths of 50x50x50 mm Cubic Samples

	Sample	Weight (gr)	Compressive Force (kN)	Compressive Stress (MPa)	Date of casting
AAC mortar	1	169.8	21.25	8.5	26.4.2019
	2	170	19.44	7.8	
	3	169.2	21.4	8.6	
CLIP Adhesive	1	173.8	28	11.2	26.4.2019
	2	174.8	22.55	9.0	
	3	174.8	22.45	9.0	
Plaster-1st layer	1	211.6	48.5	19.4	30.4.2019
	2	214.8	45.65	18.3	
	3	214.8	48.15	19.3	
Plaster-2nd layer	1	209.7	33.2	13.3	30.4.2019
	2	215.2	36.35	14.5	
	3	215.3	38.9	15.6	
	4	209.5	37.55	15.0	

B. Opensees Modeling Element Connectivity List

Element No	Start i node	End j node	Element type	Material No
1	1	12	Column	Confined1/ Unconfined 2
101	12	3	Column	Confined1/ Unconfined 2
2	2	15	Column	Confined1/ Unconfined 2
202	15	4	Column	Confined1/ Unconfined 2
3	3	9	Beam	6
4	9	4	Beam	6
5	33	61	Diagonal strut	4
6	61	2	Diagonal strut	4
7	1	62	Diagonal strut	4
8	62	44	Diagonal strut	4
9	7	63	Vertical strut	5
10	63	8	Vertical strut	5
11	1	5	Beam	6
12	5	2	Beam	6
13	13	64	Horizontal strut	5
14	64	14	Horizontal strut	5

NODES: ELEMENTS:

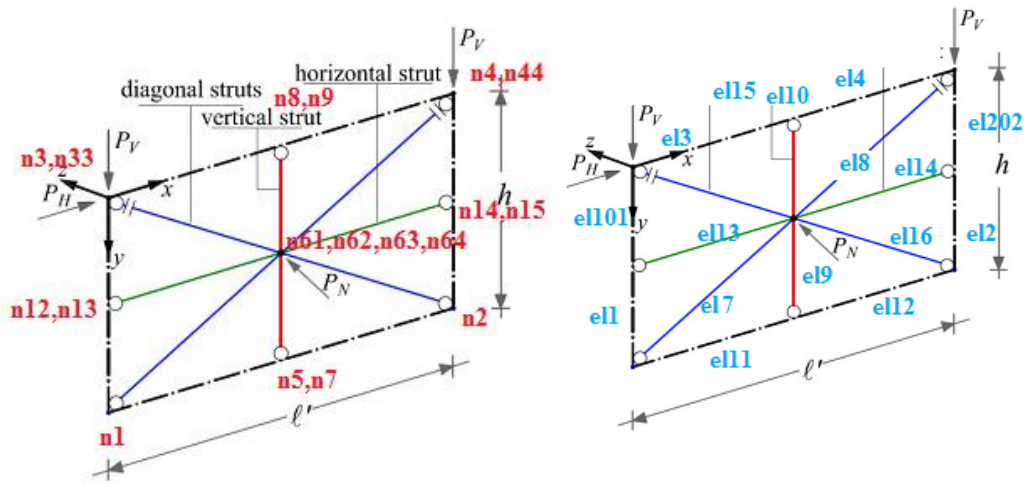

CURRICULUM VITAE

Surname, Name: Yılmaztürk, Sema Melek.

EDUCATION

Degree	Institution	Year of Graduation
MS	METU Civil Engineering-Structural Engineering	2013
BS	METU Civil Engineering	2010
High School	Gazi Anadolu High School, Ankara	2006
Middle School	TED Ankara College, Ankara	2003

FOREIGN LANGUAGES

Advanced English

PUBLICATIONS

1. Kasapgil, S.M., & Ergüner K. (2023). Structural assessment and maintenance of a balanced cantilever bridge. Bridge Engineering Association, New York Bridge Conference, August 2023. New York, USA.
2. Kasapgil, S.M., Binici, B., & Canbay, E. (2021). Seismic behavior of AAC infill walls insulated with cementitious lightweight panels in reinforced concrete frames. Engineering Structures, 248, 1-11 doi:10.1016/j.engstruct.2021.113215
3. Özel C.N., Ergüner K., Rahman A., Kasapgil S.M., Karayiğit H., Özkul Ö. & Kutsal K. (2018). Design challenges of a river crossing: Dim çayı extradosed bridge. Developments in international bridge engineering, Springer. Istanbul Bridge Conference, August 2018.Istanbul, Turkey
4. Ergüner K., Görgülü A. G., & Kasapgil, S. M. (2016). A real case study about evaluation of the existing situation of a post tensioned single span box girder bridge. Istanbul Bridge Conference, August 2016.Istanbul, Turkey.
5. Yılmaztürk, S. M., Arıcı, Y., & Binici, B. (October 2015). Seismic assessment of a monolithic RCC gravity dam including three-dimensional dam–foundation–reservoir interaction. Engineering Structures, 100, 137-148. doi:10.1016/j.engstruct.2015.05.041
6. Aldemir, A., Yılmaztürk, S. M., Yücel, A. R., Binici, B., Arıcı, Y., & Akman, A. (2015). beton barajların deprem davranışlarının incelenmesinde kullanılan analiz metotları *. İMO Teknik Dergi, 427, 6943-6968.